Long-Haul Very High Bit Rate Transmission Systems & All Optical Synchronous Multiple Access Fiber Networks Using OTDM and Optical Amplifiers

by

HANAA ISSA

A dissertation submitted to the Graduate Faculty in Engineering in partial fulfillment of the requirements for the degree of Doctor of Philosophy, The City University of New York.

1995

This manuscript has been read and accepted for the Graduate Faculty in Engineering in satisfaction requirements for the degree of Doctor of Philosophy.

4/26/95
Date

Chair of Examining Committee

Professor Samir Ahmed

4/26/95
Date

Executive Officer

Professor Gerald Lowen

Supervisory Committee

Professor Leoned Roytman
Professor Fred Moshary
Professor Umit Uyar
Dr. Kasem Sohraby

The City University of New York

ABSTRACT

Long-Haul Very High Bit Rate Transmission Systems & All Optical Synchronous Multiple Access Fiber Networks Using OTDM and Optical Amplifiers"

By : Hanaa Issa

Advisor: Herbert Kayser Professor Samir Ahmed

This thesis seeks to more effectively exploit the enormous inherent bandwidth of optical fibers by combining them with the tremendous potential functional capability of semiconductor optical amplifiers (SOAs). This can be achieved by further developing novel optical multiplexing schemes. The work proposed here, therefore, focuses on developing a novel Optical Time-Division Multiplexing technique for use in ultra high-speed transmission systems. Our emphasis is on both very high bit-rate point-to-point transmission systems and multiple-access local loop networks. The overall objective of this work is to investigate and analyze, through computer simulation and modeling, the performance of all the critical elements necessary for the implementation of high–capacity, high–performance, cost–effective, reliable point-to-point and multiaccess transmission systems based on time division optical fiber communications technology. We will investigate OTDM networking architectures and technology as well as the potential and limitations of long-haul very high bit-rate point-to-point OTDM transmission systems. The network technology element of this work aims to define the physical components and network elements that are necessary to assemble a reconfigurable, diverse OTDM network. The network architecture element specifically addresses several new topologies, such as rings and stars.

Eventually, we want to be able to model the end-to-end performance of any signal that passes through the network. This will permit us to compare and devise candidate survivable OTDM architectures and determine the appropriate field of use for each. In addition, this will enable us to determine how to use the capabilities of each architecture to best advantage and provide insight into which OTDM architecture should be stressed.

Acknowledgement

I would like to take this opportunity to acknowledge my deep appreciation to my thesis advisor Professor Samir Ahmed for his patient guidance, continued encouragement, and numerous invaluable suggestions and discussions during the course of this research. I am also grateful to my co-mentor Prof. L. Roytman for his valuable theoretical assistance.

My thankfulness goes to my fellow graduate students for their assistance, providing laughter and sunshine during my stay at CCNY.

This thesis study was made possible from the educational and financial support provided by ARPA/AFSOR Grant No. F49620-941 .

To My Parents

TABLE OF CONTENTS

List of Figures

CHAPTER 1
INTRODUCTION

1.1 Introduction and Background

Progress in very high bit-rate lightwave systems has been stimulated by consistent demands for expanded transmission capacity. These demands have led to increased interest in multigigabit-per-second pulse-code-modulated (PCM) systems, and have put an emphasis on the need for high-speed and wide-band electronics in lightwave transmitters and receivers. To date, it has generally been possible to meet these needs with high-speed Si and GaAs circuits, but at gigabit-per-second bit rates it becomes increasingly difficult to develop the necessary digital electronic circuits. One method to relieve this electronic speed bottleneck is to extend the well-known techniques of electrical multiplexing into the optical domain. The two main approaches to optical multiplexing are optical wavelength-division multiplexing (WDM) [1] and optical time-division multiplexing (OTDM) [2]. This thesis concentrates on optical time-division multiplexing.

In optical time-division multiplexing (OTDM), a high bit-rate data stream is constructed directly by time-multiplexing several lower bit-rate optical streams. Similarly, at the receiver end of the system, the very high bit-rate optical signal is demultiplexed to several lower bit-rate optical signals before detection and conversion to the electrical domain. This approach to optical time-division multiplexing and demultiplexing moves the demand for high-speed performance away from electronic devices such as transistor, and places it on the intrinsically faster optical and optoelectronic devices such as pulsed semiconductor lasers and optical

switches. The time-division multiplexing approach is a purely digital technique and is therefore compatible with the concept of an all-digital network that combines switching and transmission. In addition, OTDM offers system design flexibility, including the possibility of adjustable bandwidth allocation in different baseband channels and the possibility of simple system hardware in which only a single transmitter laser is required for all channels.

The potential of OTDM for very high bit-rate PCM systems has been recognized for more than two decades [3-5] but until recently [6-8] there have been few system-level demonstrations of the technique at multigigabit-per-second bit rates. The implementation of very high bit-rate OTDM systems has been slow because electronic multiplexing has usually served adequately and because the necessary hardware, such as high-speed optical switches and compact pulsed semiconductor lasers, have only recently reached a sufficient state of refinement.

1.2 Thesis Statement

This thesis focuses on developing a novel optical time-division multiplexing technique for use in ultra high-speed transmission systems. Our emphasis is on both very high bit-rate point-to-point transmission systems and multiple-access local loop networks. The overall objective of this work is to investigate and analyze, through computer simulation and modeling, the performance of all the critical elements necessary for the implementation of high–capacity, high–performance, cost–effective, reliable point-to-point and multiaccess transmission systems based on time division optical fiber communications technology. We will investigate

OTDM networking architectures and technology as well as the potential and limitations of long-haul very high bit-rate point-to-point OTDM transmission systems. The network technology element of this work aims to define the physical components and network elements that are necessary to assemble a reconfigurable, diverse OTDM network. The network architecture element specifically addresses several new topologies, such as rings and stars.

Simulation Tool: We will implement a flexible, powerful computer modeling tool for evaluating the end to end performance of OTDM networks. The tool will include wavelength driven and time driven capabilities. The wavelength driven capability is required to model the effects of cascading many optical amplifiers and optical filters on the output signal to noise ratio and crosstalk level of any signal on the network. The time driven capability is required to model the effects of fiber chromatic and polarization dispersion, crosstalk from adjacent channels, timing jitter due to noise and crosstalk, thermal and shot noise in the receiver, and non-perfect extinction ratio in external modulators, on the signal quality in the network.

Device and subsystems Models: We will develop models for different subsystem components, like laser sources, TWSOAS, OTDM multiplexers and demultiplexers, optical filters, and external modulators. It will be possible to combine these components in any combination, using the above tool, to allow the important network elements to be modeled. These networks elements can then be combined in an arbitrary order to allow a variety of network architectures to be modeled.

We present a model of a novel optical time-division multiple-access (OTDMA) network architecture that relates parameters at the device-level to system-level performance measures such as bit error rate (BER) and noise margin. This is accomplished by developing mathematical models of the optical and electronic devices in the system which are suitable for discrete-time simulation at the system-level. These simulation models are interconnected into a system level simulation model of the OTDMA architecture. We demonstrate some of the capabilities of the simulation model through a number of examples at both device and system level.

The simulation modeling is characterized by its consideration of the full potential for exploiting traveling-wave semiconductor optical amplifiers (TWSOAs) as multifunction components in both long haul optical transmission systems and multiple-access broad-band fiber optic networks. Specifically, the nonlinear model is used to examine the switching characteristics of TWSOAs when used for external modulation and demultiplexing at both the transmitter and receiver ends of a multi-Gb/s OTDM system. Employing TWSOAs as high-speed optical gates at both the transmitter and receiver ends of OTDM systems will, (i) provide simultaneous gain and gating, and hence increase both information capacity and transmission distance, and (ii) replace the present inherently bulky and lossy Ti: $LiNbO_3$ waveguide external modulators and demultiplexers, required at each end of each channel, with compact ones suitable for opto-electronic integrated circuit (OEIC) implementation. This approach may allow for lossless devices and future monolithic integration of external modulators with lasers and of demultiplexers with detectors or with opto-electronic integrated front-ends. Optical gating with TWSOAs is also of

particular interest for bus or broadcast network architectures where one channel on a bus is sampled and access to all channels is required.

Eventually, we want to be able to model the end-to-end performance of any signal that passes through the network. This will permit us to compare and devise candidate survivable OTDM architectures and determine the appropriate field of use for each. In addition, this will enable us to determine how to use the capabilities of each architecture to best advantage and provide insight into which OTDM architecture should be stressed by yielding estimates of comparative networking costs.

1.3 REFERENCES

[1] Charles A. Brackett, "dense wavelength division multiplexing networks: principles and application," IEEE J. on Selected Areas in communication, Vol. 8, No, 6, pp. 948-964, August (1990).

[2] R. S. Tucker, G. Eisenstien, and S. K. Korotky, "Optical time-division multiplexing for very high bit-rate transmission," IEEE J. Lightwave Technol., Vol. 6, No, 11, pp. 1737-1749, Nov. (1988).

[3] Tracy S. Kinsel, and Richard T. Denton, "Terminals for high-speed optical pulse code modulation communication system : Optical multiplexing and demultiplexing," Proceedings of the IEEE, Vol. 56, No. 2, Feb. (1968).

[4] R. T. Denton and T. S. Kinsel, "Terminals for a high-speed optical pulse code modulation communication system: I. 224-Mbit/s single channel," Proceedings of the IEEE, Vol. 56, No. 2, Feb.(1968). PP. 140

[5] Tracy S. Kinsel, "Wide-band optical communication systems : Part I -- Time division multiplexing," Proceeding of the IEEE, Vol. 58, No. 10, Oct. (1970) .

[6] G. Eisenstien, R. S. Tucker, G. Raybon, and S. K. Korotky, "8-Gb/s transmission over 40 km in a two-channel single-laser optical time-division multiplexed system experiment," OFC' 89

[7] G. Eisenstien, R. S. Tucker, and G. Raybon, "Optical time-division multiplexed transmission at 8 Gb/s using single laser and semiconductor optical power amplifier," Electron. Lett., Vol. 25, No 16, pp., 1034-1036, Aug. (1989).

[8] R. S. Tucker, G. Eisenstien, S. K. Korotky, L. L. Buhl, "16 Gbit/s Fiber transmission experiment using Optical Time-Division Multiplexing," Electronics Lett., Vol. 23, Nov. (1987).

CHAPTER 2

Principles of Optical Time-division Multiplexing and Demultiplexing

2.1 Electrical and Optical Multiplexed Systems

The basic principle of time-division multiplexing and demultiplexing is that each of the baseband data streams is allocated a series of time slots on the multiplexed channel. A multiplexer(MUX) assembles the higher bit-rate bit stream from the baseband streams and a demultiplexer (DEMUX) reconstructs bit streams at the original lower bit rate by separating bits in the demultiplexed stream. The techniques for this process are well established for electrical time division multiplexing and demultiplexing but are only now emerging in optical systems.

Fig. 2.1 highlights the similarities and the differences between electrically time-multiplexed and optically time-multiplexed lightwave systems. In this figure and in subsequent figures, thick lines are used for optical (fiber) signal paths and thin lines are used for electrical signal paths. In an electrically time multiplexed system, Fig. 2.1(a), multiplexing is carried out in the electrical domain, before the electrical-to-optical (E/O) conversion. Demultiplexing is carried out after the optical-to-electrical (O/E) conversion. For n baseband channels, each of bit rate B, the multiplexed bit rate is nB. Potential electronic bottlenecks occur in the MUX and the E/O converter, and in the O/E converter and the DEMUX, where the electronics must operate at the full multiplexed bit rate. These bottlenecks arise from a) speed limitations of digital integrated circuits, b) speed limitations of high-power and low-noise linear amplifiers used to drive the laser or modulator in the E/O converter and in the O/E

converter, c) limited modulation bandwidths of lasers and modulators, and d) the fact that the receiver sensitivity offered by an avalanche photodiode degrades by more than 3 dB for every octave increase in receiver bandwidth. These problems have so far limited the maximum bit rate for electrically multiplexed systems to about 10 Gbit/s.

In an optically multiplexed system, Fig. 2.1(b), the electronic bottlenecks are removed by moving the E/O and the O/E converters (i.e.,the transmitters and receivers) into the baseband channels. Multiplexing is carried out after the E/O conversion and demultiplexing is carried out before the O/E conversion. All electronics associated with signal processing operate only at the baseband bit rate. Note that a control signal is needed to drive the demultiplexer. In general, this control signal could be either electrical or optical, depending on the demultiplexer technology. At present the most practical optical demultiplexers are based on electrooptic switches, which use electrical control signals.

An important difference between electrically multiplexed and optically multiplexed systems is that in electrical systems the multiplexing and demultiplexing can be carried out at points in the system where the signal has been amplified to large levels. The signal-to-noise ratio is determined by the receiver and its associated low-noise front end and is not affected by loss in the multiplexing or demultiplexing operations. In an OTDM system, on the other hand, the multiplexing and demultiplexing is carried out on the optical signal. Thus, optical losses reduce the signal level relative to the receiver noise, and losses must be kept small.

2.2 Optical Time-Division Multiplexing

In this section we consider optical waveforms and timing requirements for optical multiplexing, and examine topologies for transmitters and multiplexers.

The operation of time-multiplexing several lower bit-rate baseband channels onto a higher bit-rate channel can be divided into three subfunctions: sampling, timing, and combining. The sampling function takes samples of the incoming baseband data stream, thereby identifying the value of each incoming bit. The timing function ensures that the samples are available at the correct time slots on the multiplexed channel. The combining function assembles all the sampled baseband data streams to generate the higher bit-rate multiplexed data stream. In multigigabit-per-second electrically multiplexed systems it is convenient to sample each of the input data streams using short sampling pulses that are timed to correspond to the appropriate time slots on the multiplexed bit stream. If the sampling pulsewidths are less than one bit-period of the high bit-rate multiplexed signal, the combiner can be a simple summing circuit. A similar strategy is a preferred approach to optical time-division multiplexing because it can capitalize on mode-locked and gain-switched semiconductor lasers, which are capable of generating pulses more than ten times shorter than electrical pulses. In this approach to multiplexing the sampling function is carried out in the E/O converters (i.e.,the system transmitters). Consequently, the MUX in Fig. 2.1(b) is required only to do the combining function. Fig. 2.2 shows the schematic of an E/O converter (transmitter) that can be used to sample the input data before optical combining. Short optical pulses from a laser are incident on an optical

modulator, which is driven by an input electrical data stream. The electrical data stream could be either in the return-to-zero (RZ) or the non-return-to-zero (NRZ) format, but NRZ is usually preferable because it minimizes the bandwidth requirements of the baseband digital electronics, the modulator, and its drive amplifiers. The optical pulse train from the laser samples the electrical input data via the modulator, thereby converting it from NRZ in the electrical domain to RZ in the optical domain. An important feature of the laser-modulator combination in Fig. 2.2 is that when the laser and input data are correctly timed, the modulator is either fully "on" or fully "off" when the optical pulse passes through it. This means that the modulation process does not cause the optical signal to chirp.

Sampling the baseband data in the E/O converter enable the optical combining function to be carried out using a passive device such as a fiber directional coupler power combiner. Another advantage of this approach is that, independent of the type of combiner used in the system, the RZ output format from the E/O converters leads to low multiplexing crosstalk. Furthermore, the optical power from the lasers in the E/O converters is used efficiently since the signal in each baseband channel is zero during time slots to be occupied by other channels in the demultiplexed stream. This is a significant practical consideration because semiconductor lasers are average-power limited devices.

The timing scheme for a general n-channel optical time-division multiplexed system is shown in Fig. 2.3 the n optical signals incident on the combiner are RZ pulse trains with repetition rate B and with pulsewidth T (measured at the baseline). The incoming bit streams are temporally offset

from one another by delay D. Data are encoded on each pulse train, before combining, so in general some of the individual pulses will have zero amplitude. However, in Fig. 2.3 all bits are shown as "ones" for clarity. When the pulse spacing in Fig. 2.3 is adjusted for maximum multiplexed bit rate, each pulse in the multiplexed bit stream just comes into contact with its nearest neighbors. Under these circumstances D = T, and the multiplexed bit rate is 1/T. With laser pulses that are 10 ps wide at the baseline, for example, the multiplexed bit rate could be as high as 100 Gbit/s.

Fig. 2.3 shows that the RZ signal format provides low system crosstalk. Since each baseband signal is always nominally zero except in its allotted time slot on the multiplexed bit stream, it cannot interfere with other channels. In practice, the pulse stream will have a finite on/off ratio and the resulting baseline light signal between pulses will cause a component of crosstalk. Furthermore, leading and trailing tails on the pulses will also cause crosstalk if the pulses are spaced such that tails overlap on adjacent pulses. To avoid possible overlap problems it is usually necessary to ensure that the pulses are somewhat shorter than the one bit period of the multiplexed bit stream. Since shorter pulses occupy a wider optical spectrum, reducing the pulsewidth may increase the dispersion penalty, even if the lasers operate at or near the wavelength of zero first-order chromatic dispersion in the fiber. Thus choosing the optimum pulsewidth may entail a compromise between system crosstalk and pulse spreading caused by fiber dispersion. For example in local applications requiring very high bit rates over short lengths of fiber, optimum system performance would be obtained by minimizing crosstalk. This could be

achieved using optical pulses that are significantly shorter than the multiplexed bit period. In longer distance applications, on the other hand, it may be necessary to put more emphasis on minimizing the dispersion penalty rather than crosstalk. Thus a long distance system might achieve optimum performance with longer laser pulses.

Block schematics showing two possible configurations for the E/O converters (transmitters) and combiner for an n-channel OTDM system are presented in Fig. 2.4 The first configuration, Fig. 2.4(a), uses n optical pulse generators, all driven by the same master clock. These pulse generators could be mode-locked or gain switched semiconductor lasers. The pulse streams are delayed with respect to one another using delay elements either in the electrical clock paths (as shown in Fig.) or in the optical signal paths. Electrical delays would usually be preferred because they are easily made adjustable. Data encoding and sampling can be carried out using optical modulators such as $LiNbO_3$ waveguide electrooptic devices at the outputs of the pulse generators. An alternative to using external modulators would be directly encode data on gain-switched laser. The data-encoded pulse streams in Fig. 2.4(a) are brought together in the combiner. A potential disadvantage of transmitter-combiner arrangement in Fig. 2.4(a) is that the wavelengths of all lasers need to be closely matched to avoid pulse overlap at the receiver end of the fiber caused by different propagation time. One approach to circumvent this problem is to use an active control mechanism that detects pulse overlap at the receiver end of the system and continuously adjusts the timing of the transmitter pulses accordingly. This type of control scheme could also be used to adjust the timing of bit streams originating in different locations.

The second OTDM transmitter configuration, Fig. 2.4(b), uses a single optical pulse generator. The output of the generator is split passively into n channels, which are then encoded with data and properly delayed with respect to one another. This arrangement requires only one laser a feature that cannot be achieved with other optical multiplexing methods such as wavelength-division multiplexing. In addition, all channels operate at precisely the same optical frequency and will therefore propagate through a fiber with the same delay. This minimizes the dispersion penalty and hence significantly increases the transmission distance. The main disadvantage of the second configuration is that the total transmitted power will be reduced because there is only one laser. Thus, with a single-laser source of fixed average power, time multiplexing is performed at the expense of pulse energy. Increasing the number of channels will lead to degradation of system performance. This has practically hampered attempts to take advantages of the full potential of systems using single-laser architecture.

To overcome the limitations existing with single-laser OTDM configurations, the approach we are pursuing compensates for the division of single-transmitter output power by using TWSOAs for simultaneously gating and amplifying the transmitted signal. This approach both eliminate the usual losses associated with conventional waveguide modulators and demultiplexers, usually used, and simultaneously permits the replacement of these bulky devices with integrable components.

Up to this point, we have assumed that the baseband modulation in both systems in Fig. 2.4 is synchronous with the pulse stream from the lasers. This is desirable for best performance in very high bit-rate systems but the

requirement of synchronous operation can be removed if the modulation bit rate is substantially less than the repetition rate of the lasers. Thus, one can trade off capacity for increased system flexibility. Asynchronous operation is particularly attractive for systems where the baseband channels originate in different locations.

The optical combiner in Fig. 2.4(a) and (b) can, in general, be passive or active. A passive combiner would incorporate devices such as fiber directional couplers, while active combining would use active devices such as optical switches. The passive combiner option has the advantage of simplicity but its losses can become large because each 3-dB directional coupler introduces a 3-dB combining loss. The losses in an active combiner should, in principle, be smaller because the losses per device is potentially low. An integrated array of switches on a single chip promises the lowest combining loss for systems with more than two baseband channels. In either case, optical amplification may counter the power penalties incurred.

An active combiner has the potential of reducing crosstalk, by decreasing pulse overlap caused by finite on/off ratios and leading and trailing tails on the pulses. In a passive combiner, a tail extending into the time slot of neighboring bit would be unattenuated, but in an active combiner it would be reduced by the (time-dependent) switching function. In addition to combining the baseband signals, an active combiner could also perform the sampling function required in optical multiplexing. An active multiplexer of this type could, in principle, eliminate the need for pulsed lasers. However, CW laser operations would place very stringent requirements on the switch speed and extinction if low crosstalk is to be achieved. In addition, CW operation would not be efficient because of the average

power limit of semiconductor lasers and the low duty cycle of each baseband optical signal.

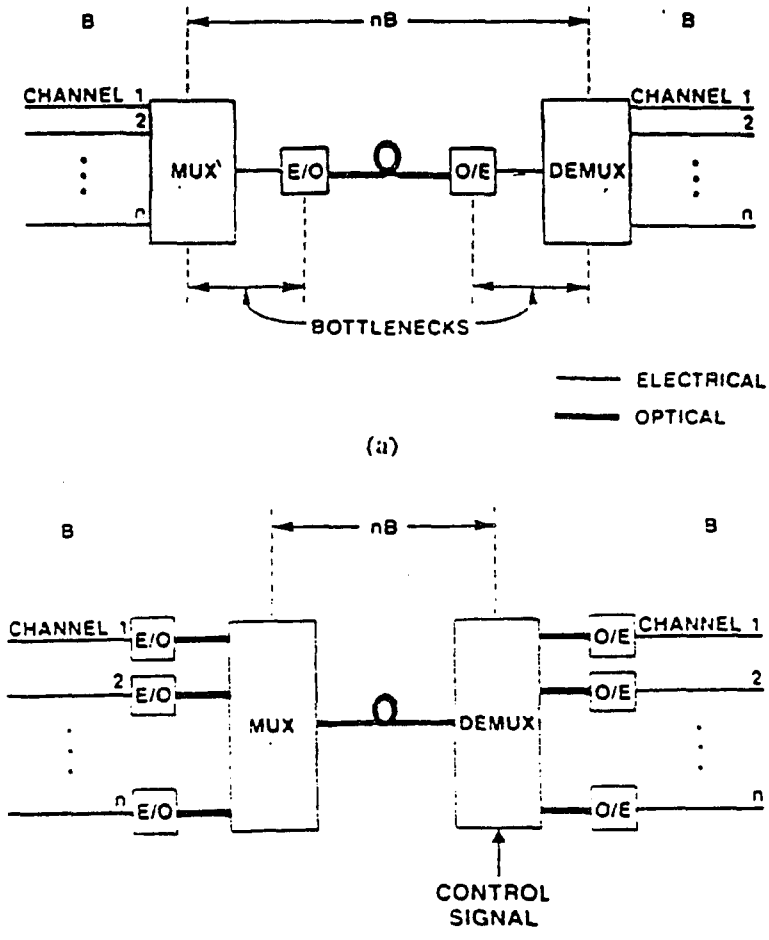

Fig. 1. Schematic of (a) electrical and (b) optical time-division multiplexed lightwave systems.

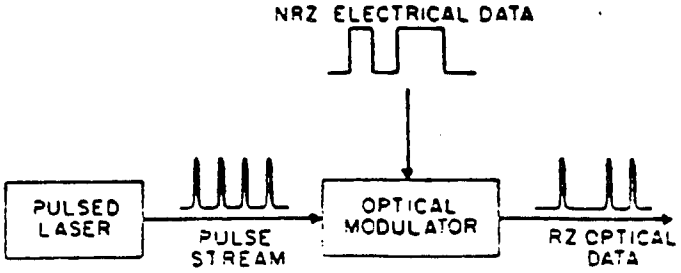

Fig. 2. Schematic of an E/O converter that samples input data.

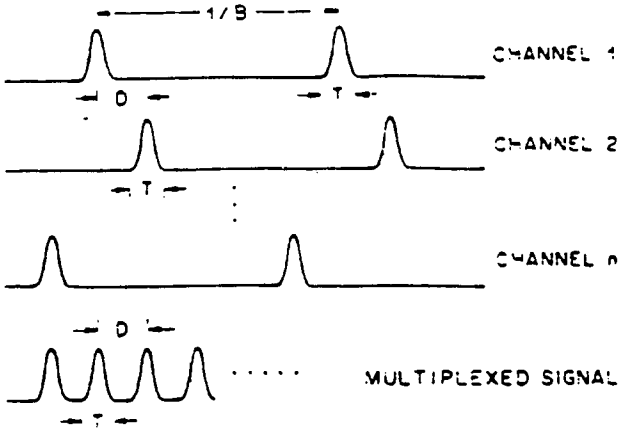

Fig. 3 Timing scheme for multiplexing in an n-channel OTDM system.

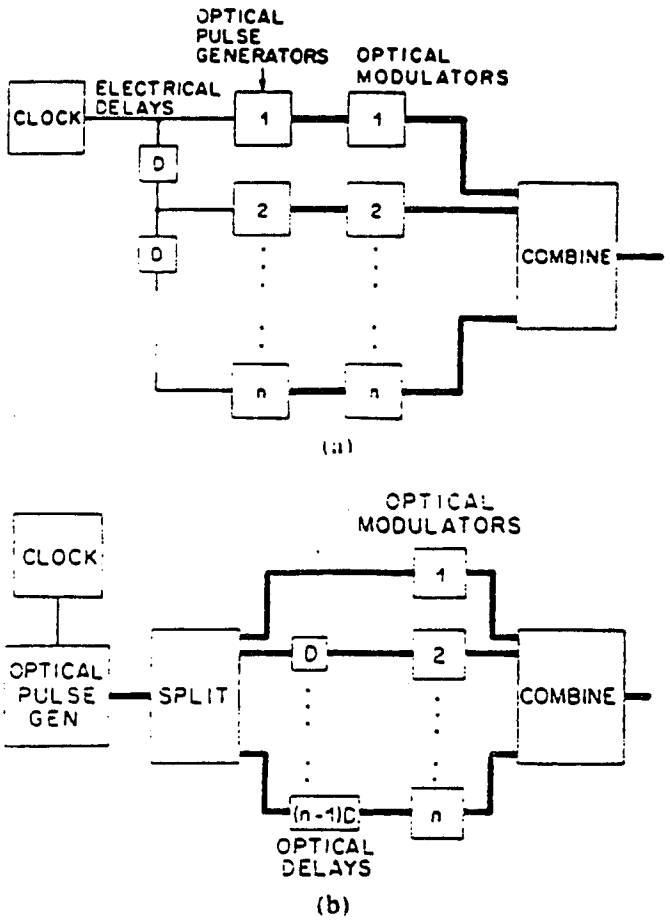

Fig. 4. Schematics of two configurations for E/O converters and combiner. (a) Multiple optical pulse generators. (b) Single optical pulse generator.

CHAPTER 3
OTDM System Architecture

3.1 OTDM Scheme

One promising way of realizing ultra high bit rate telecommunication systems that offer several tens of gigabits-per-second is to optically multiplex relatively low bit rate channels, which consist of ultra short optical pulses, into a higher bit rate channel before transmission, and to optically demultiplex the higher bit rate channel into the original low bit rate channels after transmission. This approach eliminates the speed limitations associated with electronic devices.

To date, two possible configurations for the E/O converters at the transmitter have been in use in OTDM systems. The most widely used multiple-laser transmitter configuration [1] uses a number of optical pulse generators (gain-switched DFB or mode-locked semiconductor lasers), all driven by the same master clock. A potential disadvantage of this arrangement is that the wavelengths of all lasers need to be closely matched to avoid dispersion and hence pulse overlap at the receiver end of the fiber caused by different propagation delays.

The second configuration uses a single-laser transmitter architecture where the output is split passively into n channels [1]. The channels are then encoded with data and properly delayed with respect to one another. This arrangement requires only one laser, a feature that cannot be achieved with other optical multiplexing methods such as WDM. In addition, all channels operate at precisely the same optical frequency and will therefore

propagate through a fiber with the same delay. This minimizes the dispersion penalty and hence significantly increases the transmission distance. The main disadvantage of the second configuration is that the total transmitted power will be reduced because there is only one laser. Thus, with a single-laser source of fixed average power, time multiplexing is performed at the expense of pulse energy. Increasing the number of channels will lead to degradation of system performance. This has practically hampered attempts to take advantages of the full potential of systems using single-laser architecture.

To overcome the limitations existing with single-laser OTDM configurations, the approach we are pursuing compensates for the division of single-transmitter output power by using TWSOAs for simultaneously gating and amplifying the transmitted signal. This approach both eliminate the usual losses associated with conventional waveguide modulators and demultiplexers, usually used, and simultaneously permits the replacement of these bulky devices with integrable components. It should be pointed out that, to date, systems using multiple-laser transmitter architecture are being used exclusively in order to achieve multigigabit per second (higher than 8 Gbit/s) OTDM fiber transmission systems [1]. This is because the potential of exploiting TWSOA in OTDM systems, where their use is essential for realizing the full potential of systems using single-laser transmitters, has not yet been considered.

The block diagram of the proposed OTDM scheme is shown in Fig. 3.1. The OTDM system transmitter configuration uses a single optical pulse generator, a gain-switched DFB or mode locked semiconductor laser, which is assumed to generate optical pulse trains with repetition rates B and

with pulsewidths T-ps (measured at the baseline). The output pulse train of the laser is split passively (using fiber couplers) into n channels. Each of these channels are then modulated using a TWSOA, which is driven by an input electrical data stream (amplifier driving current). The electrical data stream is assumed to be a pseudo-random NRZ (non-return-to-zero format) data pattern, while the optical input signal is assumed to be periodic Gaussian pulse train with repetition rates (B-GHz) equal to the electrical data bit rate (baseband bit rate). The n-modulated signals are properly delayed with respect to one another, by delays D using a fiber delay line, and combined in a second star coupler to form the multiplexed nB-Gbit/s signal.

When the pulse spacing is adjusted for maximum multiplexed bit rate, each pulse in the multiplexed bit stream just comes into contact with its nearest neighbors. Under these circumstances D = T, and the maximum multiplexed bit rate is 1/T. With laser pulses that are 20 ps wide at the baseline, which is the practical pulse width used in our simulation, the maximum achievable multiplexed bit rate in our proposed OTDM system can be as high as 50 Gb/s. However, in our simulation, we have increased the spacing between adjacent multiplexed pulses to larger values (D > T), than the minimum allowable values (D = T), to ensure low crosstalk, and, therefore, a transmission capacity of up to 40 Gbit/s over 100-200 km of single-mode fiber is anticipated.

The nB-Gbit/s multiplexed signal is demultiplexed at the receiver end using TWSOAs demultiplexer switching network. To fully demultiplex n-channels, a fiber directional coupler would be needed to feed the multiplexed signal to n-TWSOA switches. Each (single) TWSOA switch,

used in the simulation, is assumed to have a selection ratio of 2 : 1 and/or 4 : 1 and is, therefore, driven with a sinusoid at a frequency equal to one-half and/or one-quarter of that of the bit rate of the input optical signal to be demultiplexed. For systems with more than two baseband channels (assuming that the amplifier will have a selection ratio of 2 : 1), or with more than four channels (assuming that the amplifier will have a selection ratio of 4 : 1), larger demultiplexer switching network can be constructed by interconnecting 1 x 2 and/or 1 x 4 building blocks of TWSOAs.

The demultiplexer network assumed in our simulation is a binary tree network [1-3] which uses a specific number of TWSOAs switches. This number varies in accordance with the number of multiplexed baseband channels, bit rate of each, and the selection ratio assigned to each single TWSOA switch of the binary tree network. Its first stage is a high speed switch which demultiplexes the data stream to two and/or four data streams, each at half and/or one-fourth the multiplexed bit rate. Subsequent switches in the binary tree structure also can be driven by sinusoids, but operate at subharmonics of the drive frequency of the first stage switch.

It should be pointed out that our preliminary simulation results indicate that a single Zn-doped active region TWSOA switch should be capable of demultiplexing up to 10-12 Gbit/s. Hence, in order to demultiplex 40 Gbit/s, each first stage of the binary tree network would consist of 3-4 cascaded TWSOAs switches. It is also anticipated that the accumulated ASE (amplified spontaneous emission) noise exiting from each final amplifier in the demultiplexeing network would be the limiting factor for achieving demultiplexing speeds higher than 40 Gbit/s, since it is by far the

dominant source of receiver noise. As more channels are added, the SNR (signal to noise ratio) drops more rapidly.

Thus, in the basic form of the OTDM system proposed here, TWSOAs will be configured as:

1) low chirp external modulators to replace the conventional bulky and lossy waveguide external modulators used exclusively in OTDM system transmitters. These, in addition to modulating the transmitted signal will also amplify it and eliminate the standard 3 dB losses associated with the use of conventional bulky and lossy Ti: $LiNbO_3$ waveguide external modulators in each channel. This approach results in an increase in both the total information capacity (more channels might be multiplexed) and transmission distance (overall power budget is also increased) of the system.

2) high speed optical gates for optical demultiplexeing to replace the conventional bulky and lossy waveguide demultiplexers used exclusively in OTDM system receivers. Once again, in addition to demultiplexing the received multiplexed signal and eliminating the usual losses otherwise associated with the use of conventional bulky and lossy Ti: $LiNbO_3$ waveguide demultiplexers, the received signal is also amplified. This results in improvement in the receiver sensitivity and overall increase in the SNR at the receiver.

3) receiver preamplifier to improve the receiver sensitivity and the overall SNR at the receiver.

In the following chapter we, therefore, concentrate on developing computer simulation techniques to investigate and analyze the material and structure parameters of TWSOAs, and their effects on the overall

performance of the proposed OTDM system, for which the switching speed, rather than the gain, is the ultimate function.

3.2 REFERENCES

[1] R. S. Tucker, G. Eisenstien, and S. K. Korotky, "Optical time-division multiplexing for very high bit-rate transmission," IEEE J. Lightwave Technol., Vol. 6, No, 11, pp. 1737-1749, Nov. (1988).

[2] G. Eisenstien, R. S. Tucker, G. Raybon, and S. K. Korotky, "8-Gb/s transmission over 40 km in a two-channel single-laser optical time-division multiplexed system experiment," OFC' 89

[3] G. Eisenstien, R. S. Tucker, and G. Raybon, "Optical time-division multiplexed transmission at 8 Gb/s using single laser and semiconductor optical power amplifier," Electron. Lett., Vol. 25, No 16, pp., 1034-1036, Aug. (1989).

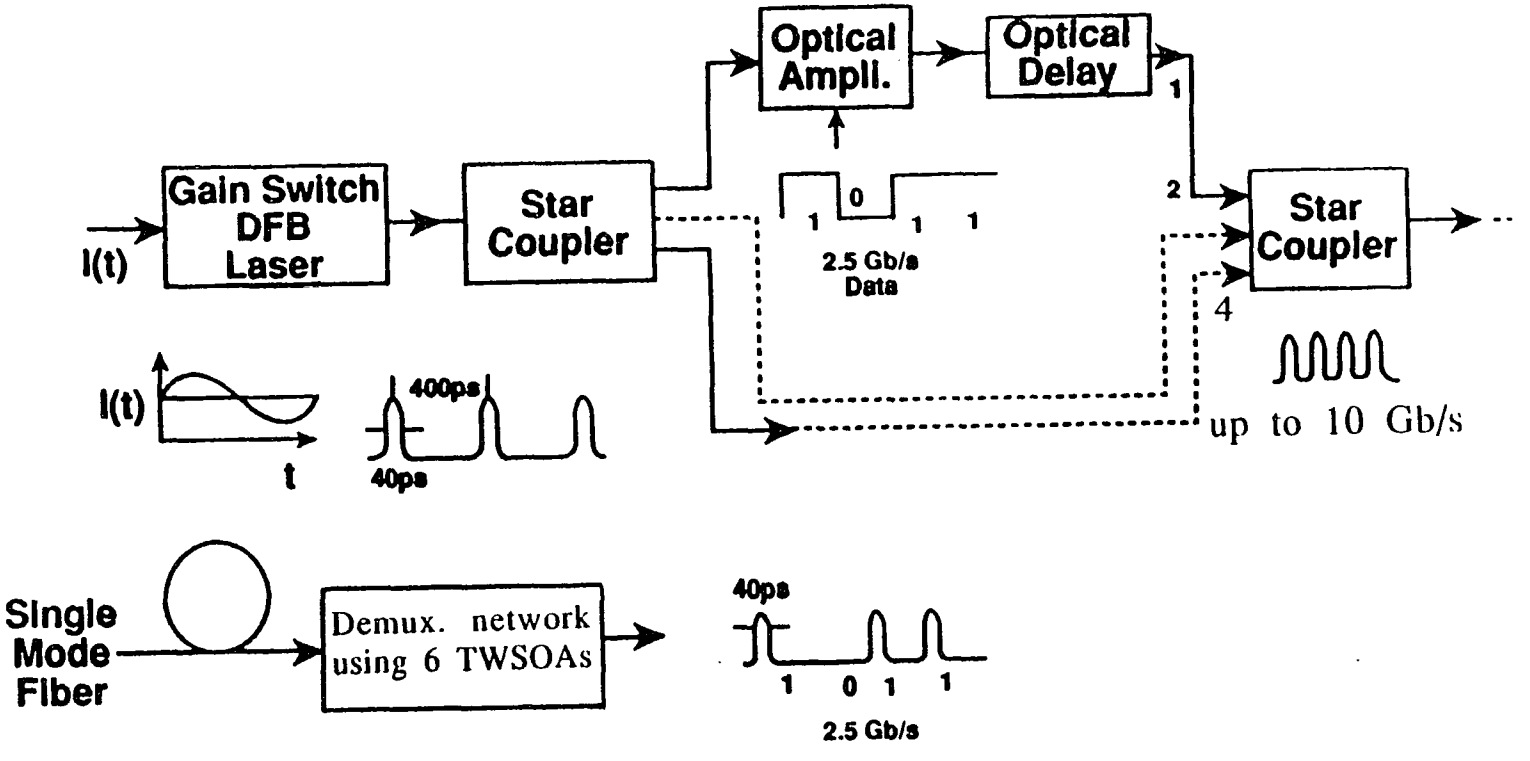

Fig. 3.1: Four channels OTDM system using TWSOAs as high speed optical gates for external modulation and demultiplexing.

CHAPTER 4

Modeling, Analysis and Simulation of SOAs for use as External Modulators at the Transmitter End of the OTDM System

4.1. Background

The rapid development of optical amplifiers will change the way system designers plan for next generation lightwave systems. In this context, Erbium doped fiber amplifiers (EDFAs) are expected to be extensively used as power boosters, repeaters and preamplifiers because of their advantageous properties, e. g., high saturation output power, polarization independence, compatibility with fiber networks, high gain and low insertion loss [1]. In a very analogous way, integrable semiconductor optical amplifiers (SOAs) offer loss compensation as well as performing sophisticated multifunctions such as switching, routing, signal tapping, pulse shape regeneration, etc. [2]. Rather than competing with fiber amplifiers, these integrated optics offer the potential for compact, cost effective solutions for next generation lightwave signal processing needs that will complement the role of discrete fiber amplifiers [1].

Travelling-wave semiconductor optical amplifiers (TWSOAs) are essential components for future high speed optical communication and switching systems [2]. In addition to their ordinary applications as gain elements, they are capable of performing a variety of optoelectronics functions in fiber networks. Some of these functions are self-clocked optical regeneration with NRZ to RZ signal format conversion, photonic switching, and external modulation [3].

4.2 Switching characteristics of TWSOAs

4.2.1 Introduction

Generally, most studies of the SOAs have focused on analyzing the material and structure parameters, which improve the device characteristics of the amplifier, for which gain is the ultimate function. SOAs have, however, attracted little attention for switching applications because the speed of present devices is determined by the carrier life time and is, thus, limited to a few Gb/s. In order to increase the switching speed of TWSOAs, it is important to increase the total carrier recombination rate (i. e., to shorten the spontaneous carrier life time). This can be achieved by doping the active region. It has been reported that Zn doping of the active region of Fabry-Perot [4] and DFB [5-6] lasers has the effect of increasing the differential gain and reducing the carrier life time. As a consequence, Zn doping can be expected to result in improvements in high-speed performances of TWSOAs. Consequently, we will investigate and analyze the material and structure parameters of TWSOAs with both an undoped (or unintentionally slightly doped) and Zn doped active regions, for which high speed switching is the ultimate function.

4.2.2 Recombination Mechanisms In SOAs with Zn-doped active layers

Recombination mechanisms can in general be classified into two groups, radiative and nonradiative. Radiative recombination occurs when an electron in the conduction band recombines with a hole in the valence band and the excess energy is emitted in the form of a photon. Radiative recombination is thus the radiative transition of an electron in the conduction band to an empty state (hole) in the valence band.

Nonradiative recombination of an electron-hole pair, as the name implies, is characterized by the absence of an emitted photon in the recombination process. This of course makes the experimental study, and hence identification, of such processes very difficult. The nonradiative recombination processes that affect the performance of long-wavelength semiconductor lasers are Auger recombination, surface recombination, and recombination at defects. The Auger recombination mechanism involves four particle state (three electrons and one hole) and is believed to be important at high temperatures and for low band-gap semiconductors.

Radiative Recombination

The total radiative recombination is given by:

$$R_{rad} = B(N)\ N(N + P_o)$$

where

$$B(N) = (B_o - B_1\ N)$$

Nonradiative Recombination

Although there are many different forms of Auger recombination [7], the discussion here will be limited to two types of band-to-band Auger recombination which have been cited as possible causes of the anomalous temperature dependence of InGaAsP light sources. In the first type [8], a conduction electron (C) and a heavy hole (H) combine and transfer their energy and momentum to a second conduction electron which is then boosted high into the conduction band. This is called the CCHC process in reference to the four particles involved. Since the initial state involves two

conduction electrons and one hole the CCHC recombination rate is proportional to n^2p.

A second Auger process, identified as dominant by several theoretical studies [9] , [10], involves one conduction electron and two heavy holes in the initial state and an excited hole (S) in the split-off band in the final state. The CHHS process is proportional to np^2. Thus, one can write the Auger recombination rate as

$$R_{Auger} = \begin{array}{ll} C_1 N^2 (N + P_o) & \text{CCHC} \\ C_2 N (N + P_o)^2 & \text{CHHS} \end{array} \qquad (1)$$

If the impurity concentration is small compared to the injected carrier density, both processes behave as Cn^3. However, if p_o is of the same order as n or larger, then the linear and quadratic term of (1) are very important and can dominant the cubic term. In fact, the presence of the linear term Cpn or a quadratic term proportional to Cp_on^2 provides a very useful method for identifying Auger recombination in more heavily doped material [11].

Several authors [12], [13], [14], who have used carrier life time date to determine Auger and radiative recombination rates, have neglected the effect of p_o and simply taken the Auger as Cn^3. In view of (1), the assumption that Auger recombination does not contribute to the quadratic recombination term can lead to incorrect interpretation of the data. This omission is justified only if Cp_o is small compared to B_o.

4.3. Amplifier Model

In this section, computer simulation techniques are used to develop a nonlinear model for the dynamic operation of TWSOAs. Specifically, the nonlinear model is used to examine the switching characteristics of these devices when used for external modulation at the transmitter end of a multi-Gb/s OTDM system. In particular, we will investigate the performance of the amplifier, when used as an optical gate, as a function of the frequency and amplitude of the RF driving signal, the precise time delay between the incident optical signal and the driving electrical signal, and the input optical signal levels. We will also consider possible degradation of crosstalk performance caused by accumulation of the ASE noise generated in the amplifiers, pulse distortion in single-channel systems due to gain saturation at multi-Gbit/s bit rates, and the introduction of pattern effects into high bit-rate optical data streams by carrier storage effects in the optical amplifier. While these effects may introduce some limitations, but our preliminary results indicate that there is little doubt that TWSOAs will greatly enhance the design flexibility of OTDM systems and will lead to significant improvements in system performance.

Our formulation, which is a pair of coupled partial differential equations, the wave equation and the rate equation, is basically along the line of the analysis reported in [15-16]. The analysis with space- and time-dependence is necessary because the gain saturation behavior is, in essence, spatially nonuniform and temporally dynamic. The characteristics of the present treatment lies in the fact that, in contrast to the frequently used linear recombination model [15-19] which assume that the gain and carrier recombination vary linearly with carrier density, we have also taken into

account the detailed non-linear carrier recombination rate, R(N). The model used here makes several reasonable simplifying assumptions, which makes it uncomplicated and economical on computational power.

In the analysis, the signal light is assumed to be single mode, and, for now, the contribution of the amplified spontaneous emission (ASE) is not considered. As will be shown, inclusion of the ASE term in the formulation does not significantly affect the results. Under these assumptions, the carrier density N(z,t) is obtained by solving the z-dependent rate equation [20-21]:

$$\frac{dN(z,t)}{dt} = \frac{I(t)}{qV} - R(N) - \frac{g(N)}{\Gamma a E_{sat}}|E(z,t)|^2 \qquad (2)$$

(a) $R(N) = N/\tau$ (Linear Model)

(b) $R(N) = AN + BN^2 + CN^3$ (Undoped active region)

(c) $R(N) = B(N)\, N(N + P_o) + R_{Auger}$ (Zn-doped active region)

$$B(N) = (B_o - B_1 N)$$

$$R_{Auger} = C_1 N^2 (N + P_o) \quad \text{CCHC}$$

$$C_2 N (N + P_o)^2 \quad \text{CHHS}$$

where the diffusion term is ignored by assuming that the transverse waveguide dimensions are smaller than the diffusion length. E(z,t) is the total optical field in the waveguide, normalized such that

$|E(z,t)|^2$ represents the optical power in watts, $E_{sat} = (h\nu A/\Gamma a)$ is the saturation energy of the amplifier, A is the cross-sectional area of the active region, and hn is the photon energy. The gain coefficient g(N) is defined by:

$$g(N) = \Gamma\, a\, [N(z,t) - N_0)] \qquad (3)$$

Other parameters and their numerical values used in the simulation are summarized in table I.

The propagation of the electromagnetic field inside the amplifier is governed by the wave equation [15-17]. Observing that the optical period is much shorter than the photon transit time through the amplifier, which, in turn, is much smaller than the timescale of envelope and gain variations [7-8], one can integrate the wave equation to get [15-16]:

$$\mathbf{E}(z,t) = \mathbf{E}(0,t)\ \exp\{(1+j\alpha)[\int_0^z g(z,t)\,dz]/2\}$$

or equivalently:

$$|E(z,t)|^2 = p_{in}(t)\ \exp\ [\int_0^z g(z,t)\,dz] \qquad (4)$$

At z = L, Eq. (3) can be rewritten as:

$$\mathbf{E}_{out}(t) = \mathbf{E}_{in}(t)\ \exp[G(t)(1+j\alpha)/2] \qquad (5)$$

where $\mathbf{E}_{in}(t) = \mathbf{E}(0,t)$ is the input field, $\mathbf{E}_{out}(t) = \mathbf{E}(L,t)$ is the output field, α is the linewidth enhancement factor, $p_{in}(t)$ is the average input power to the amplifier, $G(t) = \int_0^L g(z,t)\,dz$, and exp[G(t)] is the total large-signal optical power gain.

The set of rate equations (Eqs. 2 and 3) and the wave equation (Eq. 4) were solved numerically using a fourth-order Runge Kutta routine. This gives the values of N(t) at any point z along the amplifier, which can be used along with Eq. (5) to calculate the output power of the amplifier.

Unlike the approximate models previously proposed [15-17] to solve eq. (2), the simulation technique used here provides an exact solution. In the following, the solution claimed as "exact" is intended to mean the exact solution of (2). The technique used here does not restrict in any way the class of input signals, and can handle very large gain saturation and gain fluctuations.

The simulation block diagram of a TWSOA when used as external modulator in the proposed OTDM system transmitter configuration is shown in Fig. 4. 1. Short optical pulses from a DFB laser $\{p_{in}(t)\}$ are incident on the external modulator (TWSOA), which is driven by an NRZ input electrical data stream {amplifier input current I(t)}. The optical pulse train from the laser samples the electrical input data via the modulator, thereby converting it from NRZ in the electrical domain to RZ in the optical domain. For a TWSOA that is used as an external modulator, the set of rate equations (Eqs. 2 and 3) and the wave equation (Eq. 4) were solved numerically in response to the time-varying amplifier input current I(t). The amplifier current I(t) is assumed to be a pseudo-random NRZ data pattern of length 2^8 bits, while the input power $p_{in}(t)$ is assumed to be periodic gaussian pulses with FWHM pulse width denoted by t_p.

4.4 Results and discussion

4.4.1 General

Computer simulation techniques are used to study the modulation performance of the TWSOA at five different modulation speeds, 1, 2.5, 4, 8, and 10 Gb/s per channel. The numerical calculations are carried out in two sets:

I) In the first set, numerical calculations are carried out to examine the modulation performance of TWSOAs at modulation speeds of 1, 2.5, 4, and 8 Gbit/s per channel. The performance of devices with Zn doped active layer are compared to those with undoped or lightly-doped active layers (acceptor concentrations of 1-4 x $10^{17}/cm^3$). All numerical calculations presented in this work, for devices with Zn-doped active layers, are based on the assumption that the CHHS band-to-band Auger Recombination is the dominant nonradiative recombination process. All calculations are carried out assuming periodic gaussian pulse trains with a 40 ps FWHM pulse width.

II) In the second set, all numerical calculations of the first set are repeated, however, assuming periodic gaussian pulse trains with a 20 ps FWHM pulse width. Therefore, at the given pulse width used in the second set (= 40 ps at the base line), the multiplexed bit rate can be as high as 25 Gbit/s (twice the multiplexed bit rate of the first set) in our proposed OTDM system, if the pulse spacing is adjusted for the maximum multiplexed bit rate.

In general, the simulation results indicate that the modulated output pulses are sensitive to the precise time delay between the incident optical pulse and the electrical injection current pulse driving the TWSOA modulator. It is found that best modulation performance is obtained when the peak of the

input optical pulse $p_{in}(t)$ coincides with the trailing edge of the injection current pulse I(t). Therefore, all the simulation results presented in this work will be based, unless otherwise specified, on the assumption that optical input pulses satisfy this condition.

4.4.2 Simulation results of the first set (τ_p = 40 ps)

4.4.2.1 Modulation performance at 1 Gb/s per channel

In this section, all calculations are carried out assuming a peak drive current of 100 mA and optical input of periodic 1-GHz gaussian pulse trains (baseband bit rate) with 40 ps at FWHM. Fig. 4. 2 shows the simulation results of the modulated output power $p_{out}(t)$ at 1 Gb/s per channel, for three different values of input pulse energy, normalized with respect to the saturation energy. The amplifier driving current pulses used in the simulation has a peak pulse amplitude of 100 mA . It can be seen from Figs 4.2a ($E_{in}/ E_{sat} \approx$ -20 dB, corresponding to a pulse peak power of 0.75 mw) and 4.2b ($E_{in}/ E_{sat} \approx$-10 dB, corresponding to a pulse peak power of 7.5 mw) that the output peak power of a pulse preceded by 1 or a series of ones is slightly higher than that of a pulse preceded by zero or a series of zeros. In other words, the modulated (legitimate) output pulses depend on the driving random bit pattern. This means that these pulses which are preceded by 1 or a series of ones experience a gain higher than those which are preceded by zero or a series of zeros.

To understand these effects, it is important to note that input pulses are separated by times (1 ns) long compared with the gain decay time. Therefore, during a zero or a series of zeros, the amplifier carrier density has ample time to drop sharply and hence clamp the gain down to a zero

value. If the next consecutive bit is 1, the carrier density and hence gain has then to build up starting from the zero value. On the other hand, during a series of ones, the depletion in the carrier density is only that caused by the induced stimulated emission sweeping out the gain. The extent to which the gain will be depleted will depend on the strength of the induced stimulated emission. At relatively low input pulse energy ($E_{in}/E_{sat} \leq$ -10 dB), the induced stimulated emission causes little depletion in gain and carrier density. Therefore, during a second consecutive 1, the gain will start building up from a value that is relatively higher than that for a pulse preceded by zero or a series of zeros. The exact starting value is determined by the ratio of E_{in}/E_{sat}, and is higher for a lower ratio. This explains why the modulated output pulses in Fig. 4.2a, which have a smaller input signal, are more pattern dependent than those in Figs. 4.2b and 4.2c.

At high input pulse energy, $E_{in} \approx E_{sat}$, corresponding to a pulse peak power of 75 mw), Fig. 4.2c, the induced stimulated emission is strong enough to sharply deplete the carrier density and thereby clamp the gain down to a lower (near zero) value. In this higher intensity case, the gain during the second consecutive 1, will therefore start building up from a lower value and the pulse will experience the same gain as is experienced by a pulse preceded by 0 or a series of zeros. This can be seen in Fig. 4.2c ($E_{in} \approx E_{sat}$) where the peak power of all modulated output pulses are pattern independent. However, eventhough the modulated output pulses are pattern independent, the modulation performance obtained at 1 Gbit/s, for large input signal levels, is unsatisfactory, due to the generation, Fig. 4.2c,

of those false output pulses (at every 0 bit) which have a peak power $\approx$ 1/7 of that of the legitimate output pulses (at every 1 bit).

We define the extinction ratio (on/off ratio), r, as the ratio of the optical power in the least-favored "1" pulse (i.e., a "1" pulse which is preceded by the longest series of zeros) to the power in the most-favored "0" pulse. Strictly speaking, it is not the generation of those false output pulses which render the modulation performance inadequate, it is the low value of r, that is the problem.

Thus, as shown in Figs. 4.2a and 4.2b, satisfactory modulation performance at 1 Gb/s, over a practically useful range of input signal levels, is possible provided that $E_{in}/E_{sat} \leq$ -10 dB. Note that in this case, the two conditions required for achieving adequate modulation performance are met, that is: 1) all the modulated legitimate output pulses are almost pattern independent, and 2) the extinction ratio, r, must be as high as possible is ($r > 15$ dB).

Finally, as a specific example of the modulation performance that results for an incident optical pulse not coinciding with the trailing edge of the injection current pulse, Fig. 4.3 shows the simulation results of the modulated output power $p_{out}(t)$ at 1 Gb/s for $E_{in} = E_{sat}$. These results are obtained assuming 500 ps time delay between the peak of the input optical pulse $p_{in}(t)$ and the leading edge of the injection current pulse I(t). It can be seen from the figure that the modulated output pulses are distorted due to the generation of false output pulses at every 0 bit (zero driving injection current) preceded by a one or a series of ones. This is because the input optical pulses are separated from the trailing edge of the injection

current bits by times (500 ps) short compared to the gain decay time. In these circumstances, the initial input pulses passing through the amplifier with 0 driving current are not fully attenuated, since the gain, during their passage, has not had enough time to totally drop to an exact zero value.

4.4.2.2 Modulation performance at 2.5 Gb/s per channel

Fig. 4. 4 shows the simulation results of the modulated output power p_{out} (t) at 2.5 Gb/s per channel for three different values of input pulse energy normalized with respect to the saturation energy. These results are obtained assuming a peak drive current of 100 mA and optical input of periodic 2.5-GHz gaussian pulse trains with 40 ps at FWHM. Note that as the modulation speed increases (input optical pulses are separated by times (400 ps) comparable with the gain recovery time), the gain has not had enough time to completely decay and/or recover, and, therefore, the pattern dependence effects become more pronounced, Figs. 4.4a and 4.4b. In this case, extinction ratio values of 12 dB and 10 dB are obtained at input signal levels of $E_{in}/E_{sat} \approx$ -20 dB and $E_{in}/E_{sat} \approx$ -10 dB, respectively.

At high input pulse energy ($E_{in} \approx E_{sat}$), Fig. 4.4c, although the modulated output pulses are pattern independent, the modulation performance obtained at 2.5 Gbit/s, for large input signal levels, is unsatisfactory, due to the generation, Fig. 4.4c, of false output pulses (at every 0 bit) which have a peak power $\approx$ 1/5 of that of the legitimate output pulses. Note that the modulation performance in this case is almost the same as that obtained at 1 Gb/s (Fig. 4.2c).

In general, increasing the pulsed electrical drive amplitude to the amplifier results in both faster gain recovery and decay times, and consequently improves the modulation performance of the amplifier. Faster gain recovery time means that successive legitimate pulses are almost uniform (pattern dependence is less) and shorter gain decay time ensures a higher on/off ratio. Note that the upper limit on the amplitude of the driving current pulses are set by two factors:

1) Reliability considerations due to increased thermal effects.

2) The carrier concentration within the active region must be maintained below threshold (N_{th}) to prevent significant emission from the amplifier itself. It has been shown, however, that for the purpose of short pulse amplification, surpassing the carrier threshold by a few percent is sustainable since the optical output is much weaker on a much longer time scale and potentially spectrally much wider than the amplified signal pulse. Thus synchronously "super-pumping" the cavity could be a method of gain improvement in optical amplifiers. Not only is the on/off ratio improved by high gain levels but also if the carrier level is forced below the transparency threshold N_0, then the amplifier actually introduces loss into the optical path.

As a specific example which illustrates the significance of increasing the drive current, Fig. 4.5 shows the modulated output pulses at 2.5 Gb/s, under the same operating conditions of Fig. 4.4a, however, with a 200 mA drive current pulses (twice of that used in Fig. 4.4a). As can be seen from the figure, the modulated output pulses are almost pattern independent (faster gain recovery time) and there is about 5 dB improvement in the

extinction ratio (-17 dB vs -12 dB obtained at 100 mA drive current) due to a shorter gain decay time.

4.4.2.3 Modulation performance at 4 Gb/s per channel

Fig. 4.6 shows the optimum extinction ratio at 4 Gb/s versus E_{in}/E_{sat}. These results are obtained assuming a peak drive current of 200 mA. Although the modulated output pulses are slightly pattern-dependent, however, as can be seen from the figure, satisfactory modulation performance at 4 Gb/s, over a practically useful range of input signal levels, is possible provided that $E_{in}/E_{sat} \leq$ -10 dB. Note that, at such high repetition rate, where pulse repetition period (250 ps) is shorter than the gain recovery time, the gain if compressed, will not recover completely between pulses, causing a slight degradation of modulation performance. Note also that the gain compression also decreases as the pulse repetition rate increases.

4.4.2.4 Modulation performance at 8 Gb/s per channel

At such a high modulation speed, where pulse repetition period (125 ps) is much shorter than the gain recovery time, we need to further shorten both the gain recovery and decay times. This is achieved as follows: a) By increasing the drive current pulses amplitude, however, subject to the constraint that the carrier level must be maintained below the lasing threshold to prevent significant emission from the amplifier itself.

b) By using Zn-doped active layers with different doping concentrations.

Fig. 4.7 shows the optimum value of the extinction ratio at 8 Gb/s, for an amplifier with undoped active layer, versus peak drive current pulses at a given input signal level of $E_{in}/E_{sat} \approx$ -20 dB. It can be seen that there is an optimum value of the peak drive current pulses ($\approx$ 450 mA) where the the extinction ratio is maximum ($\approx$ 11 dB). Note that any further increase of the peak drive current pulses results in lower values for the extinction ratio. This is because at such high drive currents the "0" pulses experience higher gain.

Fig. 4.8 shows the optimum extinction ratio at 8 Gb/s versus E_{in}/E_{sat} for both undoped and Zn-doped active layers. These results are obtained assuming an optimum peak drive current pulses of 450 mA. For an amplifier with intrinsic active region, although the modulated output pulses are slightly pattern-dependent, however, as can be seen from the figure, satisfactory modulation performance at 8 Gb/s, over a relatively small range of input signal levels, is possible provided that $E_{in}/E_{sat} \leq$ -20 dB. Note also that the extinction ratio is marginal ($\approx$ 10 dB) at E_{in}/E_{sat} = -20 dB. However, for an amplifier with Zn-doped (P = 3 x 10^{18} cm^{-3}) active region, satisfactory modulation performance at 8 Gb/s over a relatively wider range of input signal levels, is possible provided that $E_{in}/E_{sat} \leq$ -10 dB. Furthermore, there is about 3 dB improvement in the extinction ratio values obtained over that useful range.

Two comments are in order here. First, the dependence of gain compression on output pulse energy is shown to be linear for any pulse separation and is characterized by a repetition-rate dependent effective saturation energy $E_{sat,eff}$ [20-21]. At high repetition rate, such that the

separation between pulses is much smaller than the gain recovery time, as well as under CW injection, gain compression is shown to depend on the average input power rather than on the pulse energy, and to be characterized by a saturation power P_{sat}. The saturation power p_{sat} is related to E_{sat} and to the gain recovery time τ by $P_{sat} = E_{sat}/\tau$ [22-24]. At low repetition rate, such that the separation between pulses is comparable or larger than the gain recovery time, the saturation energy is a function only of device parameters ($E_{sat} = h\nu A/\Gamma a$), and $E_{sat,eff}$ becomes equal to E_{sat}.

Second, By using specific pulse shapes and intensities rather than assigning a constant value of average input power or pulse energy, we are effectively free to normalize the input signal levels in terms of any parameter. Consequently, we have chosen to normalize the input signal levels with respect to the saturation energy E_{sat}, which is physically a constant parameter for a given amplifier, merely for convenience and simplicity.

4.4.3. Simulation results of the second set (τ_p = 20 ps)

In this section, all numerical calculations of the first set are repeated, however, assuming periodic gaussian pulse trains with a 20 ps FWHM pulse width. All simulation results obtained with τ_p = 20 ps, are almost similar to those obtained with τ_p = 40 ps, and are not repeated again. Therefore, at the given pulse width used in this section ($\approx$ 40 ps at the base line), the multiplexed bit rate can be as high as 25 Gbit/s (twice the multiplexed bit rate of the first set), if the pulse spacing is adjusted for the maximum multiplexed bit rate.

The following summarizes the results of this chapter:

1) Satisfactory modulation performance at a bit rate ranging from 1 Gb/s up to 8 Gb/s, over a practically useful range of input signal levels, is possible provided that $E_{in}/E_{sat} \leq$ -10 dB.

2) At high modulation speeds (> 2.5 Gb/s), such that the separation between pulses is comparable and/or shorter than the gain recovery time, satisfactory modulation performance can be achieved by: a) Increasing the drive current pulses amplitude, however, subject to the constraint that the carrier level must be maintained below the lasing threshold to prevent significant emission from the amplifier itself; and, b) Using Zn-doped active layers with different doping concentrations.

3) As will be shown later, an on/off ratio of 20:1 or better will in all circumstances gives a power penalty of 1 dB or less.

4.5 REFERENCES

[1] R. C. Alferness, "optical amplifiers for photonic circuits," Technical Digest on Optical Amplifiers and their Applications Topical Meeting, SANTA FE, New Mexico, Vol. 17, Paper FA1-1 (1992).

[2] M. J. O'Mahony. "Semiconductor laser amplifier for use in future systems," IEEE J. Lightwave Technol., Vol. 5, No. 4, pp. 531-543, Apr. (1988).

[3] A. Elrefaie, H. Izadpanah, and A. Alhamdan, "8 Gb/s current modulation of semiconductor optical amplifiers," ECOC' (1990).

[4] C. B. Su, and V. Lanzisera, App. Phys. Lett. 45, PP. 1302 (1984).

[5] K. Kamite, H. Sudo, and H. Ishikawa, "14 GHZ single-mode picosecond optical pulse train generation in Zn-doped distributed-feedback lasers," App. Phys. Lett., 45 (3), PP. 208-209, (1989).

[6] R. Olshansky, C. Su, and W. Powazink, " Measurement of radiative and nonradiative recombination rates in InGaAsP and AlGa As light sources," IEEE J. Qu. Elec., Vol. 20, PP. 838-854 (1984).

[7] A. R. Beattie and P. T. Landsberg, "Auger effects in semiconductors," Proc. Roy. Soc. London, Vol. 249, PP. 16-29, 1956.

[8] N. K. Dutta and R. J. Nelson, "The case of Auger combination InGaAsP," J. Appl. Phys., Vol 53, PP. 74-92, Jan. 1982.

[9] A. Sugimura, "Band-to-band Auger recombination in InGaAsP lasers," Appl. phys. lett., Vol. 39, PP. 21-23, July 1981.

[10] A. Haug, "Auger recombination in InGaAsP," Appl. phys. lett., Vol. 42, PP. 512-514, Mar. 1983.

[11] C. B. Su, J. Schlafer, J. Manning, and R. Olshansky, "Measurement of radiative and Auger recombination rates in p-type InGaAsP diode lasers," Elect. Lett., Vol. 18, PP. 595-596, July 1982.

[12] T. Uji, K. Iwamoto, and R. Lang, "Non-radiative recombination in InGaAsP/InP light sources causing light emitting diode output saturation and strong laser-threshold-current temperature sensitivity," Appl. phys. lett. Vol. 38, PP. 193-195, Feb. 1981.

[13] G. H. B. Thompson, "Analysis of radiative and nonradiative recombination law in lightly doped InGaAsP lasers," Elect. Lett., Vol. 19, PP. 154-155, Mar. 1983.

[14] T. Uji, K. Iwamato, and R. Lang, "Dominance of Auger recombination in InGaAsP light emitting diode current-power characteristics," IEEE Trans. Electron Dev., Vol. ED-30, PP. 316-320, Apr. 1983.

[15] A. Saleh, "Nonlinear models of traveling-wave optical amplifiers," Electron. Lett., Vol. 24, No 14, pp., 835-837, July (1988).

[16] A. Saleh, "Modeling of nonlinearity in semiconductor optical amplifiers," IEEE Globecom, (1989).

[17] G. P. Agrawal and N. A. Olsson, "Self-phase modulation and spectral broadening of optical pulses in semiconductor laser amplifiers," IEEE J. QE., vol. 25, pp. 2279-2306, (1989).

[18] M. J. O'Mahony. "Semiconductor laser amplifier for use in future systems," IEEE J. Lightwave Technol., Vol. 5, No. 4, pp. 531-543, Apr. (1988).

[19] M. J. Adams, J. V. Collins, and I. D. Henning, " Analysis of semiconductor laser optical amplifiers," Proc. IEE, Optoelectron., Vol. 132, pp. 58-63 (1985).

[20] M. Ali, A. Elrefaie, and S. Ahmed, "Simulation of 12.5 Gb/s optical time-division multiplexer using semiconductor optical amplifiers as external modulators," IEEE PTL., Vol. 11, PP. 1018-1020, Mar. (1992).

[21] M. Ali, and S. Ahmed, "Simulation of semiconductor optical amplifiers for external modulation and demultiplexing in multi-Gb/s optical time-division multiplexed systems," International Conf. on lasers, 91, Proceedings, Session WD.7

[22] Per Bang Hansen, and R. Tucker, " Repetition-rate dependence of gain compression in InGaAsP optical amplifiers using picosecond optical pulses," IEEE J. Qu. Elec., Vol. 25, PP. 2611-2619 (1984).

[23] Tadashi Saitoh, and T. Mukai,"Gain saturation characteristics of traveling-wave semiconductor laser amplifiers in short optical pulse amplification," IEEE J. QE., vol. 26, pp. 2086-2094, (1990).

[24] A. E. Siegman, Lasers. Mill Valley, CA: University Science Books, 1986, Ch. 10.

Parameter	Symbol	Value
Volume of Active Region	V	
Cavity Length	L	300 μm
Width of Active Region	w	1.5 μm
Thickness of Active Layer	d	0.1 μm
Confinement Factor	Γ	0.2
Nonradiative Recombination Rate	A	1.1×10^{8} s^{-1}
Radiative Recombination Coefficient	B	1×10^{-10} cm^3/s
Auger Recombination Coefficient	C	4×10^{-29} cm^6/s
Gain Coefficient	a	2.5×10^{-16} cm^{-2}
Carrier Density at Transparency	N_O	1×10^{18} cm^{-3}
Small signal chip gain for 100 mA dc bias current		33 dB

Table I
Model parameters.

Zn-doped

$B_o = 1.3 \times 10^{-10}$ cm^3/s $B_1 = 2.3 \times 10^{-29}$ cm^6/s

$C_2 = 10^{-28}$ cm^6/s

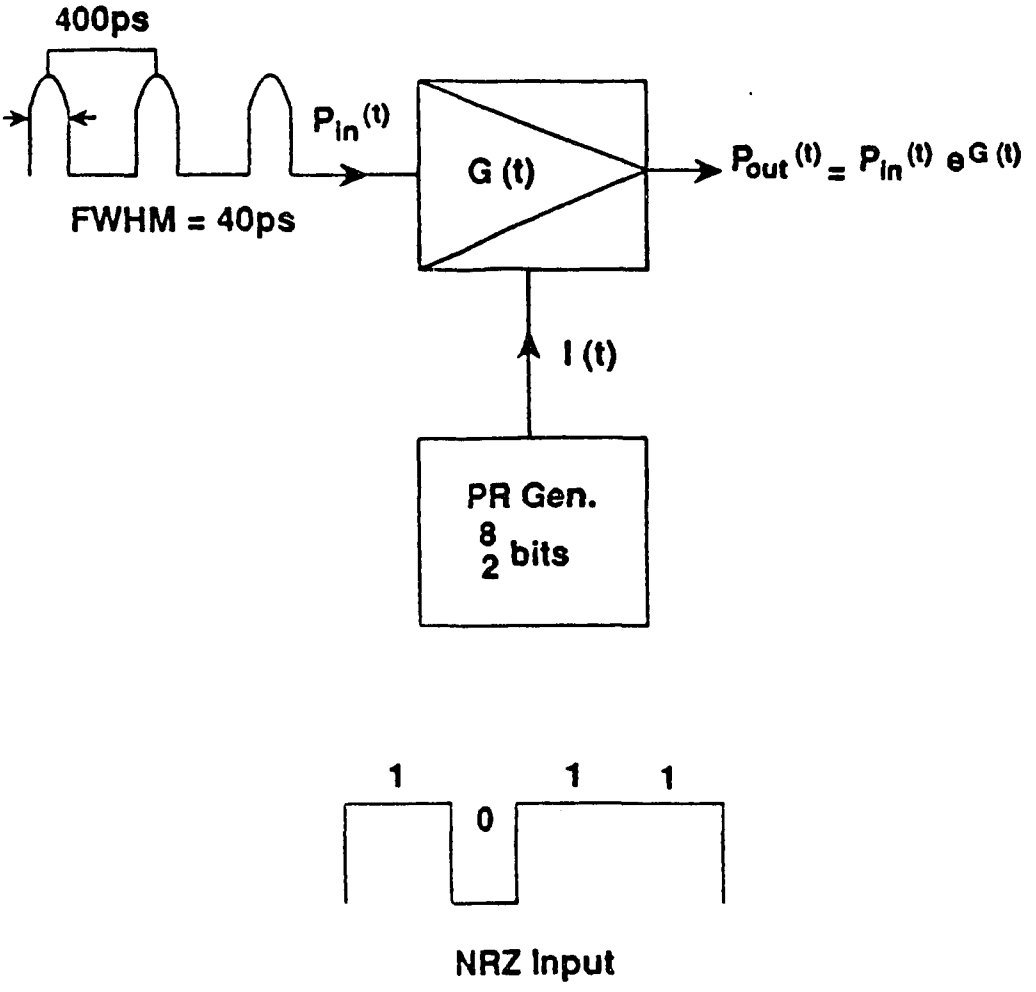

Fig. 4.1: Simulation block diagram of a TWSOA external modulator at the transmitter end of the OTDM system.

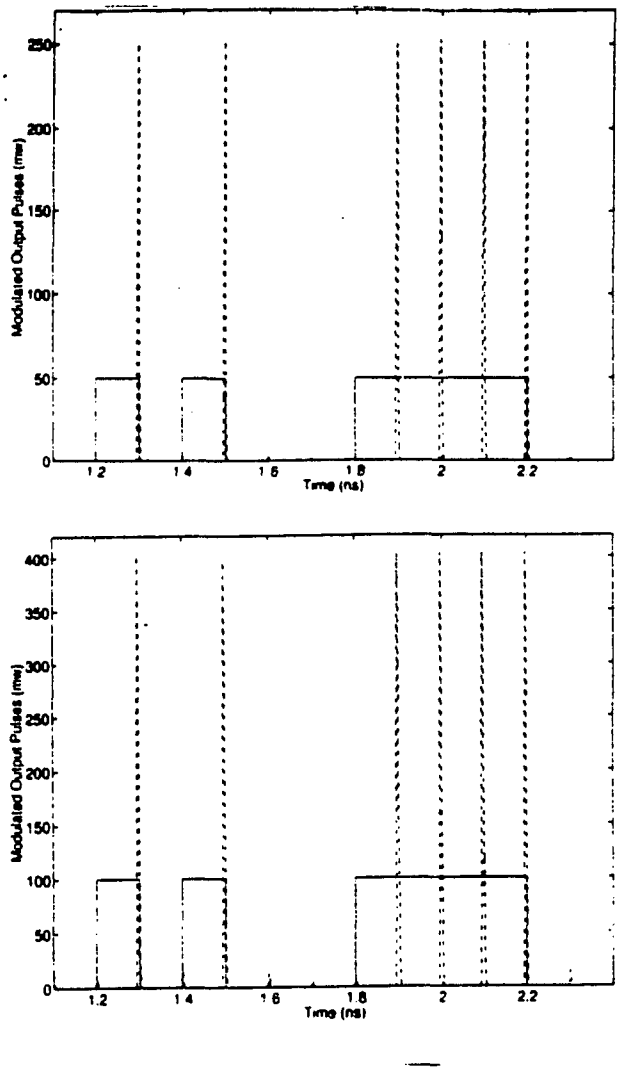

Fig. 4.2 (a) Modulated output pulses ---- at 1 Gbit/s per channel and a 100 mA injection current pulses _____ for E_{in}/E_{sat} = - 20 dB. Input pulse peak power = 0.75 mw. **(b)** Modulated output pulses ---- at 1 Gbit/s per channel and injection current pulses _____ for E_{in}/E_{sat} = - 10 dB. Input pulse peak power = 7.5 mw.

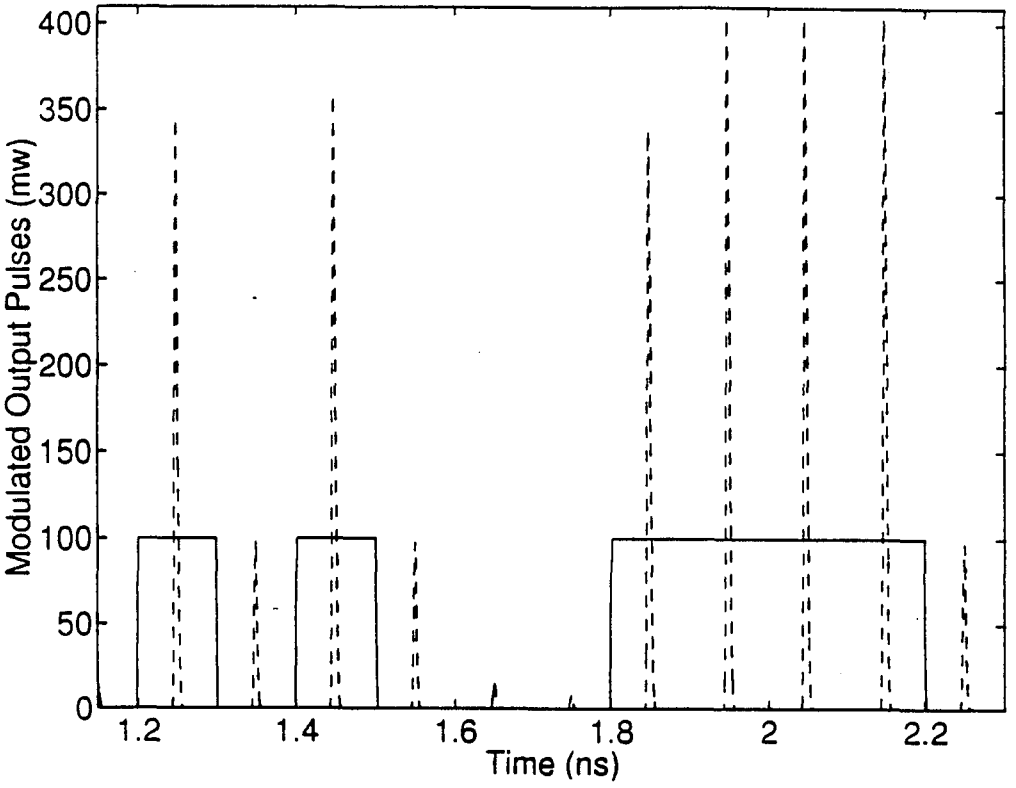

Fig 4.3: Same as Fig. 4.2b. however. with 500 ps time delay between the peak of the input optical pulses and the leading edge of the drive current pulses. i.e.. optical pulses are approximately in middle of current pulses.

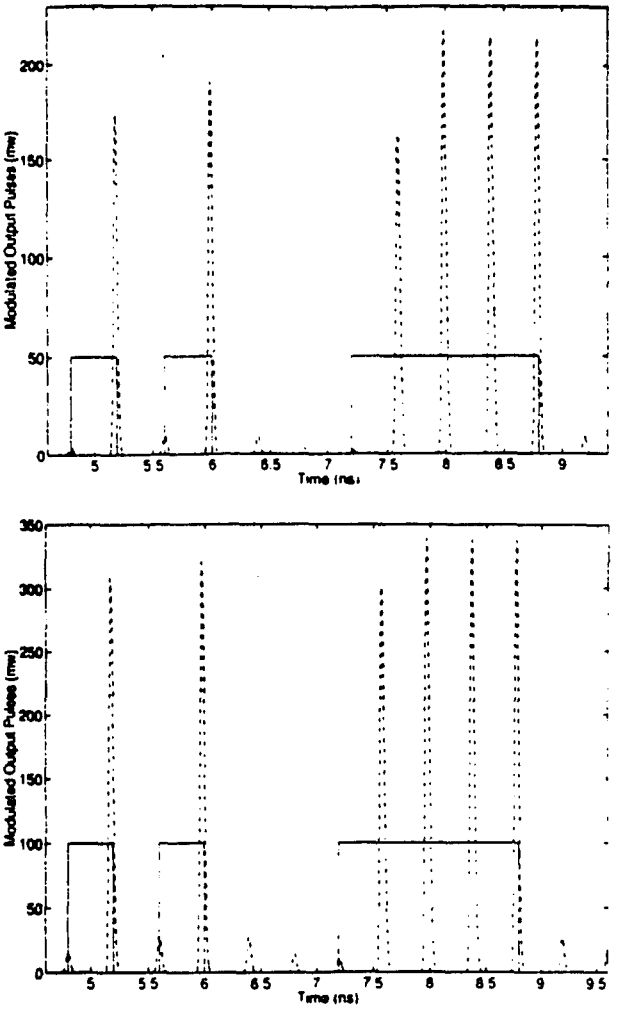

Fig. 4.4 (a) Modulated output pulses ---- at 2.5 Gbit/s per channel and a 100 mA injection current pulses _____ for E_{in}/E_{sat} = - 20 dB. Input pulse peak power = 0.75 mw. (b) Modulated output pulses ---- at 2.5 Gbit/s per channel and injection current pulses _____ for E_{in}/E_{sat} = - 10 dB. Input pulse peak power = 7.5 mw.

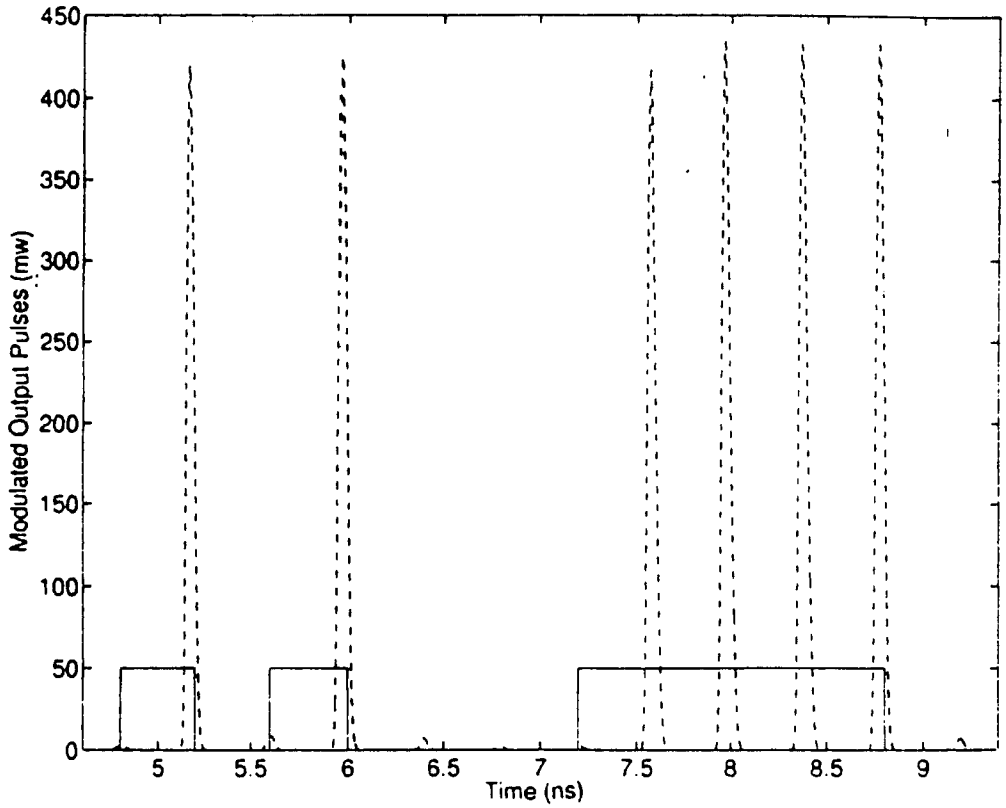

Fig. 4.5: Same as Fig. 4.4 (a) except with a 200 mA injection current pulses.

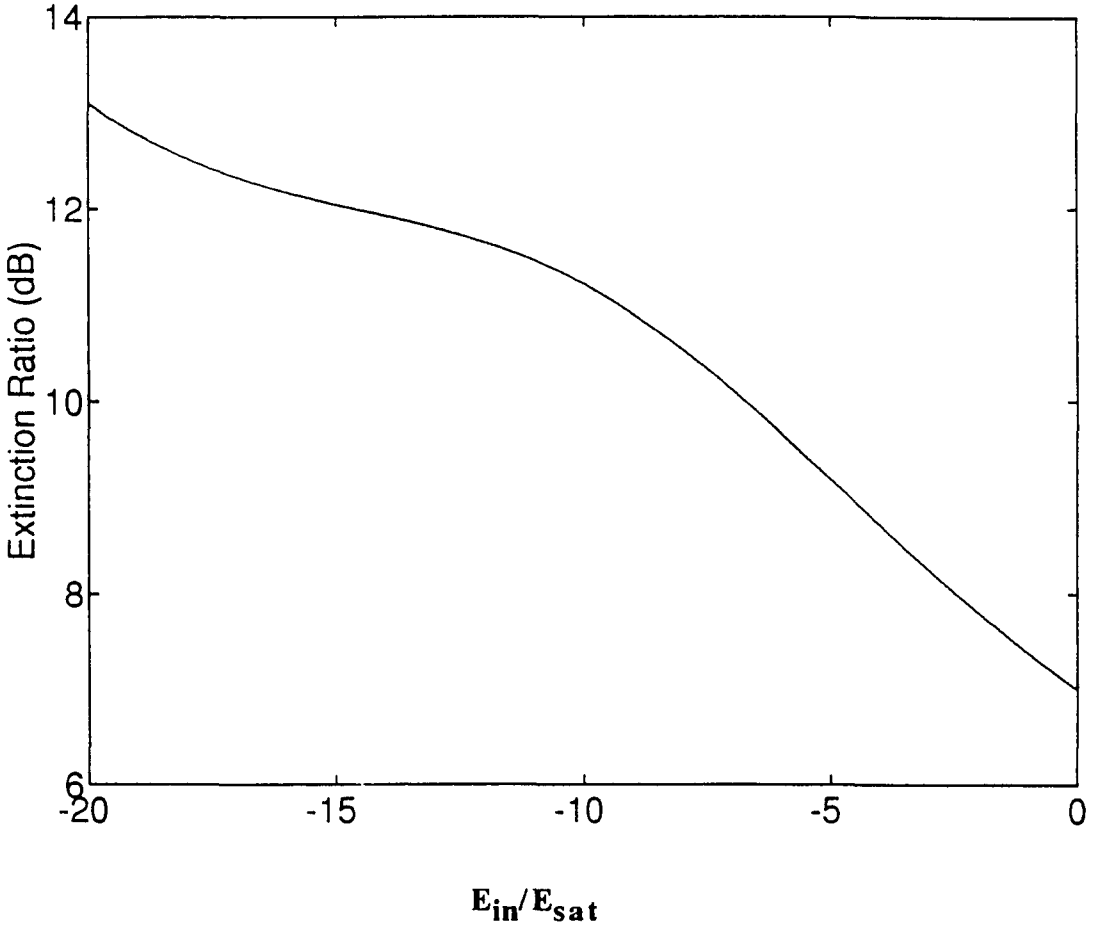

Fig. 4.6: Optimum values of the Extinction ratio at 4 Gb/s versus E_{in}/ E_{sat}. Peak drive current pulses = 200 mA.

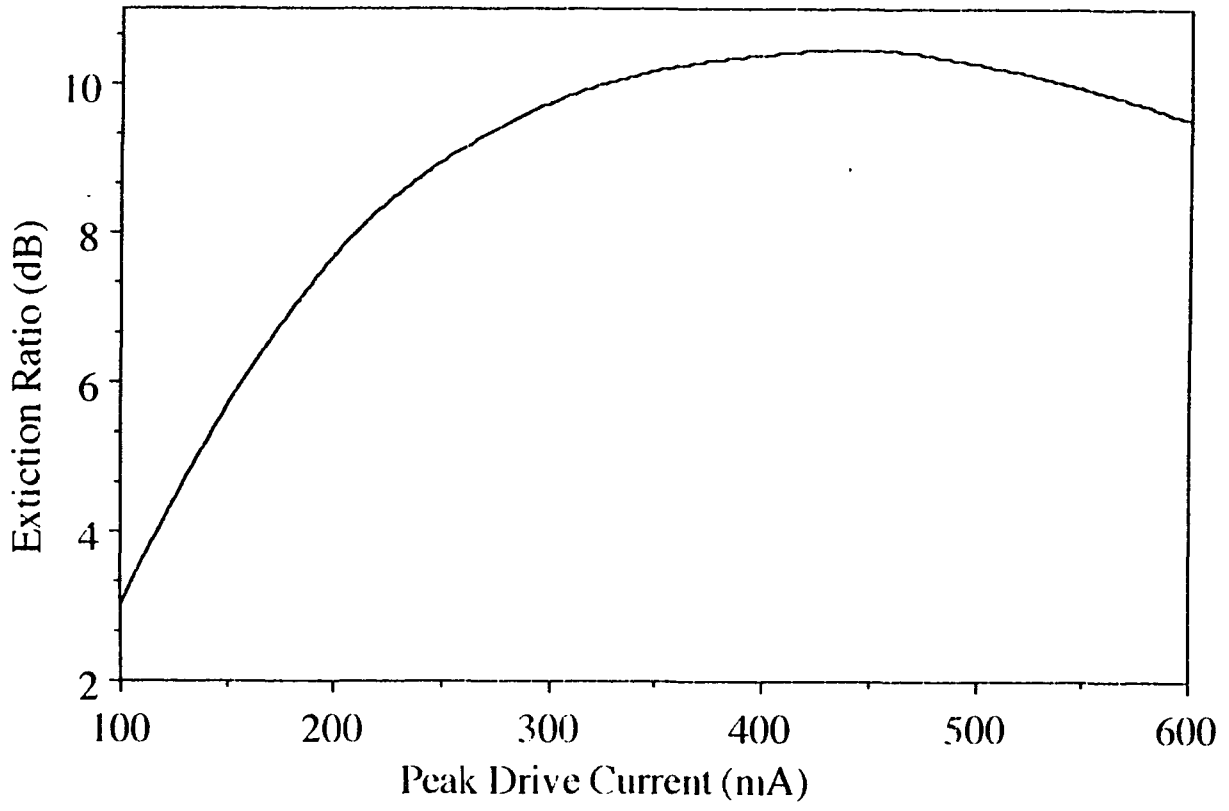

Fig. 4.7: Optimum values of the Extinction ratio at 8 Gb/s for an amplifier with intrinsic active region versus peak drive current pulses at an input signal levels of E_{in}/ E_{sat} = -20 dBm.

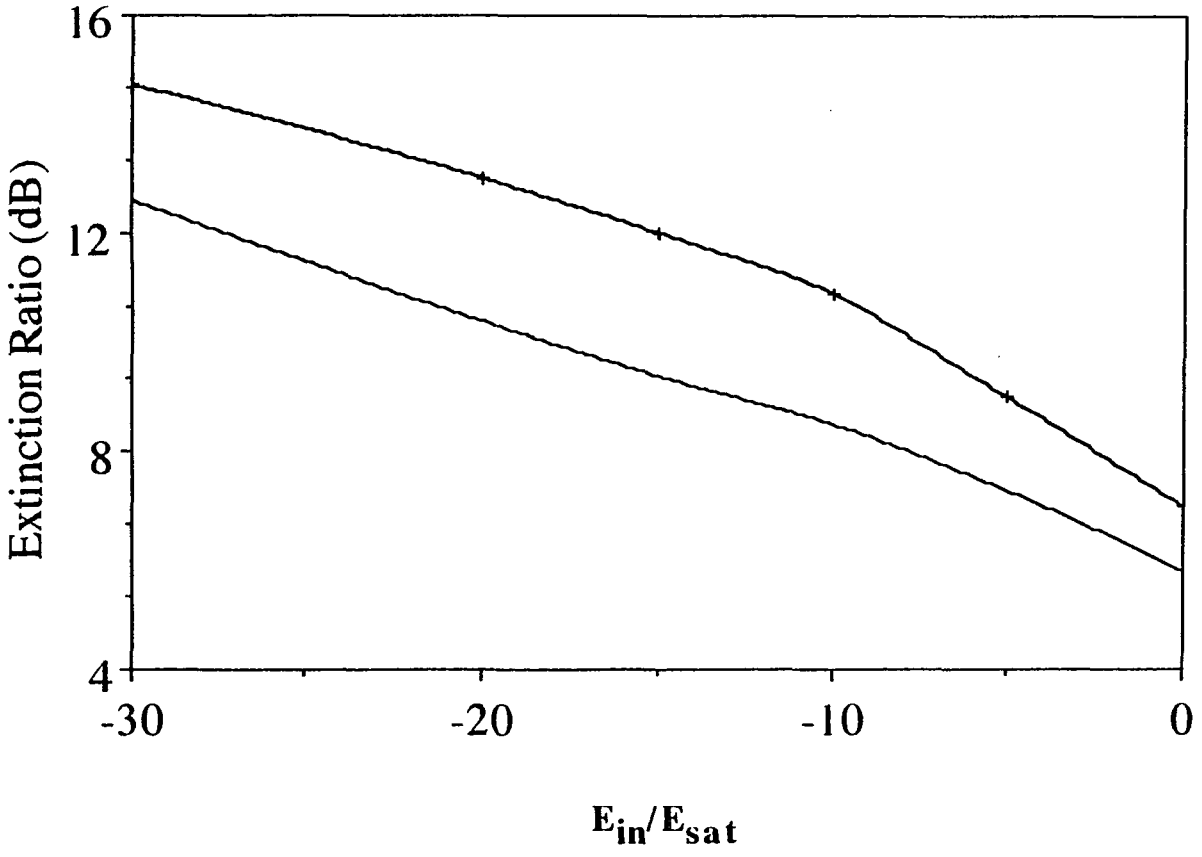

Fig. 4.8: Optimum values of the Extinction ratio at 8 Gb/s versus E_{in}/E_{sat}. Peak drive current pulses = 450 mA.

_____ Amplifier with intrinsic active region.

- - - - Amplifier with Zn-doped active region.

CHAPTER 5

Modeling and Simulation of SOAs when used as Optical Demultiplexers at the Receiver End of the OTDM System

5.1. Background

Optical time division multiplexing (OTDM) has been demonstrated as an efficient way of increasing transmission capacity of fiber links [1]. Several schemes have been demonstrated or suggested for performing the optical demultiplexing, including, Ti:$LiNbO_3$ switches, and modulators [1-2], sagnac fiber loops [3], and four-wave mixing in fibers [4]. TWSOAs have, however, attracted little attention for use as optical demultiplexers because the speed of present devices is determined by the carrier life time and is, thus, limited to a few Gb/s. In spite of speed limitations, however, providing simultaneous gain and gating may allow for lossless devices and future monolithic integration of demultiplexers with a detector or with an opto-electronic integrated front-end. Optical gating with TWSOAs is also of particular interest for bus or broadcast network architectures where one channel on a bus is sampled and access to all channels is required. In this chapter, the potential of TWSOAs will be further extended by using them at the receiver end of the proposed OTDM system for optical demultiplexing. Again simultaneous gain and gating may allow for lossless devices and future monolithic integration of the demultiplexer with a detector or with an opto-electronic integrated front-end.

The nB-Gbit/s multiplexed signal is demultiplexed at the receiver end using TWSOAs demultiplexer switching network. To fully demultiplex n-channels, a fiber directional coupler would be needed to feed the

multiplexed signal to n-TWSOA switches. Each (single) TWSOA switch, used in the simulation, is assumed to have a selection ratio of 2 : 1 and/or 4 : 1 and is, therefore, driven with a sinusoid at a frequency equal to one-half and/or one-quarter of that of the bit rate of the input optical signal to be demultiplexed. For systems with more than two baseband channels (assuming that the amplifier will have a selection ratio of 2 : 1), or with more than four channels (assuming that the amplifier will have a selection ratio of 4 : 1), larger demultiplexer switching network can be constructed by interconnecting 1 x 2 and/or 1 x 4 building blocks of TWSOAs.

The demultiplexer network assumed in our simulation is a binary tree network [5-7] which uses a specific number of TWSOAs switches. This number varies in accordance with the number of multiplexed baseband channels, bit rate of each, and the selection ratio assigned to each single TWSOA switch of the binary tree network. Its first stage is a high speed switch which demultiplexes the data stream to two and/or four data streams, each at half and/or one-fourth the multiplexed bit rate. Subsequent switches in the binary tree structure also can be driven by sinusoids, but operate at subharmonics of the drive frequency of the first stage switch.

To investigate demultiplexing performance, we will use the dynamic model developed in chapter 4 to investigate the performance of both undoped and Zn-doped active layers TWSOAs driven by sinusoidal current signals, serving as optical gates for demultiplexing multi Gb/s OTDM input signals with demultiplexing ratios of 2 : 1 and/or 4 : 1. We will also investigates the potential for increasing the switching speed of these devices by cascading two amplifiers and/or using amplifiers with Zn-doped active region to perform the optical demultiplexing.

We show that maximum demultiplexing speed can be increased from the 6 Gb/s maximum speed achievable using undoped single TWSOA gate [8], to 10-12 Gb/s by using an optical gate consisting of two cascaded undoped TWSOAs and/or a single Zn-doped TWSOA gate [9-10]. The effect of the ASE noise on the receiver sensitivity will be considered in chapter 6, when evaluating the end-to-end performance of the whole OTDM system.

We will also show that consideration of the detailed non-linear carrier recombination rate, $R(N) = AN + BN^2 + CN^3$, is essential to reliably model the use of electrically modulated TWSOAs as high speed optical gates [10], rather than the frequently used linear recombination rate, $R(N) = N/\tau_s$ [11-15]. Finally, by comparing the simulation results of our model with the linear recombination model [11-15], we propose a wide range of values for the spontaneous carrier life time, τ_s, which give the same results for both models.

5.2. Simulation Results

5.2.1. General

The simulation results of this section will be divided into three different sets. In the first set, in order to validate the model, the simulation results of the demultiplexing performance at 6 Gb/s , of a single TWSOA gate, are compared with results of experiments to date [8]. In the second set, simulation results of the demultiplexing performance, at higher speed, for an optical gate consisting of two cascaded TWSOAs are presented. Finally, in the third set, the simulation results of our model are compared with those of the linear recombination model [11-15]. Based on this comparison, we propose values for the spontaneous carrier life time, τ_s, which gives the

same results for both models. All simulation results presented in this section are for conventional undoped active region TWSOA.

5.2.2. Demultiplexing performance of undoped single TWSOA gate with a selection ratio of 2 : 1

Each (single) TWSOA gate, used in the simulation, is assumed to have a selection ratio of 2 : 1 and therefore is driven with a sinusoid at a frequency equal to one-half of that of the bit rate of the input optical signal to be demultiplexed (on and off states are 180^{o} out of phase). To fully demultiplex two channels, a fiber directional coupler would be needed to feed the multiplexed signal to two TWSOA gates. The driving current I(t), used in the simulation, is a 3 GHz 200 mA amplitude sinusoidal signal superimposed on a 40 mA dc current. All simulation results presented in this chapter, unless otherwise specified, assume TWSOAs gates with undoped active region.

To avoid driving the amplifier with a negative current, a zero value is always assigned to I(t) during the period for which its value would otherwise be negative (by chopping off that portion of the negative cycle of the sine wave which makes the value of I(t) negative). Thus, the amplifier driving current I(t) varies from zero mA to 240 mA (40 mA dc bias + 200 mA peak RF). For these conditions, the peak small-signal chip gains were calculated, as shown in Fig. 5.1, to be 37 and 35 dB at 3-GHz and 5-GHz driving signals frequencies, respectively.

To investigate the demultiplexing performance at 6 Gb/s, numerical calculations are carried out for a wide range of input pulse energy (E_{in})

normalized with respect to the saturation energy (E_{sat}). The input optical signal to be demultiplexed is assumed to be a pseudo-random bit sequence of 6 Gb/s gaussian pulse trains with 40 ps at FWHM (a long input sequence of ones is used in the simulation to account for worst crosstalk conditions). The point of zero time delay is defined as the point at which the peak of the on-state optical pulse (channel to be selected), coincides with the positive peak of the RF sinusoidal current signal.

The simulation results showing output optical pulses for a long input sequence of ones are shown in Fig. 5.2a. These results are obtained for a signal level of $E_{in}/E_{sat} \approx$ -20 dB, corresponding to a pulse peak power of 0.75 mw, and for an optimum time delay, as shown in Fig. 5.2b, between the RF driving signal and the input optical pulses. As can be seen from Fig. 5.2b, the peak of the selected on-state second channel pulses is delayed from the positive peak of the sinusoidal current signal by a time equivalent to one-fourth ($\approx$ 83 ps) of its period. It can also be seen from Fig. 5.2a that the peak gain (i.e., the ratio of peak output power to peak input power) of these on-state selected pulses is $\approx$ 24 dB. Ideally, the off-state first channel pulses should be totally extinguished. However, as shown in Fig. 5.2a, those pulses experience peak gains $\approx$ 14 dB. This is because the on and off states optical pulses are separated by times (166 ps) short compared to the gain decay time, consequently, the gain has not had enough time to totally drop to an exact zero value during the passage of the off state pulses.

The extinction ratio (maximum on-off ratio) is defined as the ratio of the peak output power of the on-state pulse to that of the off-state pulse. This ratio $\approx$ 9.5 dB at 6 Gb/s. This value is in good agreement with the value

obtained experimentally [8] under similar input signal levels and driving conditions, and is sufficient for demultiplexing a 6 Gb/s signal without significant penalty in receiver sensitivity [8,16].

A specific example, shown in Fig. 5.3a, of the worst demultiplexing performance is that which results for a zero time delay between the on-state pulses and RF driving signal. As can be seen from the figure, in this situation, the off-state output pulses $\approx$the on-state output pulses (maximum on-off ratio $\approx$ 2.1 dB), and therefore, no effective demultiplexing is performed. This case occurs, as shown in Fig. 5.3b, when the peak of the on-state pulses coincides with the positive peak of the sinusoidal current signal (zero time delay).

Fig. 5.4 shows the extinction ratio, at 6 Gb/s, for a signal level of $E_{in}/E_{sat} \approx$ -20 dB, as a function of the time delay between the optical pulse and the RF driving signal. As can be seen from the figure, the extinction ratio reaches its maximum value at a time delay of $\approx$ 83 ps between the optical and the RF driving signals, it then deteriorates rapidly for a time delay longer than 1/4 of the RF driving signal period. It is important to emphasize that the optimum time delay value, calculated from the simulation results, is independent of changing driving conditions, i. e., bias current, amplitude and frequency of the sinusoidal signals used in the simulation, and are also independent of the input optical signal levels. This happens because these delay values are arrived at by optimizing ratios of peak on-state pulse outputs to the off-state ones.

It is further noted that the demultiplexing performance deteriorates with increasing input signal levels. This is shown in Fig. 5.5 where the optimum value of the extinction ratio, at 6 Gb/s, is drawn as a function of input pulse energies normalized with respect to the saturation energy. Thus, at a signal level of $E_{in}/E_{sat} \approx$ -10 dB, the optimum value of the extinction ratio reduces to $\approx$ 8 dB, while at the highest signal level used in the simulation, $E_{in} \approx E_{sat}$, this value reduces to $\approx$ 6 dB. Two comments are in order here. First, the simulation results, which are in good agreement with experimental results [8], show that satisfactory demultiplexing performance at 6 Gb/s is only possible when the input signal level is kept well below the saturation energy. Second, the simulation results clearly set an upper limit on the maximum input signal level (given by $E_{in}/E_{sat} \leq$ -20 dB), above which it is no longer possible to obtain an adequate demultiplexing performance.

To investigate the maximum speed at which a single TWSOA gate can be used for demultiplexing, the optimum value of the extinction ratio is calculated as a function of the driving signal frequency. The simulation results showing these values, are shown in Fig. 5.6, for a signal level of $E_{in}/E_{sat} \approx$ -20 dB. As can be seen, the extinction ratio deteriorates rapidly at frequencies above 2 GHz and is reduced from 20 dB at 1 GHz to only 6.8 dB at 5 GHz. However, at 3 GHz, we are still able to obtain an on-off ratio of 9.5 dB. Thus, the simulation results indicate that 6 Gb/s (3 GHz driving signal frequency) is the maximum speed at which a single TWSOA gate can be used for demultiplexing. Again, these results are in

good agreement with the experimental results reported in [8], which further validates the model used here.

It should be emphasized that the value of the amplifier driving current I(t), 240 mA (40 mA dc bias + 200 mA peak RF), used in the simulation, was chosen after initial simulation results indicated that this was the appropriate value needed to get adequate extinction ratios at 6 Gb/s. For instance, when the driving sinusoidal current I(t), used in the simulation at 6 Gb/s, was reduced to 150 mA amplitude superimposed on a 30 mA dc current, we were not able to obtain an on-off ratio of more than 8 dB, which might not be considered sufficient for effectively demultiplexing a 6 Gb/s signal without significant penalty in receiver sensitivity [8,17].

Finally, to take the ASE into account in our nonlinear model, an equivalent average spontaneous emission input power term [18-19] is added to the original input power $p_{in}(t)$ in equation (3). The simulations results showed almost no difference between the extinction ratio values obtained previously and those obtained taking the ASE into account particularly at large input signal levels. However, the effect of the ASE noise on the receiver sensitivity will be considered in chapter 6, when evaluating the end-to-end performance of the whole OTDM system.

5.2.3. Demultiplexing performance of an optical gate consisting of two cascaded TWSOAs

5.2.3.1 Demultiplexing performance with a 2 : 1 selection ratio

In this section, we will investigate the potential of increasing the switching speed of these devices by cascading two amplifiers to perform

optical demultiplexing. Each amplifier is assumed to have a selection ratio of 2 : 1. Numerical calculations are carried out for a wide range of input pulse energies normalized with respect to the saturation energy, as follows:

1) the input optical signal to the first amplifier is assumed to be a pseudo-random bit sequence of 10 Gb/s gaussian pulse trains with 40 ps at FWHM (a long input sequence of ones is used in the simulation to account for worst crosstalk conditions).

2) the demultiplexed output pulses from the first amplifier are taken as inputs to the second amplifier. The input signal levels (E_{in}/E_{sat}) are assumed to be the same for both amplifiers. This is done by scaling down the demultiplexed output pulses of the first amplifier to the required level before using them as inputs to the second amplifier. It is also assumed that the input pulse energy to the second amplifier is that of the on state selected pulse.

3) both amplifiers are assumed to have the same driving conditions, a 5 GHz 200 mA amplitude sinusoidal signal superimposed on a 40 mA dc current (a selection ratios of 2:1), and an optimum time delay between the optical and the RF driving signals (same as in the previous section).

Fig. 5.7 shows the optimum value of the extinction ratio, at 10 Gb/s, as a function of input pulse energies normalized with respect to the saturation energy. As can be seen from the figure, satisfactory demultiplexing performance at 10 Gb/s is now possible over a wide range of input signal levels (-20 dB $\leq E_{in}/E_{sat} \leq$ 0 dB). Thus, at a signal level of $E_{in}/E_{sat} \approx$ -20 dB, the optimum value of the extinction ratio $\approx$ 13.7 dB {compare this value to the value obtained from Fig. 5.6 (6.8 dB) using a single TWSOA

gate}, while at the highest signal level used in the simulation, $E_{in} \approx E_{sat}$, we are still able to obtain an adequate on-off ratio of $\approx$ 9.6 dB.

In order to further explore the possibility of obtaining satisfactory demultiplexing performance at higher speeds, under same previous operating conditions, numerical calculations are carried out at 12 and 16 Gb/s. However, the FWHM of the input optical pulses is reduced from 40 to 20 ps. At an input signal level of $E_{in}/E_{sat} \approx$ -20 dB, we are able to obtain optimum on-off ratios of 11.4 and 8.9 dB at 12 and 16 Gb/s, respectively. Thus, by using two cascaded TWSOAs as an optical gate, satisfactory demultiplexing performance at 12 Gb/s is feasible.

Summarizing the results of this section, it is clear that using two cascaded TWSOAs as an optical gate have potentially two basic advantages: 1) satisfactory demultiplexing performance at higher speeds up to 12 Gb/s (and possibly up to 16 Gb/s) can be achieved. 2) Those satisfactory high speeds demultiplexing performances are also achievable over a wide range of input signal levels (-20 dB $\leq E_{in}/E_{sat} \leq$ 0 dB). This is in contrast to the results obtained using a single TWSOA as an optical gate, where satisfactory demultiplexing performance (only up to 6 Gb/s) is only possible when the input signal level is kept well below the saturation energy.

5.2.3.2 Demultiplexing performance with a 4 : 1 selection ratio

In this section, we investigate the performance of an optical gate when it is used to select one channel out of four (4 : 1 selection ratio). The optical gate consists of two cascaded TWSOAs, each is assumed to have

a selection ratio of 4 : 1, and is therefore driven with a sinusoid at a frequency equal to one-quarter of that of the bit rate of the input optical signal to be demultiplexed. This will permit the demultiplexing of a high speed signal into four baseband channels using a single stage switching network.

As a specific example, numerical calculations are carried out to decompose a 10 Gb/s RZ signal to one of its four-2.5 Gb/s baseband components using a two cascaded amplifier gate. The driving current used in the simulation is a 2.5 GHz 200 mA amplitude sinusoidal signal superimposed on a 40 mA dc current. The simulation results giving the output optical pulses from the first and second amplifier of the twin gate are shown in Figs. 5.8a and 5.8b, respectively. These results are obtained for a signal level of $E_{in}/E_{sat} \approx$ -20 dB and for an optimum time delay between the RF driving signal and the input optical pulses. The simulation results also indicate that the optimum time delay occurs when the peak of the selected on-state fourth channel pulses of the first amplifier lags the positive peak of the RF signal by slightly less than one-sixth (62 ps) of its period. The optimum delay for the second amplifier is found to be slightly less than that of the first (57 ps).

It should be emphasized that it is not a coincidence that the optimum time delay obtained for an amplifier with a 2 : 1 selection ratio is different than that for an amplifier with a 4 : 1 selection ratio. This is because for the 2 : 1 selection ratio case, there should be one and only one off-state pulse preceded and followed by the on-state pulses where the optimum time delay must be adjusted to achieve the complete or partial extinction

of that particular single off-state pulse. However, for the 4 : 1 selection ratio, there are three consecutive off-state pulses which, ideally, must all three be totally extinguished. Thus, the time delay has to be adjusted accordingly to achieve the best compromise for the extinction of these three off-state pulses.

It can be seen from Figs. 5.8a and 5.8b that the peak gain of these on-state selected pulses is $\approx$ 24 and 25 dB, respectively. Ideally, the pulses of the other three channels, channel 1, 2, and 3 (the channels corresponding to the off-state), should be totally extinguished. However, as shown in Fig. 5.8a, the first and third channel pulses experience peak gain $\approx$ 17.7 dB, while the second channel pulses experience peak gain $\approx$ 13 dB. The extinction ratio (maximum on-off ratio) must therefore be redefined as the ratio of the peak output power of the on-state pulses to that of the maximum peak power of the off-state pulses. Thus, this ratio, for the first amplifier, $\approx$ 6.3 dB. However, as can be seen from Fig. 5.8b, after cascading the second amplifier, the extinction ratio has been increased to $\approx$ 10.7 dB.

5.2.3.3. Comparison between the linear recombination model and non-linear recombination model

In this section, the detailed nonlinear recombination model described above in section II is compared with the linear recombination model [11-15]. Using the detailed nonlinear recombination model, we first calculate the gain experienced by a given input optical signal for a given drive condition. Then, using the linear model, we derive the values of τ_s which

give the same results as those obtained from the nonlinear model for a wide range of input signal levels.

As a specific example, Fig. 5.9 shows the calculated values for t_s, which give the same gain for both models, as a function of input pulse energies normalized with respect to the saturation energy. These results are obtained assuming a 100 mA dc driving current for both models. The input optical signal used in the simulation is assumed to be a 6 Gb/s gaussian pulse train with 40 ps at FWHM. As can be seen from the figure, the value of τ_s increases from 445 ps at small signal gain to 1500 ps at the highest signal level used in the simulation ($E_{in} \approx E_{sat}$). Thus, it is therefore clear that the same results can be obtained by both models for a wide range of values of τ_s. This is true even if input signal levels are constrained to a narrow range.

5.3 Demultiplexing performance of Zn-doped single TWSOA gate with a selection ratio of 2 : 1

At high demultiplexing speeds (> 6 Gb/s), where pulse repetition period is much shorter than the gain recovery time, we need to further shorten both the gain recovery and decay times. This is achieved as follows: a) By increasing the drive current pulses amplitude, however, subject to the constraint that the carrier level must be maintained below the lasing threshold to prevent significant emission from the amplifier itself.
b) By using Zn-doped active layers with different doping concentrations.

Fig. 5.10 shows the optimum value of the extinction ratio, at 10 Gb/s for an a single amplifier gate with Zn-doped active layer ($p = 4 \times 10^{18}$ cm^{-3}), as a function of input pulse energies normalized with respect to the saturation energy. These results are obtained assuming a drive current of 5 GHz 500 mA peak RF signal superimposed on a 20 mA dc current. As can be seen from the figure, satisfactory demultiplexing performance at 10 Gb/s is now possible over a wide range of input signal levels ($E_{in}/E_{sat} \leq$ -10 dB). Thus, at a signal level of $E_{in}/E_{sat} \approx$-20 dB, the optimum value of the extinction ratio $\approx$ 13 dB {compare this value to the value obtained from Fig. 5.6 (6.8 dB) using a single TWSOA gate with undoped active region}.

5.4 Conclusion

The following summarizes the results of this chapter:

1) The maximum achievable satisfactory demultiplexing speeds using conventional undoped active region TWSOA is 6 Gb/s.

2)The maximum demultiplexing speeds can be increased from the 6 Gb/s maximum speed achievable using undoped single TWSOA gate, to 10-12 Gb/s by using an optical gate consisting of two cascaded TWSOAs. Those satisfactory high speeds demultiplexing performances are also shown to be achievable over a wide range of input signal levels (E_{in}/E_{sat} $\leq$ 0 dB), using an optical gate consisting of two cascaded TWSOAs, each with a 2 : 1 and/or 4 : 1 selection ratios.

3) Satisfactory demultiplexing performance at 10 Gb/s can also be achieved using a single Zn-doped active layer TWSOA gate.

5.5 REFERENCES

[1] R. S. Tucker, G. Eisenstien, and S. K. Korotky, "Optical time-division multiplexing for very high bit-rate transmission," IEEE J. Lightwave Technol., Vol. 6, No, 11, pp. 1737-1749, Nov. (1988).

[2] S. K. Korotky and J. J. Veselka, "Efficient switching in a 72-Gb/s Ti:$LiNbO_3$ binary multiplexer/ demultiplexer," Conf. Opt. Fiber Commun., Paper TuH2, San Francisco, CA, 1990.

[3] A. Takada, K. Aida, and M. Jinno, "Demultiplexing of a 40- Gb/s optical signal to 2.5 Gb/s using a nonlinear fiber loop mirror driven by amplified, gain-switched laser diode pulses," Conf. Opt. Fiber Commun., Paper TuN3, San Diego, CA, 1991.

[4] P. A. Andrekson, N. A. Olsson, J. R. Simpson, T. Tanbun-EK, R. A. Logan, and M. Haner, "16 Gb/s all-optical demultiplexing using four-wave mixing," Electron. Lett., vol 27, pp 922-924, 1991.

[5] R. S. Tucker, G. Eisenstien, and S. K. Korotky, "Optical time-division multiplexing for very high bit-rate transmission," IEEE J. Lightwave Technol., Vol. 6, No, 11, pp. 1737-1749, Nov. (1988).

[6] G. Eisenstien, R. S. Tucker, G. Raybon, and S. K. Korotky, "8-Gb/s transmission over 40 km in a two-channel single-laser optical time-division multiplexed system experiment," OFC' 89

[7] G. Eisenstien, R. S. Tucker, and G. Raybon, "Optical time-division multiplexed transmission at 8 Gb/s using single laser and semiconductor optical power amplifier," Electron. Lett., Vol. 25, No 16, pp., 1034-1036, Aug. (1989).

[8] P. Hansen, G. Raybon, J. Wiesenfeld, C. Burrus, R. Logan, T. Tanbun-Ek, and H. Temkin, "Optical demultiplexing at 6 Gb/s using a

semiconductor laser amplifier as an optical gate," IEEE PTL., Vol. 11, PP. 1018-1020, Nov. (1991).

[9] M. Ali, and S. Ahmed, "Simulation of semiconductor optical amplifiers for external modulation and demultiplexing in multi-Gb/s optical time-division multiplexed systems," International Conf. on lasers, 91, Proceedings, Session WD.7

[10] M. Ali, H. Issa, A. Elrefaie, and S. Ahmed, " High speed optical time-division demultiplexer using semiconductor optical amplifiers," IEEE J. Lightwave Technol., Vol. , NOv. (1992).

[11] A. Lomax, and I. White, "Modulation of picosecond pulses using semiconductor laser amplifiers," IEE Proc., Part J, Vol.138, no. 3, PP. 178-184, (1991).

[12] A. Saleh, "Nonlinear models of traveling-wave optical amplifiers," Electron. Lett., Vol. 24, No 14, pp., 835-837, July (1988).

[13] A. Saleh, "Modeling of nonlinearity in semiconductor optical amplifiers," IEEE Globecom, (1989).

[14] G. P. Agrawal and N. A. Olsson, "Self-phase modulation and spectral broadening of optical pulses in semiconductor laser amplifiers," IEEE J. QE., vol. 25, pp. 2279-2306, (1989).

[15] M. J. O'Mahony. "Semiconductor laser amplifier for use in future systems," IEEE J. Lightwave Technol., Vol. 5, No. 4, pp. 531-543, Apr. (1988).

[16] M. J. Adams, J. V. Collins, and I. D. Henning, " Analysis of semiconductor laser optical amplifiers," Proc. IEE, Optoelectron., Vol. 132, pp. 58-63 (1985).

[17] R. G. Smith, and S. D. Personic, "Receiver design for optical fiber communication systems," Topics in App. Phys., H. Kressel, Ed. New York: Spring-Verlag, 1987, Vol. 39, ch. 4.

[18] C. H. Lee and P. J. Delfyett, "limits on amplification of picosecond pulses by using semiconductor laser traveling-wave amplifiers," IEEE J. QE., vol. 25, pp. 2279-2306, (1991).

[19] C. H. Henry, " theory of spontaneous emission noise in open resonators and its application to lasers and optical amplifiers," IEEE J. Lightwave Technol., Vol. LT-4, pp. 288-297 (1986).

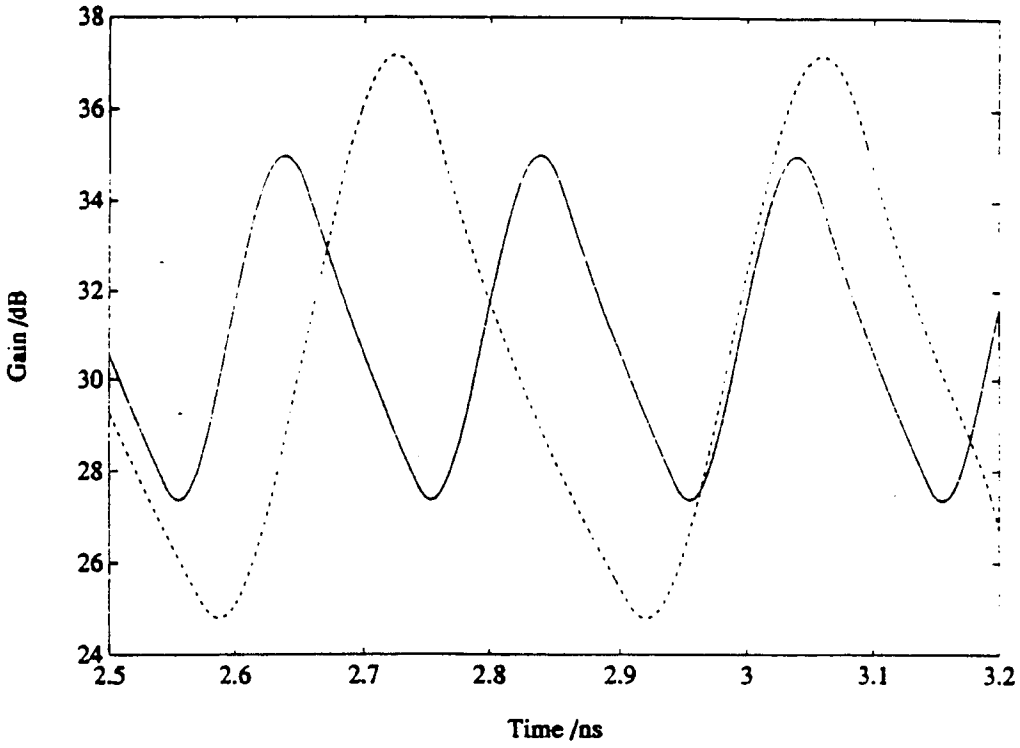

Fig. 5.1: Small signal chip gains. Drive conditions: 40 mA DC bias + 200 mA amplitude RF signal. Driving signals frequencies: ----- 3 GHz —— 5 GHz.

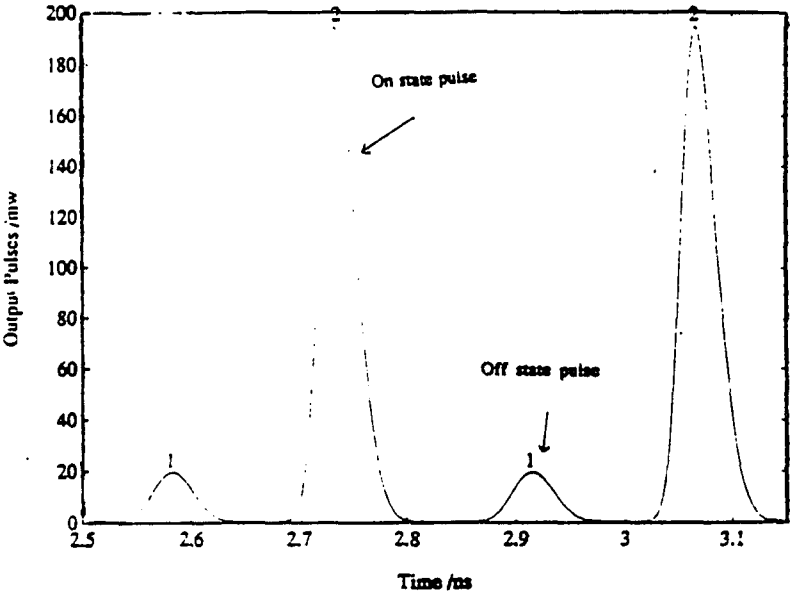

(a)

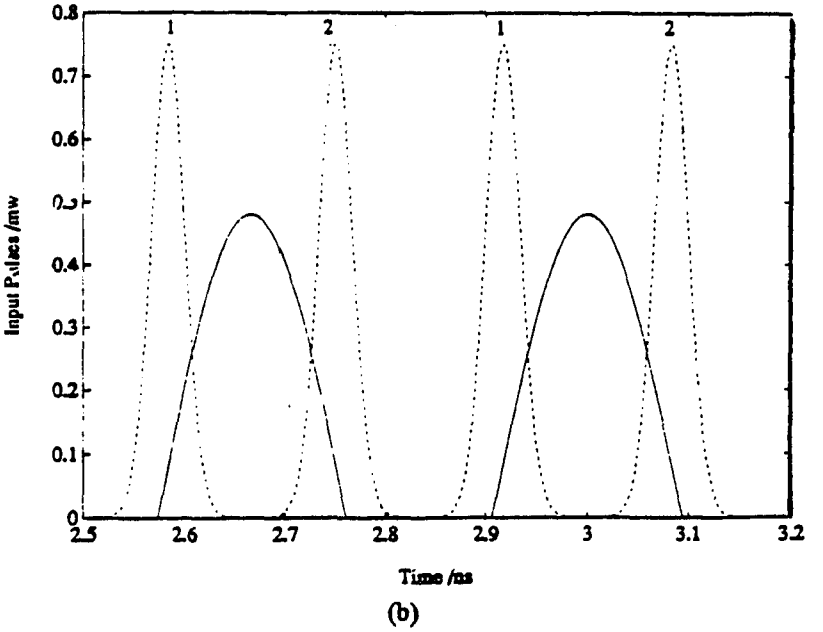

(b)

Fig. 2. (a) Output pulses selected by a single TWSOA gate with a 2:1 selection ratio, and for an optimum time delay between the 6 Gb/s input optical pulse train and the RF driving signal. $E_{in}/E_{sat} \approx -20$ dB (Input pulse peak power = 0.75 mw). Drive conditions: 40 mA DC bias + 3 GHz 200 mA amplitude RF signal. (b) ____ input optical pulses, and _____ RF driving signal. Relative delay $\approx 1/4$ (83 ps) the RF driving signal period.

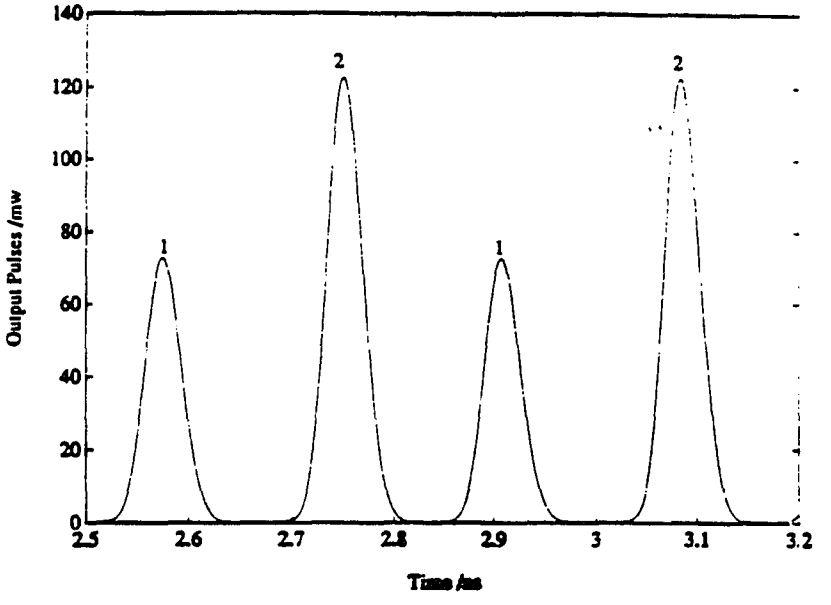

(a)

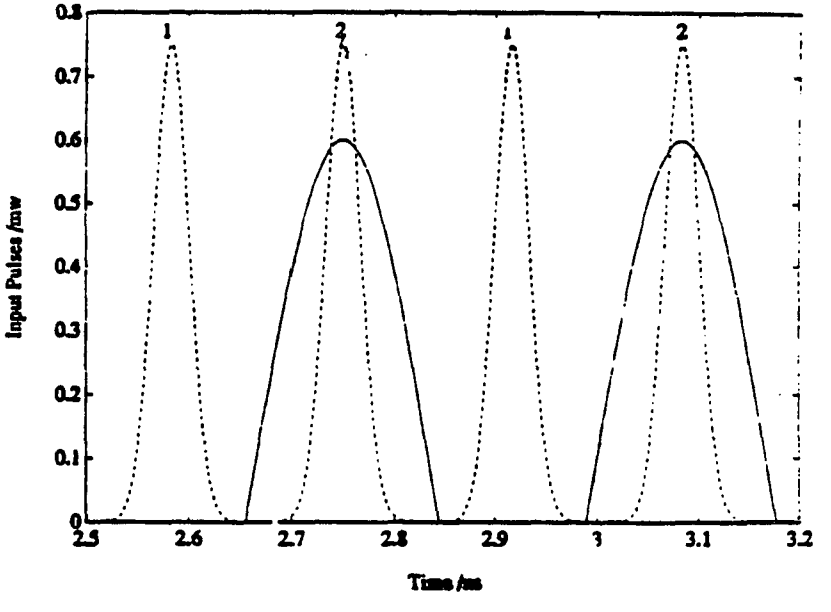

(b)

Fig. 3. (a) Output pulses with a zero time delay (worst demultiplexing performance) between input optical pulses and the RF driving signal. Operating conditions: same as Fig. 2. (b) ____ input optical pulses, and _____ RF driving signal. Peak of the on-state pulses coincides with the positive peak of the RF driving signal.

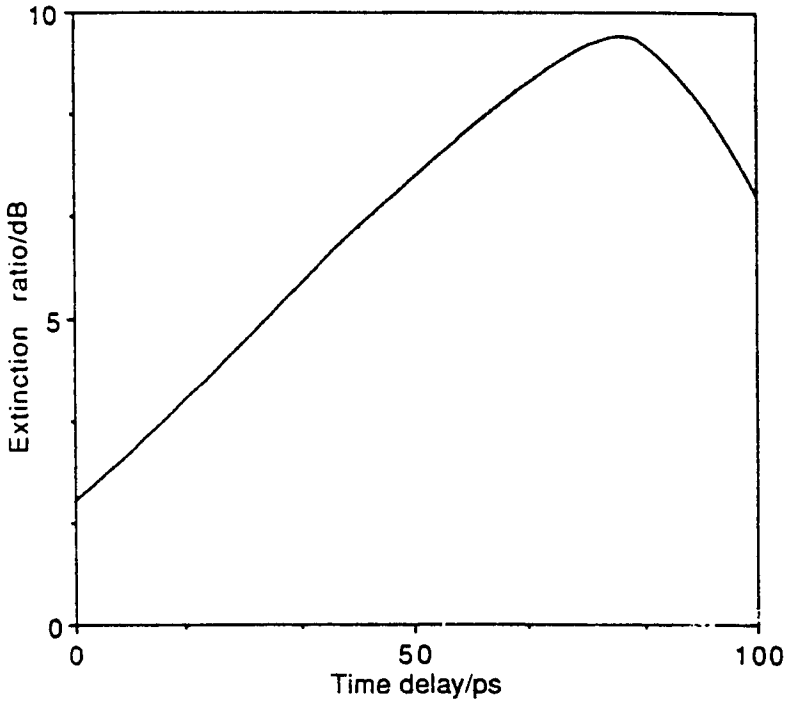

Fig. 5.4: Extinction ratio versus time delay between input optical pulses and RF signal. Operating conditions: same as Fig. 5.2.

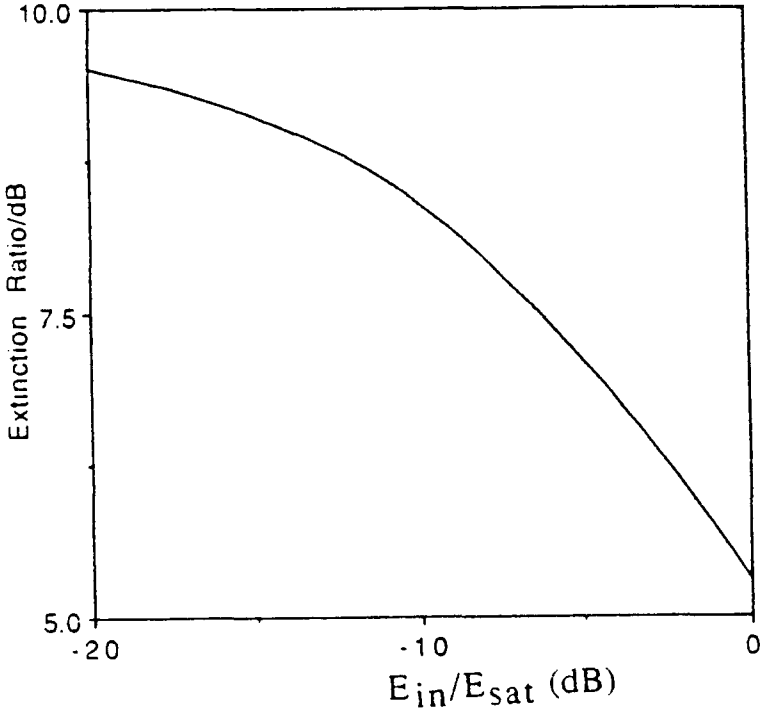

Fig. 5.5: Optimum value of the Extinction ratio versus input pulse energies with respect to the saturation energy. Operating conditions: same as Fig. 5.2.

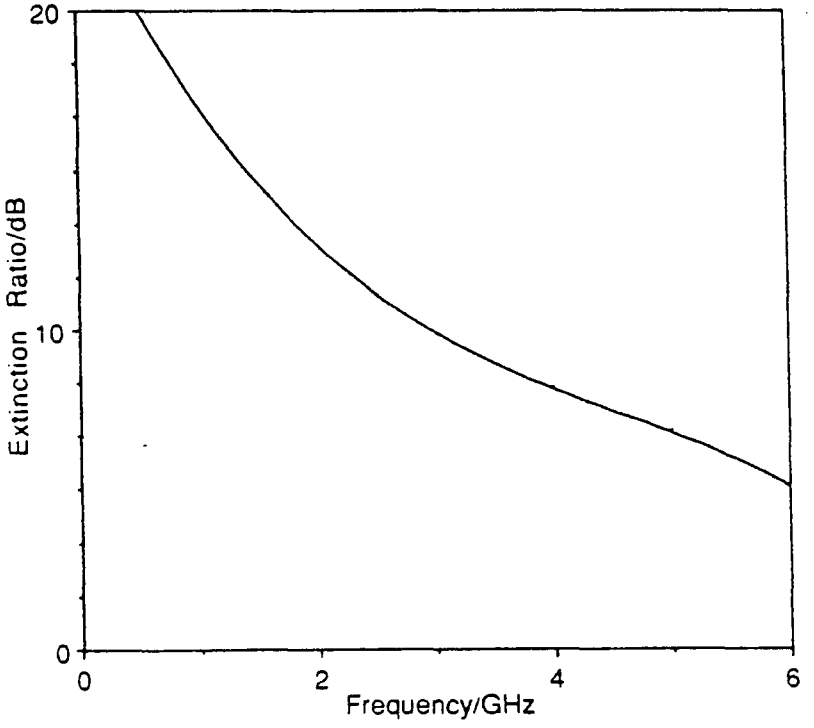

Fig. 5.6: Optimum value of the Extinction ratio versus driving signal frequency for signal level of E_{in}/E_{sat} = -20 dB. Operating conditions: same as Fig. 5.2, with 40 mA bias + 200 mA amplitude RF signal.

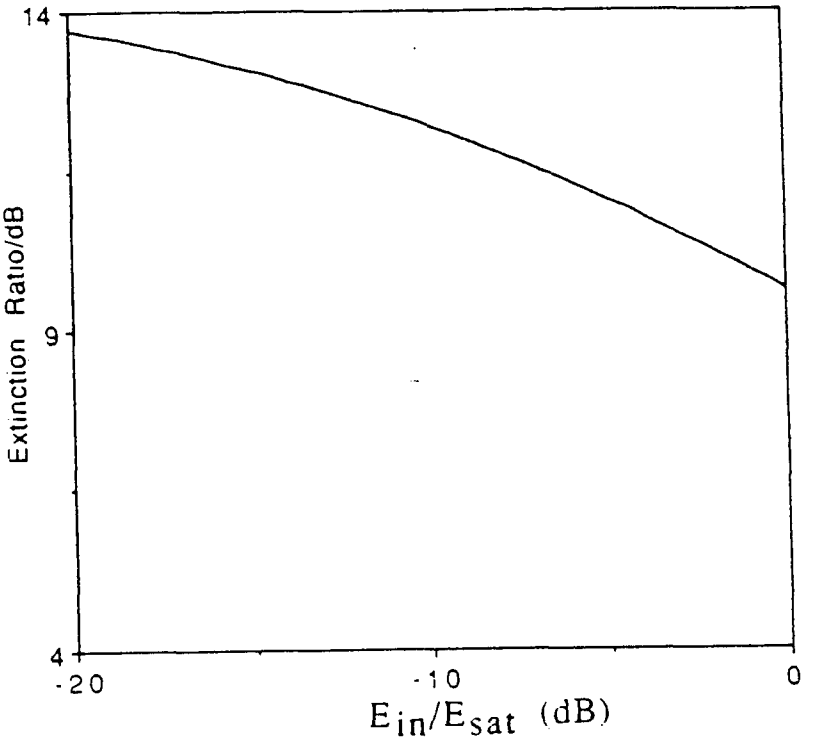

Fig. 5.7: Optimum value of the Extinction ratio at 10 Gb/s, for an optical gate of two cascaded TWSOAs, each with a 2 : 1 selection ratio, versus input pulse.

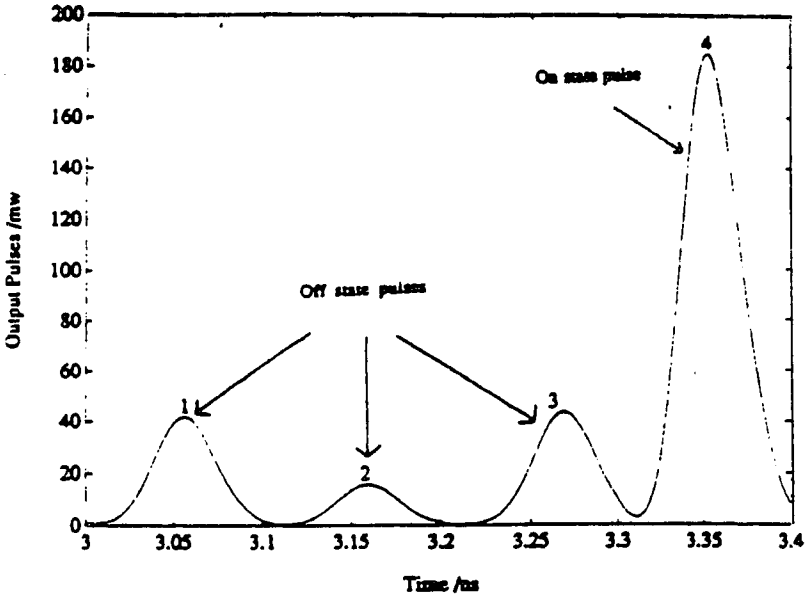

(a)

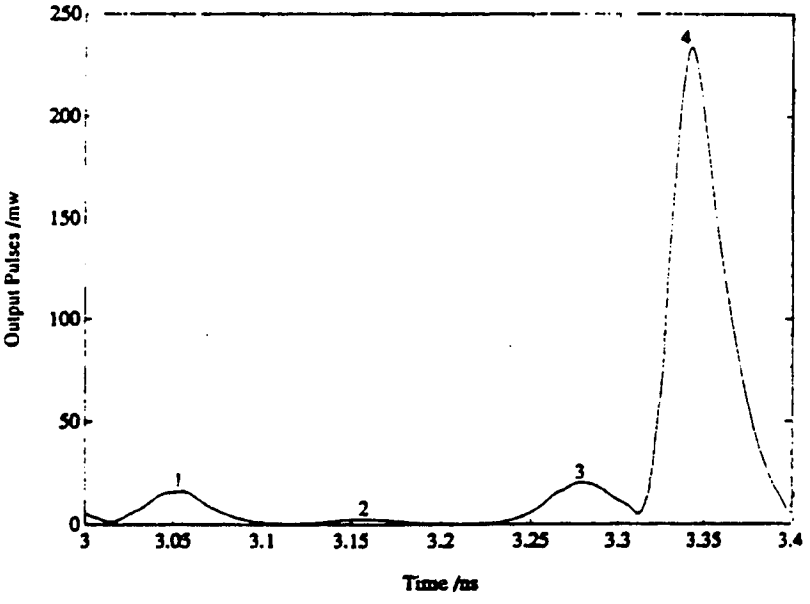

(b)

Fig. 8. (a) Output pulses selected by the first amplifier of the twin gate for an optimum time delay between the 10 Gb/s input optical pulse train and the RF driving signal. Each amplifier of the twin gate is assumed to have a selection ratio of 4:1. $E_{in}/E_{sat} \approx -20$ dB. Drive conditions: 40 mA DC bias + 2.5 GHz 200 mA amplitude RF signal. (b) Output pulses selected by the second amplifier of the twin gate. Operating conditions: same as Fig. 8(a).

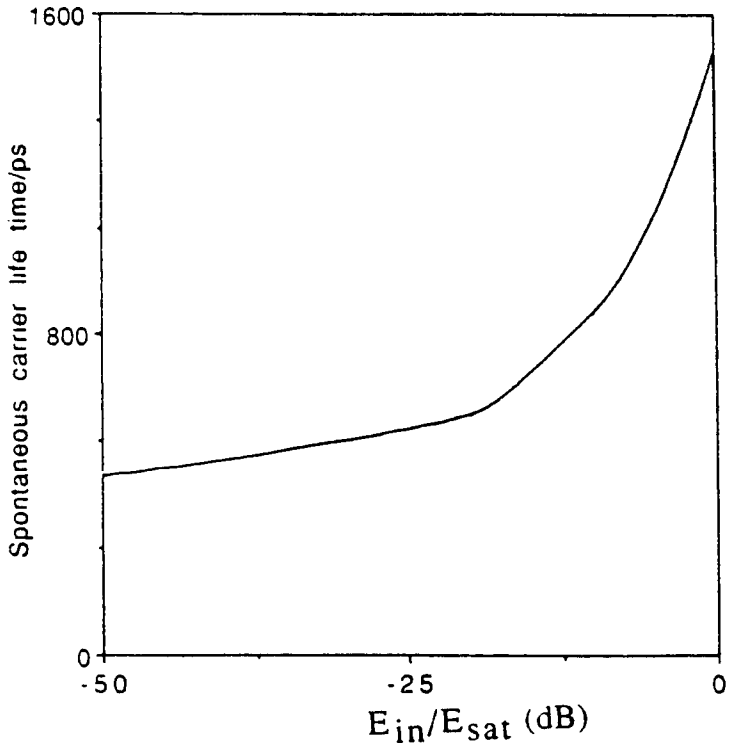

Fig. 5.9: Derived values of τ_s using the linear recombination model, which give the same results as those obtained using the detailed non-linear recombination model, versus input pulse energies normalized with respect to the saturation energy. The input optical signal used in the simulation is assumed to be a 6 Gb/s gaussian pulse train with E_{in}/E_{sat} = - 20 dB . Drive conditions: 100 mA DC bias

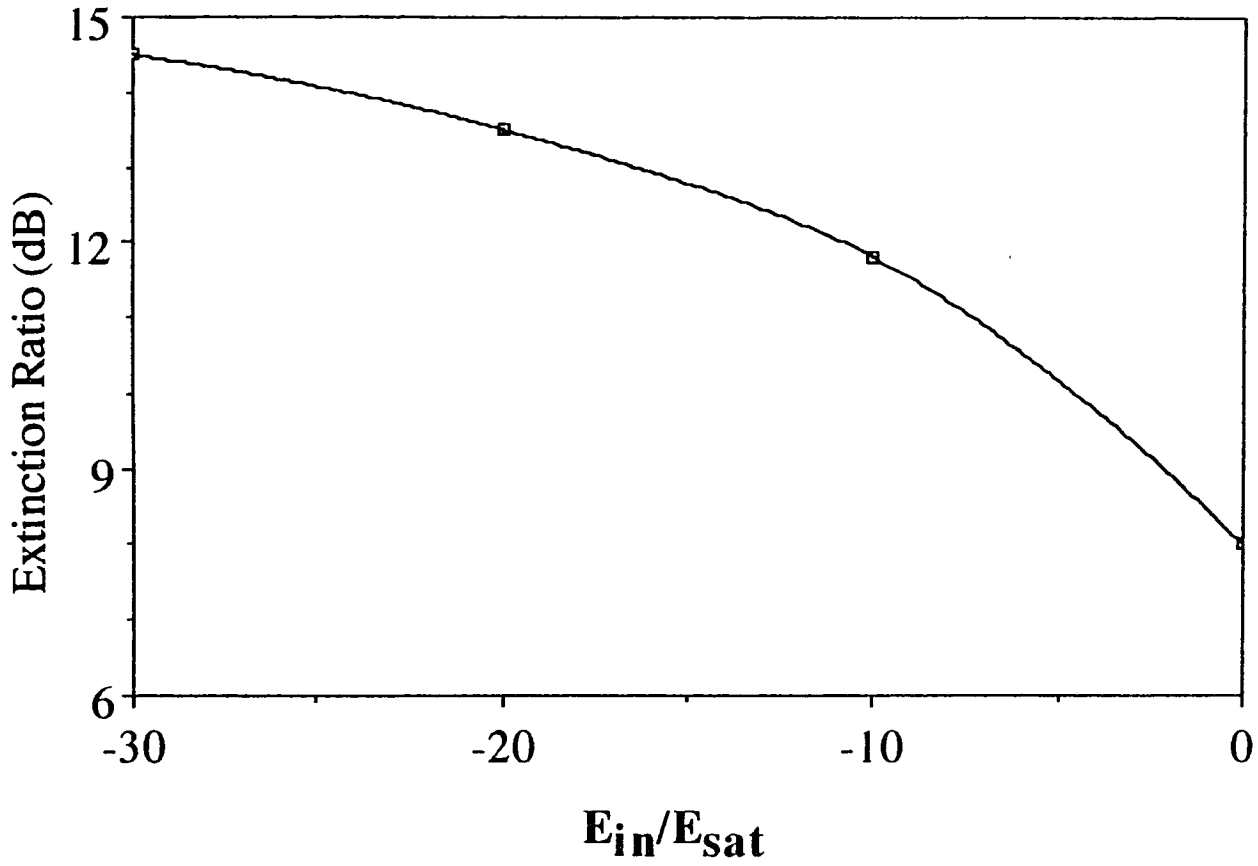

Fig. 5.10: Optimum values of the Extinction ratio at 10 Gb/s for a single amplifier gate with Zn-doped active region ($p = 4 \times 10^{18}$ cm^{-3}) versus E_{in}/ E_{sat} . Drive conditions: 20 mA Dc bias + 5 GHZ 500 mA RF signal.

CHAPTER 6
End-to-End Performance of the OTDM System

6.1 Optical Receivers:

6.1.1 Background:

The role of the optical receiver is to recover the data that was originally transmitted by the light source and which has been sent through the optical-fiber communication system. Its main components are a photodetector, an electronic preamplifier, and some electronic signal-processing elements. Fig 6.1 shows a block diagram of a representative optical digital data receiver.

The photodetector converts the modulated optical input into an electronic signal through the photoelectric effect. The ideal photodetector would have a high optoelectrical conversion efficiency, add no noise to the signal, not limit the system's operating bit rate, be highly reliable and inexpensive, have a size comparable to the fiber-core size, and, possibly, be electronically compatible with integrated circuits. These requirements are best met with semiconductor photodiodes, which are at present universally employed within optical receivers for fiber systems. Two types of semiconductor photodiodes are commonly used: the so called PIN photodiode and the avalanche photodiode (APD).

Because the received optical signal impinging on the photodiode is typically weak, the photodetected signal is first amplified by a preamplifier. The main goal of the preamplifier is to provide a signal level compatible with the following circuitry used for further processing. The

combination of the photodiode and the preamplifier is referred to as the receiver front-end. It is crucial that the noise added by the preamplifier be minimized because the receiver performance is essentially determined by the noise introduced within the front-end. Since there is a tradeoff between noise and bandwidth, the lowest noise preamplifier designs suffer from bandwidth limitation and an equalizer is sometimes used to alleviate the problem of pulse spreading within the front-end. This equalizer as an optional element in Fig. 6.1 because there are receiver front-end designs that partially avoid the problem of bandwidth limitation (for instance transimpedance front-end).

The next step following the (optional) equalizer is to boost the signal with a postamplifier, usually with an automatic gain control (AGC) that adjusts the gain as a function of the input signal strength. The average output voltage of the AGC is fixed at an adequate level irrespective of the incident average optical power at the receiver. The filter following the postamplifier removes unwanted frequency components that might have been generated at this point. The last step at the receiver is the actual data recovery. In some low cost poorly performing optical receivers, data recovery is done asynchronously by merely using a comparator to decide whether a pulse is present or not. The simplified data recovery scheme is practical only for low data rate signals for which the signal pulses sharp rise and fall times compared to the bit duration. For high data rate system a clock recovery circuit is necessary to achieve optimum performance. The recovered clock is fed onto the data decision circuit, which samples the input signal at the optimum times corresponding to the situation where the signal level difference between bits "1" and bits "0" is maximum (usually in

the middle of the bit slot). The output of the decision circuit is the recovered data stream, which may contain some errors.

6.1.2 Direct Detection (DD) Receiver:

The present section is intended to review the characteristics and performances of direct detection (DD) optical receivers used in optical-fiber communication systems and will be exclusively used in our work. With DD, the receiver recovers the original data by deciding on the presence or absence of light in each bit slot. Therefore, the only way the original data stream can be imposed on the optical carrier at the transmitter is by modulating the intensity of the emitted light. Systems based on such schemes are referred to as intensity modulation with direct detection (IM/DD).

Direct detection receivers are called so because the incident optical signal is directly converted into an electrical form by the photodiode. In essence, DD receivers are based on photon counting as bits "0" and "1" are decoded, depending whether or not there is optical power within the allocated bit slot.

If the responsivity of the photodetector has a finite value, then an electrical current is always generated even if the incident optical power approaches to zero. For example, a binary digital signal could (ideally) be recovered by DD without error provided that each bit "1" carries at least η photons while each bit "0" corresponds to the absence of any light. However, this is never the case even for a perfect photodetector, and all

receivers require more "photons per bit" than this hypothetical limit to operate reliably.

The reasons are the quantum nature of light and the noise mechanisms that lead to fluctuations in the generated photocurrent. these mechanisms prevent error-free data recovery because a bit "1" can be decided at the receiver while a bit "0" was originally transmitted, and vice versa. The optical receiver will thus produce only an " estimate" of the originally transmitted message.

The performance of an optical receiver is specified by the minimum received optical power (or equivalently, the minimum number of photon per bit) required to achieve a given bit error rate between the original message at the transmitter and its estimate at the receiver. In telecommunication networks, the BER is typically set at 10^{-9}, or one error per billion bits on average, while for computer networks a BER of 10^{-15} (ie., six orders of magnitude lower) is often highly desirable. The minimum optical power required to achieve the specified BER is referred to as the receiver sensitivity.

6.1.3 Signal-to-Noise Ratio (SNR) of DD Receivers

The power SNR at the output of the an optical receiver is defined by:

$$SNR = \frac{Signal\ power\ from\ photodetector}{photodetector\ noise\ power + Amplifier\ noise\ power} \quad (1)$$

The noise sources in the receiver arise from the photodetector noises resulting from the statistical nature of the photon-to-electron conversion process and the thermal noises associated with amplifier circuitry. For most application it is the noise currents which determine the minimum optical power level that can be detected, since the photodiode quantum efficiency is normally close to the maximum possible value.

The signal and noise components are as follows:

1) The average photocurrent due to the signal power is given by:

$$I_{ph} = I_{sig} = q\,\eta\,[\overline{P}_{in}/h\upsilon_s] = \Re\,\overline{P}_{in} \qquad (2)$$

where:

$\Re$: is the photodiode's responsivity (A/w).

η: is the photodiode's quantum efficiency.

$h\upsilon_s$: is the incident signal's photon energy.

q: is the electron charge.

$\overline{P}_{in}$: is the steady-state average optical power incident on the photodetector.

For PIN photodiodes the mean square signal current:

$$\left\langle I_{sig}^2 \right\rangle = \left\langle I_{ph}^2 \right\rangle = (\Re P_o)^2 \qquad (3)$$

2) The photodetector load resistor, R_L, contributes a mean square thermal noise current:

$$N_{th} = \left\langle I_{th}^2 \right\rangle = \sigma_{th}^2 = 4\,k_B T\,B_E/R_L \qquad (4)$$

Where

k_B is Boltzmann's constant.

T is the absolute temperature.

σ is the standard deviation (square root of the variance).

B_E is the electrical bandwidth of the receiver (bandwidth of the matched filter), usually taken as:

$B_E = (B/2) = (1/2T_b)$, where T_b is the bit duration and B (bit/s) is the bit rate, as long as the received signal is integrated and then sampled in the low-pass version of the integrate-and-dump filter (matched filter) of Fig. 6.1.

3) The component of the shot noise intrinsic to the signal has a mean square value which is proportional to the average value of the signal photocurrent I_{sig}:

$$N_{Sh} = \left\langle I_{sh}^2 \right\rangle = \sigma_{sh}^2 = 2q\, I_{sig}\, B_E \qquad (5)$$

4)The noise sources associated with both the active and passive elements of the amplifier are referred to as the preamplifier noise and depends on the front-end design and the type of preamplifier used, e. g., FET, BJT, MOSFET, and MESFET (note that Eq. (4) expresses the thermal noise generated by the load resistor alone). The mean square noise current introduced by the preamplifier is given by:

$$N_{Amp} = \left\langle I_{Amp}^2 \right\rangle = \sigma_{Amp}^2 = 2q\, I_{Amp}\, B_E \qquad (6)$$

5) We shall ignore here the dark current (bulk and surface) noise components.

The total noise (variance) is the sum of the different noise terms, since these processes are statistically independent zero-mean processes (we are assuming that there is enough light for the shot noise to be considered a gaussian process, rather than a Poisson process), and is given by adding Eqs. (4), (5), and (6):

$$N_{ToT} = \sigma_{ToT}^2 = \left\langle I_{ToT}^2 \right\rangle = \left\langle I_{sh}^2 \right\rangle + \left\langle I_{th}^2 \right\rangle + \left\langle I_{Amp}^2 \right\rangle \tag{7}$$

Substituting Eqs. (3) and (7) into Eq. (1) yields:

$$SNR = \frac{\left\langle I_{sig}^2 \right\rangle}{\left\langle I_{sh}^2 \right\rangle + \left\langle I_{th}^2 \right\rangle + \left\langle I_{Amp}^2 \right\rangle} \tag{8}$$

6.2 DD Receivers Using Semiconductor Optical Preamplifiers

We have just seen that in the case of even the most efficient PIN photodiodes, the shot noise is usually dominated by the thermal noise of the preamplifier input. The performance limits imposed by this noise component naturally lead one to question whether the signal can somehow be amplified before reaching the electrical amplifier input. There are two competing approaches to doing this. In the first approach one could obtain internal gain, through impact ionization by using an APD. In the second approach, one could use coherent detection and swamp the thermal component with a strong local-oscillator input. The trouble with these two approaches is that the first does not buy very much because of randomness of the avalanche gain and their inability to handle extremely

high bandwidths (more than about 1-2 Gb/s), while the second entails considerable system complexity that usually causes performance to fall many dB short of the relevant quantum limits.

A third approach is to use an optical amplifier especially of the travelling-wave type, when placed immediately before the photodetector, has neither of these difficulties. A TWSOA, for example, offers a high gain over a very large bandwidth, e. g., 30 dB over 5 x 10^{12} Hz, which is unmatched by any conventional photodetector (the best APD's for example, have a gain bandwidth product of 5 x 10^{12} Hz [5]). However, it has its own problem, namely random sponteneous-emission events that occur within the amplifier and appear at the output as ASE (amplified spontaneous emission).

However, we shall find in this section that the best solution of the three seems to be photonic preamplification, particularly in the case of the very convenient IM-DD system. It will turn out that the detectability limit for such an arrangement, which is physically simple and is capable of being greatly cost-reduced, is close to that of the shot noise imposed quantum limit of a coherent heterodyne ASK system.

In this section, the potential of TWSOAs will be further extended by using them as receiver preamplifiers, to enhance the receiver sensitivity, and line amplifiers, to boost the signal along the fiber, in the proposed OTDM system.

6.2.1 Amplifier Noise

The dominant noise generated by the amplifier is the amplified spontaneous emission (ASE). The amplification of spontaneous emission is triggered by the spontaneous recombination of electrons and holes in the amplifier medium. This spontaneous noise can be modeled as a random process in which the events are infinitely short pulses distributed all along the active medium. This random process is characterized by a flat noise-power spectrum, and the ASE power at the output of an amplifier is given by [1-3]:

$$P_{ASE} = 2 \chi N_{sp} h\upsilon_s (G-1) B_o \qquad (9)$$

where

B_O: is the optical filter bandwidth.

2: Two polarizations.

N_{sp}: is the spontaneous emission factor, given by [4]

$$N_{sp} = \frac{N}{N - N_o} \frac{\Gamma g}{\Gamma g - \alpha} \qquad (10)$$

Γ: is the optical gain confinement factor of the active layer.

α: is the effective loss coefficient per unit length which includes scattering and absorption losses both inside and outside the active region.

g: is the material gain coefficient.

In general, N_{sp} ranges from 1.4 to more than 4 depending both on the pumping rate and the operating wavelength [2-4].

χ: is the excess noise factor given by [1-2]:

$$\chi = \frac{(1 + R_1 G)(G - 1)}{(1 - R_1)G} \tag{11}$$

R_1: is the input facet reflectivity of the amplifier. From (9) and (11), we see that the noise power decreases when the input facet reflectivity R_1 decreases. The reason is that the part of the noise that has the greatest impact on the amplifier performance degradation is that which occurs where the signal is the weakest, that is, at the input of the amplifier. With R_1 small, the spontaneous emission that is directed towards the input facet can escape from the cavity and no longer contributes to the ASE.

Since for TWA, $R_1 \approx 0$ and $G >> 1$, $\chi \approx 1$

When the total output from the amplifier (amplified signal + ASE) is detected by a photodiode, two distinct types of noise are created in addition to electronic (thermal) noise, the well-known shot noise and the beat noise. Since the power spectrum of the electrical current out of the photodiode is the result of a squaring operation upon the input optical power, the power spectrum of the photodiode output will contain not only a spike at DC, the signal-signal cross-product term, which is the squared optical signal, but will also contain two noise cross-product continuum spectra, signal-ASE, and ASE-ASE. The latter has a spectral density much smaller than that of the signal-ASE component.

These noises will now be quantified following the analysis given by Olsson [4]. For simplicity, we assume an ideal TWA with flat gain across both the modulation bandwidth and the optical bandwidth B_O, and that

the optical carrier signal is centered in the middle of B_o. The simulation block diagram of the optical preamplifier receiver is shown in Fig. 6.2. The incoming signal P_{in} is amplified with a frequency flat gain, polarization filtered, bandlimited (through an optical bandpass filter with B_o bandwidth) and received with a PIN front end receiver. The optical filter is assumed to have an ideal rectangular bandpass characteristics centered at the signal wavelength. For the receiver of Fig. 6.2, the detector output is sampled once each bit interval, and depending on the results, the receiver decides whether a binary "0" or a binary "1" has been transmitted.

The average photocurrent signal generated by the average optical signal power $\bar{P}_{in}$ is:

$$I_{sig} = q\eta \left[\frac{\bar{P}_{in}}{h\upsilon_s}\right] \tag{12}$$

and the received average photocurrent signal is:

$$I_{sig,rec} = G\ \Gamma_1 I_{sig} \eta_{in} \eta_{out} \tag{13}$$

After square law detection in the receiver, the received signal power is:

$$S = [G\ \Gamma_1 I_{sig} \eta_{in} \eta_{out}]^2 \tag{14}$$

where

Γ_1: is the Optical loss between amplifier and receiver.

η_{in}: is the amplifier input coupling efficiency.

η_{out}: is the amplifier output coupling efficiency.

For an amplitude modulated signal of average power $\bar{P}_{in}$, 50-percent duty cycle and an extinction ratio of r ($r = P_1/P_o$, where P_1 is the optical power transmitted for a "1" bit and P_o is the power transmitted for a "0" bit), the photocurrent signal equivalents of the input power for a mark "1" $\{I_{sig}(1)\}$ and a space "0" $\{I_{sig}(0)\}$ are:

$$I_{sig}(1) = q\eta\left[\frac{2\bar{P}_{in}}{h\upsilon_s}\right]\left[\frac{r}{1+r}\right]$$

$$I_{sig}(0) = q\eta\left[\frac{2\bar{P}_{in}}{h\upsilon_s}\right]\left[\frac{1}{1+r}\right] \qquad (15)$$

The photocurrent generated by the ASE is:

$$I_{ASE} = q\eta\left[\frac{P_{ASE}}{h\upsilon_s}\right] = q\eta\, N_{sp}(G-1)B_o \qquad (16)$$

and the photocurrent equivalent of the ASE noise power at the receiver is:

$$I_{ASE,rec} = \eta_{out}\,\Gamma_1\, I_{ASE} \qquad (17)$$

The noise terms are [2-4]:

$$N_{shot\text{-}sig} = 2q\, I_{sig,rec}\, B_E \qquad (18)$$

$$N_{shot\text{-}ASE} = 2q\, I_{ASE,rec}\, B_E \qquad (19)$$

$$N_{sig\text{-}ASE} = 4\, I_{sig,rec}\, I_{ASE,rec}\, B_E/B_o \qquad (20)$$

$$N_{ASE\text{-}ASE} = (I_{ASE,rec})^2\, B_E\,(2B_o - B_E)/B_o^2 \qquad (21)$$

$$N_{ciruit} = I_{circuit}^2\, B_E \qquad (22)$$

where

$N_{shot\text{-}sig}$: shot noise due to the signal.

$N_{shot\text{-}ASE}$: shot noise due to ASE.

$N_{sig\text{-}ASE}$: beat noise between the signal light and ASE.

$N_{ASE\text{-}ASE}$: beat noise between ASE components.

N_{ciruit}: circuit noise due to the receiver front-end electronic circuit.

I_{ciruit}: Equivalent input noise current of the receiver front-end electronic circuit. $(pA/\sqrt{HZ})$.

The total noise is:

$$N_{Tot} = N_{shot\text{-}sig} + N_{shot\text{-}ASE} + N_{sig\text{-}ASE} + N_{ASE\text{-}ASE} + N_{ciruit} \qquad (23)$$

Combining Eqs. (14) and (18)-(22) yields:

$$SNR = \frac{\left(G\Gamma_1 I_{sig}\eta_{in}\eta_{out}\right)^2}{N_{shot-sig} + N_{shot-ASE} + N_{sig-ASE} + N_{ASE-ASE} + N_{circuit}} \qquad (24)$$

The BER is given by [2-5]:

$$BER = \frac{1}{\sqrt{2\pi}} \frac{\exp\left[-\frac{Q^2}{2}\right]}{Q} \qquad (25)$$

where Q is given by:

$$Q = \frac{\sqrt{S(1)} - \sqrt{S(0)}}{\sqrt{N_{Tot}(1)} + \sqrt{N_{Tot}(0)}} \qquad (26)$$

where S(1), S(0), $N_{Tot}(1)$, and $N_{Tot}(0)$ are the signal and total noise for mark and space, respectively. Note that these values can be obtained by using Eqs. (12)- (15), and (23). A BER of 10^{-9} require Q= 6. Eqs. (9)-(26) form the basis from which the performance of the amplifier systems are evaluated.

6.2.2 Performance of DD Receivers incorporating TWSOAs as Preamplifier and In-Line Amplifier

I) Optical Preamplifier performance

Since our proposed OTDM system will operate at a baseband bit rate of 2.5 Gb/s per channel, therefore, we will analyze a 2.5 Gb/s receiver with 1.25-GHZ electrical bandwidth. The following amplifier and system parameters, unless otherwise specified, are used in the calculations:

* The optical amplifier is assumed to be a conventional TWSOA with undoped active layer and same parameters as those used in previous chapters and are listed in table 4.I. The optical amplifier is assumed to operate at a signal wavelength which coincides with the gain maximum. $\eta_{in} = \eta_{out} = 0.4$, i. e., coupling losses of 4 dB/facet. The spontaneous emission factor, N_{sp}, is assumed to be 1.4 [4-5]. The optical bandwidth, B_o, was 1-nm with insertion losses of about 2 dB. Optical isolators are assumed to be inserted both before and after the amplifier for more stable operation.

* A PIN/FET receiver front-end is used in the simulation. The photodetector is a commercially available high-speed PIN diode followed by a high impedance (5 kΩ front-end FET amplifier). The receiver

sensitivity without optical preamplifier was - 26 dBm at 2.5 Gb/s (i., e., the value chosen for the thermal noise current, I_{ciruit} = 12 $(pA/\sqrt{HZ})$ corresponds to a base receiver sensitivity of - 26 dBm at 2.5 Gb/s).

* A value of r = 20, is assumed for the extinction ratio.

The BER characteristics for the receiver with the optical preamplifier, assuming a net fiber-to-fiber gain of 15 dB at the 1.55 μm operating wavelength, is shown in Fig. 6.3. The "received power" in Fig. 6.3 refers to the average optical power in the input fiber to the preamplifier. As can be seen from the figure, with the optical preamplifier, the receiver sensitivity is - 36 dBm which is about 10 dB better than the base receiver sensitivity.

The simulation results of the achievable receiver sensitivity versus the amplifier gain for a BER of 10^{-9} are shown in Fig. 6.4. At low amplifier gains, the receiver is limited by the thermal noise and consequently the receiver sensitivity improves 1 dB for every decibel of gain. For higher gains, the signal-ASE and ASE-ASE beat noise becomes dominant, and the best achievable receiver sensitivity depends on the bandwidth of the optical filter.

Like APD receivers, optical preamplifier receivers have signal dependent noise. Therefore, the sensitivity degradation from a nonperfect extinction ratio is worse than in a traditional PIN receiver. The effect of the extinction ratio is shown in Fig. 6.5 as the power penalty (receiver sensitivity degradation in decibels at a fixed BER (10^{-9}), as compared with the sensitivity for a perfect extinction ratio) at amplifier internal gains

of 20 dB and 35 dB. The higher the gain, the more dominant is the signal-ASE beat noise term ($N_{sig\text{-}ASE}$) and consequently the higher is the extinction ratio penalty. As shown in figure 6.5, an extinction ratio of 20 : 1 or better will in all circumstances gives a power penalty of 1 dB or less.

Overall, using very reasonable and achievable values for the amplifier and system parameters (G = 25 dB, $\eta_{in} = \eta_{out} = 0.4$, $N_{sp} = 1.4$, r = 20, B_o= 1 nm, B_E = 1.25 GHz), the achievable sensitivity for a 1.25-GHz receiver is about - 36 dBm at 2.5 Gb/s.

II) In-Line Amplifier Chain performance

In this section, we will analyze a system with multiple in-line amplifiers. For evaluating the overall performance of our OTDM system, the main concerns are how the system performance is affected by gain, optical bandwidth and the input power of cascaded in-line amplifiers. Also of interest is the ultimate number of amplifier stages, n, that can be cascaded while maintaining reasonable system performance. These issues have been addressed previously and, for this case, it has been shown that the most important parameter is the optical input power to the amplifier [3-5]. Here, using our amplifier and system parameters, we will merely calculate the power penalty incurred at the receiver as function of n and with the amplifier input power as a parameter. The calculation is made as follows:

1. We will assume that the gain of each amplifier exactly equals the loss in between two successive amplifiers. With this assumption, the cumulative effect of the amplifier noise is obtained by replacing N_{sp} in Eqs. (16)-(26) by nN_{sp}, where n is the number of cascaded amplifiers.

2. For each given input power and optical bandwidth, the loss between the last amplifier and receiver is varied such as to produce a signal power at the receiver that gives an BER of 10^{-9}. No approximations are made and all of the noise terms in equations (18)-(23) are used to evaluate the BER. This receiver sensitivity is then compared to the baseline receiver sensitivity (no amplifiers) and the power penalty is taken as the sensitivity difference.

Fig. 6.6 shows the power penalty versus number of in-line amplifiers at 20 Gb/s for amplifier input powers of - 30 dBm, -20 dBm, and -10 dBm. Note that for this calculation we have used $\eta_{in} = 1$, so the amplifier input power refers to the power actually coupled into the amplifier. Other system and amplifiers parameters used in this calculation are: G = 25 dB, $\eta_{out} = 0.4$, $N_{sp} = 1.4$, r = 20, $B_o = 1$ nm, and $B_E = 10$ GHz. As can be seen from the figure, for amplifier input powers of - 30 dBm, -20 dBm, and -10 dBm, the maximum (2-dB penalty) number of in-line amplifiers are 3, 6, and 20 respectively.

6.3 End-To-End Performance of 8-channel, 20 Gb/s 300 Km OTDM Transmission System:

The OTDM system transmitter configuration uses a single-laser architecture (see chapter 3). The following summarizes the system components and parameters assumed in the simulation:

1) A gain-switched DFB semiconductor laser, driven by a 2.5 GHz sinusoidal current, is assumed to generate 20 ps pulses (FWHM) at a

repetition rate of 2.5 GHz. The average power coupled into the single-mode fiber is assumed to be + 4 dBm [6].

2) The output pulse train of the laser is split passively into eight-channels by a 1 x 8 fused fiber couplers.

3) Each of the 2.5 GHz pulse trains at the eight coupler output ports is modulated using a TWSOA, whose drive signal is assumed to be a 2.5 Gb/s pseudo-random NRZ electrical data pattern, synchronized to the 2.5 GHz laser drive. Each TWSOA switch is assumed to have a net gain of 15 dB.

4) The 8-modulated signals are properly delayed with respect to one another by 50 ps using a fiber delay line (to allow inter-leaving with the correct delay), and then combined using a 8 x 1 fused fiber coupler to form a single 20 Gb/s RZ data stream. The mean output power from the interleave (combiner) is -1 dBm.

5) The transmission section of the system consists of four 75 Km lengths of dispersion-shifted (DS) fiber with an average wavelength of zero-dispersion at 1.55 μm. The mean loss and anomalous group delay dispersion, $D(\lambda)$, of the fiber spans are 15 dB (0.2 dB/Km) and 0.1 ps/(nm .Km) at the signal wavelength of 1.55 μm. Note that the wavelength of zero-dispersion of the fiber is assumed to coincides with both the signal wavelength and the gain peak wavelength of the amplifier at 1.55 μm.

6) Three in-line TWSOAs were placed at 75 km intervals along the transmission path of the fiber, each followed by an optical bandpass filter of 1-nm flat bandwidth to reduce the effect of ASE noise accumulation. It is also assumed that the net gain of each amplifier (15 dB) compensates the mean loss of each 75-Km fiber span. In order to avoid detrimental optical nonlinearities effects in the fiber, the average power of the signal pulse at the output of the amplifier was set to -1 dBm (.79 mw), and thus the penalty was mostly due to the accumulation of ASE noise from the amplifiers and the linear waveform distortion due to the linear group velocity dispersion from the fiber.

7) The 20 Gb/s signal is split passively into eight-20 Gb/s pulse stream using a 1 x 8 fused fiber couplers paced at the receiver end of the system.

8) Each of the 20 GHz pulse trains at the eight coupler output ports is demultiplexed using two cascaded TWSOAs gates (as described before in chapter 5), each of a selection ratio od 8 : 1, and, therefore, is driven 100 ps 2.5 GHz electrical pulses which is generated by extracting the timing information from one of the demultiplexed 2.5 Gb/s signals [6]. Consequently, each channel require two TWSOAs gates to perform the demultiplexing and a total of 16 amplifiers gates are required to retrieve the 8-2.5 Gb/s baseband channels. Just as the TWSOAs modulators at the the transmitter, the TWSOAs gates is not being used to shape the output and is acting as only as an on/off switches. The overall on/off ratio of the two TWSOAs gates is more than 15 dB. Different channels may be selected by changing the phase (delay) of the electrical drive to the

demultiplexer. This can also be achieved using fiber delay lines to obtain the correct timing for all switches.

Another approach to demultiplex the 20 Gb/s signal is to use the binary tree demultiplexing network shown in Fig. 6.7 which consists of 16 TWSOAs gates, however, each with a selection ratio of 2 : 1. Therefore, as explained before in chapter 3, its first stage is a high speed switch which demultiplexes the 20 Gb/s data stream into 10 Gb/s data streams, and is, therefore driven by a 10 GHz sinusoidal signal. Subsequent switches in the binary tree structure also can be driven by sinusoids, but operate at subharmonics of the drive frequency of the first stage switch. The reason that we have chosen to directly demultiplex the incoming signal with a gate which have an 8 : 1 selection ratio will be explained in detail later when considering the crosstalk power penalty.

9) The receiver used here has the same configuration and parameters as the one described in details in section 6.2. Note that the second TWSOA gate at each channel, used primarily as a switch, will also act as a preamplifier.

In order to assess the overall performance of the system, in terms of evaluating the receiver sensitivity, the dispersion penalty, and the crosstalk penalty, all these degradation mechanisms must be taken into account to determine the actual sensitivity of the receiver. Although the dispersion penalty can be viewed as an additional crosstalk penalty but we use the term "dispersion penalty" here to separate clearly the crosstalk penalty inherent in the demultiplexer from the additional penalty caused by dispersive characteristics of the fiber.

6.3.1 Sensitivity Degradation Mechanisms:

Degradation mechanisms must be taken into account to determine the actual sensitivity of DD receivers. Some of these mechanisms, such as the nonperfect extinction ratio at the transmitter, has already been taken into account. Others may occur when the optical signal propagates through the fiber (e.g., dispersion effect). Other may occur at the receiver end (e.g., crosstalk penalty inherent in the demultiplexer). Still other may occur at the decision circuit itself (e.g., timing jitter). This degradation in the receiver sensitivity is referred to as the power penalty. In this section, we will determine the power penalty arising from each of these Degradation mechanisms individually, and then combine all the power penalties to calculate the actual receiver sensitivity. Some of these may also be added directly as a noise term to total noise of the system. For instance, as will be shown below, the crosstalk resulting from cascading two TWSOAs gates, at each channel to perform the demultiplexing at the receiver end of the system, will be assessed as a mean square noise term to be added to Eq. (23).

I. Fiber Dispersion Penalty

The maximum bit rate distance product, BL, achievable with single-mode fibers is limited because of dispersion-induced pulse broadening. However by allowing a certain amount of pulse broadening, we implicitly degrade the receiver sensitivity. This is because optical pulse broadening is accompanied by a reduction of pulse energy within the allocated bit slot. Such a reduction decreases the SNR at the decision point. In order to

maintain the same SNR as in the absence of pulse broadening, and thereby maintain the same system performance, the receiver requires more average optical power. This increase in the required optical power is referred to as "dispersion-induced power penalty".

Furthermore, waveform distortion due to fiber dispersion is a serious problem in in-line amplifiers systems because the optical signal is transmitted over long distance without undergoing regeneration. Since an amplifier is merely amplifies the input signal, it should not increase the dispersion of the optical signal. Provided that the effective bandwidth of each amplifier is wide enough even if a large number of amplifiers are cascaded, waveform distortion due to dispersion is determined only by fiber dispersion. Thus the dispersion limit for in-line amplifier systems can be derived in the same manner as conventional systems employing no in-line amplifiers.

As is well known, the limit due to fiber chromatic dispersion is given by [7-8]:

$$B^2 L = \gamma . \frac{c}{\lambda^2 |D(\lambda)|} \qquad (27)$$

where γ is the chromatic dispersion limit coefficient depending on the modulation format [7-8] and B is the bit rate. The optical dispersion penalty depends on the factor γ as shown in Fig. 6.8 for IM-DD systems [7-8]. The product of the transmission distance and the square of the data rate is limited by the chromatic dispersion and the modulation-modulation scheme employed, not by the characteristics of the in-line amplifiers.

Another rough estimate of the chromatic dispersion power penalty is given by [9]:

$$P_D = 21\ (\sigma_t B)^2 \quad \text{(dB)} \qquad (28)$$

where σ_t is the rms impulse spread. As an approximate rule we can say that the dispersion penalty is about 1 dB when the rms impulse spread is one-quarter of a bit period. For system design purposes we may use:

$$\sigma_t B < 1/4 \qquad (29)$$

as a condition for avoiding excessive dispersion penalty [9].

Polarization dispersion can also causes signal waveform distortion, and thus may limit the system length. The limit due to this is given by [8]:

$$B^2 \cdot L = (\gamma_p / D_p)^2 \qquad (30)$$

where γ_p is the coefficient related to the modulation-demodulation format and D_p is the polarization dispersion. Values of γ_p have been determined experimentally for various modulation-demodulation formats [8]. For IM-DD, a value of γ_p = 0.5, corresponds to a 1 dB penalty [8]. The measured Polarization dispersion coefficient D_p of the fiber ranges from 0.1 to 2 ps/$\sqrt{Km}$ [8].

Based on Eqs. (27)-(29) and by using Fig. 6.7, the power chromatic dispersion penalty,P_D, for our 20 Gb/s 300 Km transmission system, is calculated to be about 0.1 dB. Using Eq. (30), the power penalty due to polarization dispersion is almost zero.

II. Crosstalk Penalty

In this section, we will consider crosstalk in a switching system consisting of N cascaded TWSOAs. In the worst case, crosstalk is present in each switching element and the polarization of each crosstalk event matches the signal polarization. Then, the optical field at the photodiode is the sum of the signal wave and various crosstalk components. When the data signal passes through N TWSOAS switching elements with independent crosstalk events, the variance due to crosstalk is given by [10]:

$$\sigma_{CT}^2 = N_{CT} = I_{sig}^2 \left[\frac{5}{6}\frac{N}{r} + \frac{N}{6r^2} + \frac{17}{96}(N^2 - N)\frac{1}{r^2} \right] \qquad (31)$$

where r is the extinction ratio (on/off) of the TWSOA demultiplexing switch and I_{sig} is given by Eq (12) above. The shot noise due to crosstalk power, $N_{shot\text{-}CT}$, is given:

$$N_{shot\text{-}CT} = 2q\, I_{CT}\, B_E \qquad (32)$$

where I_{CT} is the photocurrent equivalent of the crosstalk power and is given by:

$$I_{CT} = q\,\eta\,[\bar{P}_{in}/h\upsilon][N/r] \qquad (33)$$

Beat noise between crosstalk and ASE components, $N_{CT\text{-}ASE}$, is expected to have a negligible contribution to the total noise and is not considered here. Therefore, based on these results, the total noise term of Eq. (23) has to be modified to include both the shot noise and the variance (Eqs. 31 and 32) due to crosstalk components, The total noise , taking into account crosstalk noise is now:

$$N_{Tot} = \{N_{shot\text{-}sig} + N_{shot\text{-}ASE} + N_{sig\text{-}ASE} + N_{ASE\text{-}ASE} + N_{ciruit}\} + \{N_{shot\text{-}CT} + N_{CT}\}$$

(34)

where the last bracket is the total crosstalk noise contribution.

The results of the calculation of the power penalty due to crosstalk, P_{CT}, is summarized in Fig. 6.9. These calculations were made as follows: Using Eq. (26), the receiver sensitivity without crosstalk noise is calculated by setting Q = 6 (BER = 10^{-9}) and using Eq. (23) as the total noise (i.,e., no crosstalk). These calculations are repeated, however, using Eq. (34) as the total noise (i.,e., taking into account crosstalk noise) and the corresponding value of the receiver sensitivity is calculated. This receiver sensitivity is then compared to the baseline receiver sensitivity (no crosstalk) and the power penalty is taken as the sensitivity difference.

Based on the analysis of this section and Fig. 6.8, the crosstalk power penalty P_{CT} in our 20 Gb/s system is estimated to be about 3 dB. Note that this relatively large penalty is mainly due to the fact that we are using two cascaded TWSOAs, each of a selection ratio of 8 : 1, to perform the demultiplexing function at the receiver end of the system. However, if we have used the binary tree demultiplexing network shown in Fig. 6.7, where each signal has to traverse four cascaded TWSOA gates, the crosstalk penalty would have been increased to about 4.5 dB.

III. Timing Jitter

The output of the clock-recovery circuit provides the sampling times used by the decision device. Since this timing information is recovered from the noisy input signal, the sampling time fluctuate around a mean

value usually centered at the middle of the bit slot. Such fluctuations are referred to as timing jitter. The consequence of timing jitter is that different portion of the received signal waveform are sampled from bit to bit. Therefore, the sampled values fluctuate by an amount that depends on both the received signal waveform and the timing jitter. These unwanted fluctuations translate into a reduction of the SNR at the sampling instant and result in performance degradation.

The power penalty induced by timing jitter is defined as the increase of the received optical power required to maintain the same SNR as that expected in the absence of timing jitter. The evaluation of this power penalty is complicated by the fact that it depends not only on the statistical properties of the timing jitter, but also on the exact waveform of the received signal. Since the received waveform depends on details of the transmitter (through relaxation oscillations, frequency chirping, etc.) the fiber (through dispersion phenomena), and the receiver (through equalizer, filters,etc.) the power penalty must generally be computed on a per-case basis by means of numerical simulations. In general the rms value of the timing jitter should be below 10% of the bit slot for a negligible power penalty.

Fig. 6.10 shows the BER performance of the system versus the received power in one of the 2.5 Gb/s receivers. The figure compares the 20 Gb/s system with 300 Km of fiber to a single 2.5 Gb/s channel without any fiber. The total system penalty from the 2.5 Gb/s baseline is about 9 dB. As shown above, this penalty is mainly due to both amplifiers noise and crosstalk. The system sensitivity at the input to the preamplifier is

about -27 dBm for a BER of 10^{-9}. The "received power" in Fig. 6.10 refers to the average optical power in the input fiber to the preamplifier (second TWSOA gate of the demultiplexer). From overall power budget of the system, the power at the input fiber to the preamplifier is about - 26 dBm, indicating that adequate transmission of the 20 Gb/s over 300 Km is possible.

6.4 REFERENCES

[1] J. C. Simon, "GaInAsP semiconductor laser amplifiers for single mode fiber comunications," J. Lightwave Technol., vol. 5, pp. 1286-1295 (1987).

[2] T. Mukai, Y. Yamamoto, and T. Kimura, "S/N and error rate performance in AlGaAs semisonductor laser preamplifier and linear repeater systems," IEEE Trans. Microwave Theory Tech., Vol. MIT-30, No. 10, PP. 1548-1554 (1982).

[3] T. Saitoh, and T. Mukai, "1.5-μm GaInAs TWSOA," IEEE J. Qu. Elec., Vol. 23, No. 6, PP. 1010-1020 (1987).

[4] N.A.Olsson "Lightwave system with optical amplifiers," IEEE J. Lightwave Technol., Vol. 7, No. 7, pp. 1071-1082 (1989).

[5] M. J. O'Mahony. "Semiconductor laser amplifier for use in future systems," IEEE J. Lightwave Technol., Vol. 5, No. 4, pp. 531-543, (1988).

[6] G. Eisenstien, R. S. Tucker, and G. Raybon, "Optical time-division multiplexed transmission at 8 Gb/s using single laser and semiconductor optical power amplifier," Electron. Lett., Vol. 25, No 16, pp., 1034-1036 Aug. (1989).

[7] A. Elrefaie, R. Wagner, and D. Daut, "Chromatic dispersion limitations in coherent lightwave transmission systems," IEEE JLT., Vol. 6, No, 5, pp. 704-709 (1988).

[8] S. Saito, and T. Ito, "System performance of coherent transmission over cascaded in-line amplifiers," (Invited paper), IEEE J. Lightwave Technol., Vol. 11, No, 2, pp. 331-342, (1993).

[9] P. Henry, "Lightwave primer," IEEE J. Qu. Elec., Vol. 21, No. 12, PP. 1862-1879 (1985).

[10] A. Ehrhardt, et.al., "Semiconductor laser amplifier as optical switching gate," IEEE JLT., Vol. 11, No, 8, pp. 1287-1295 (1993).

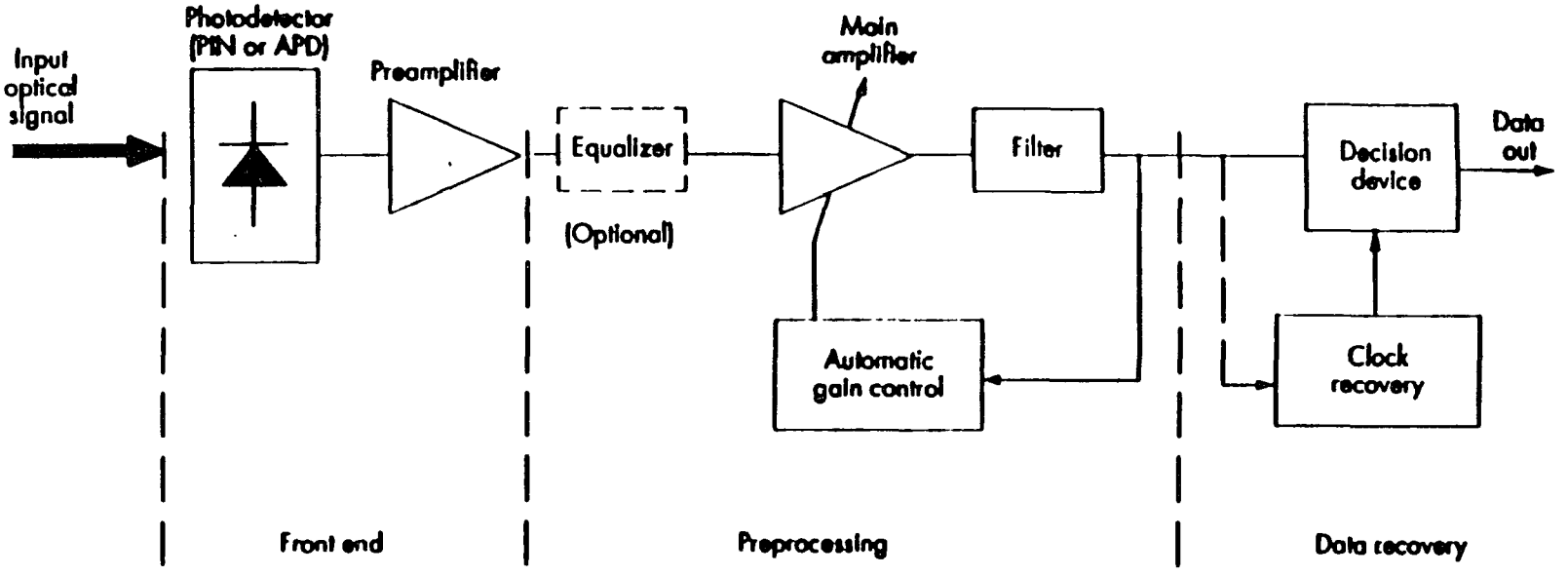

Fig. 6.1: Block diagram of a direct detection optical receiver for a digital data link.

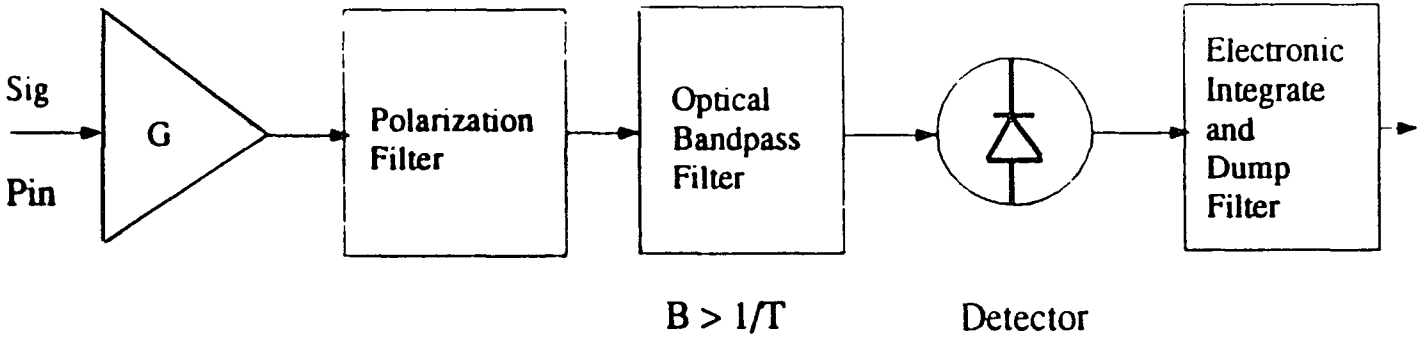

Fig. 6.2: Direct detection receiver with optical preamplifier.

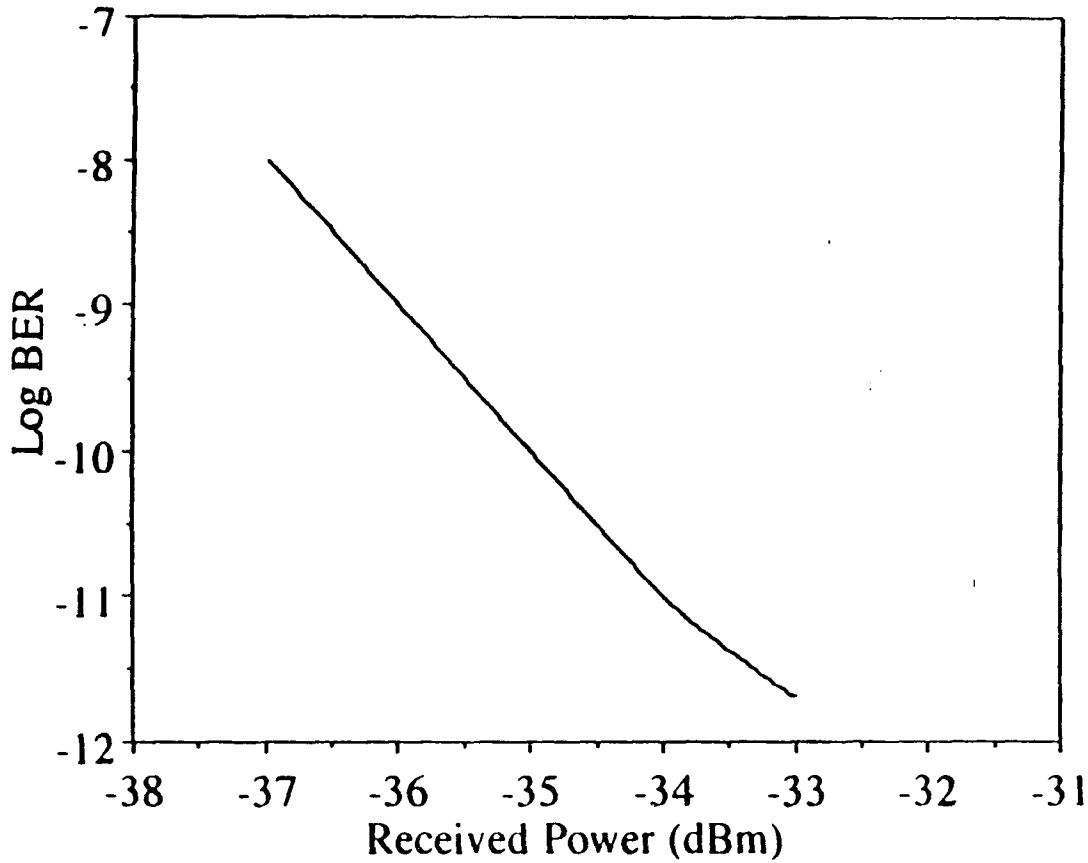

Fig. 6.3: BER characteristics for optical preamplifier receiver at 2.5 Gb/s. "Received Power" is the average optical power in the input fiber. G = 25 dB, $\eta_{in} = \eta_{out} = 0.4$, $N_{sp} = 1.4$, $r = 20$, $B_o = 1$ nm, $B_E = 1.25$ GHz.

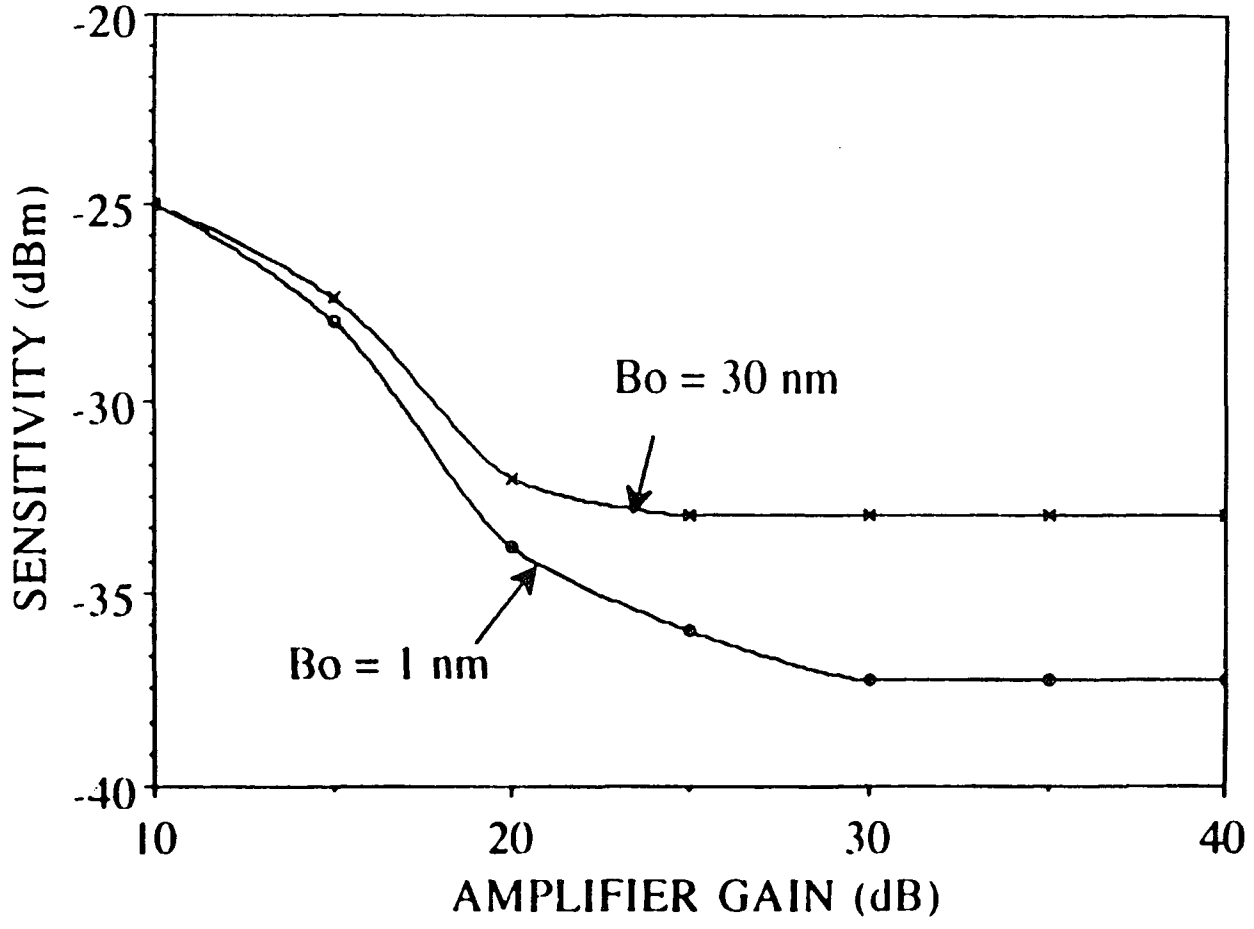

Fig. 6.4: Optical preamplifier sensitivity versus amplifier gain.
$\eta_{in} = \eta_{out} = 0.4$, $N_{sp} = 1.4$, $r = 20$, $B_E = 1.25$ GHz. BER = 10^{-9}.

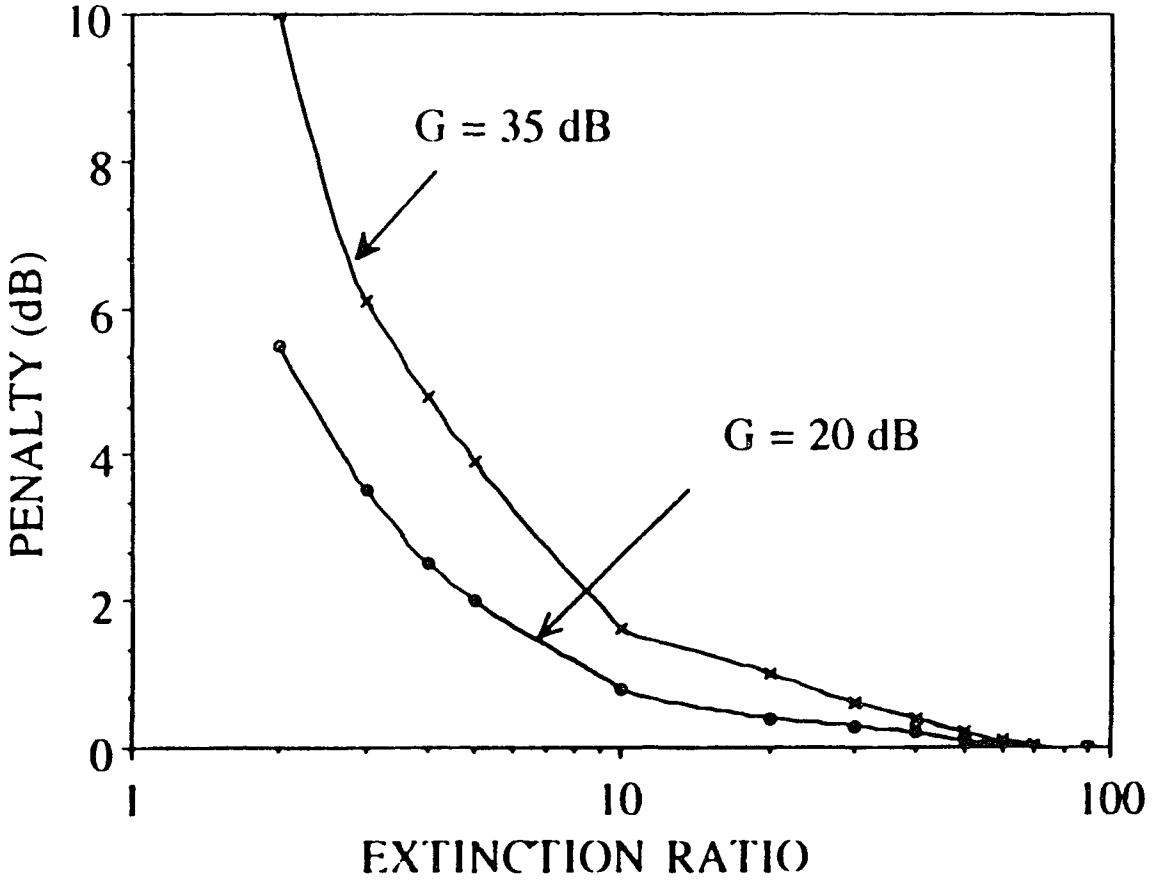

Fig. 6.5 Optical preamplifier sensitivity penalty versus extinction ratio. η_{in} = η_{out} = 0.4, N_{sp} = 1.4, B_o = 1 nm, B_E = 1.25 GHz. BER = 10^{-9}.

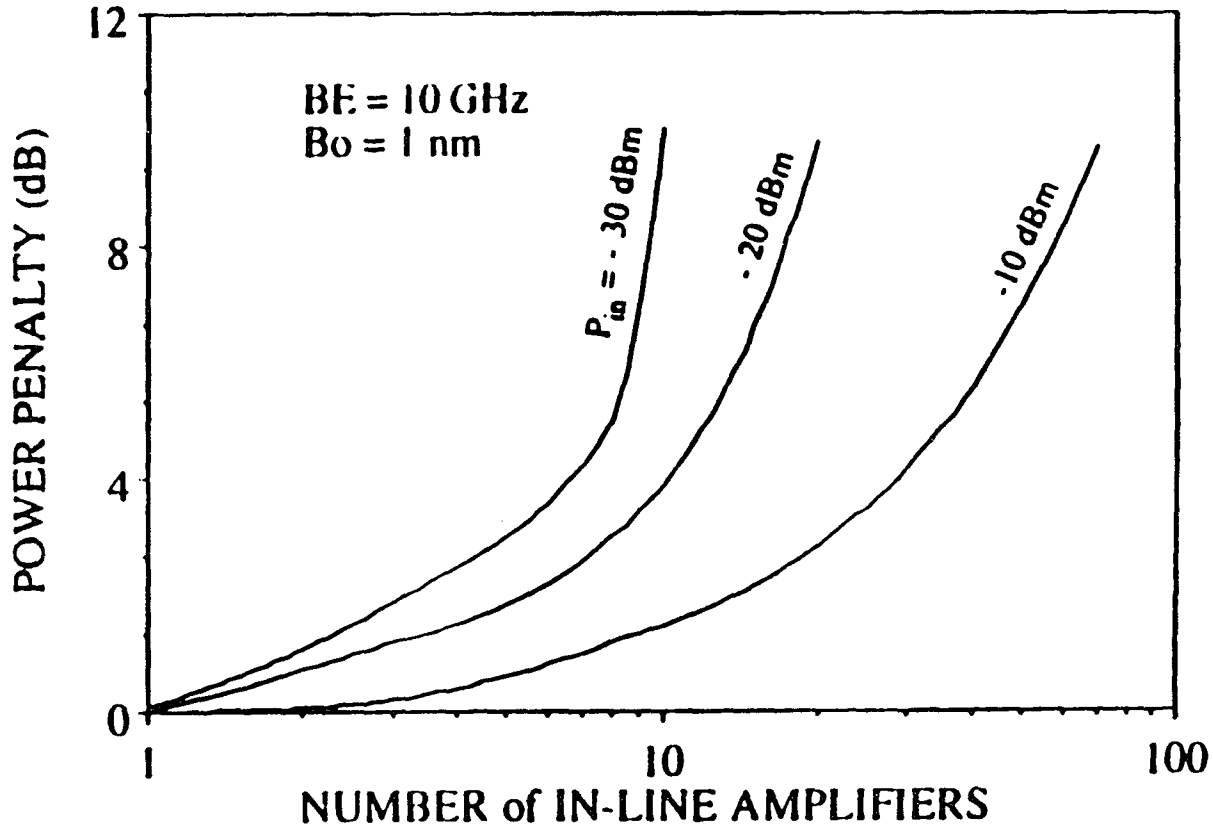

Fig. 6.6: Power Penalty versus number of in-line amplifiers at 20 Gb/s. Plotted for amplifier input powers of -30, -20, and -10 dBm. G = 25 dB, η_{in} = η_{out} = 0.4, N_{sp} = 1.4, r = 20, B_o= 1 nm, B_E = 10 GHz.

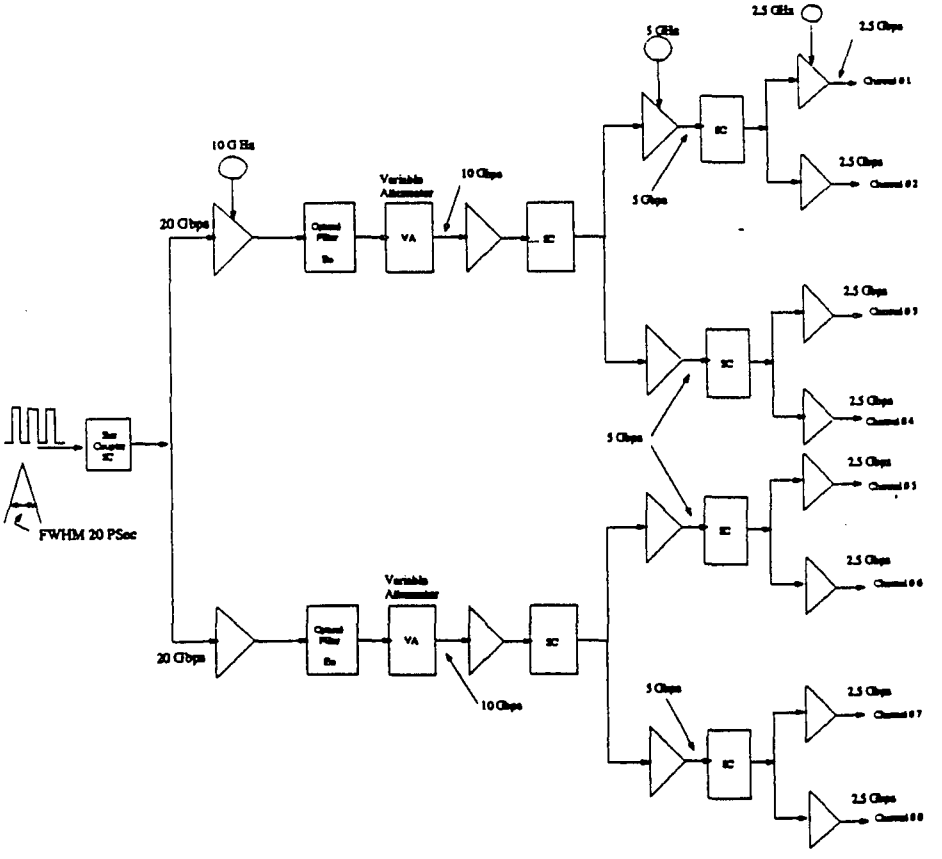

Fig. 6.7 Binary Tree Demultiplexing Network consisting of 16 TWSOA Gates for Demultiplexing 20 Gbps to eight 2.5 Gbps.

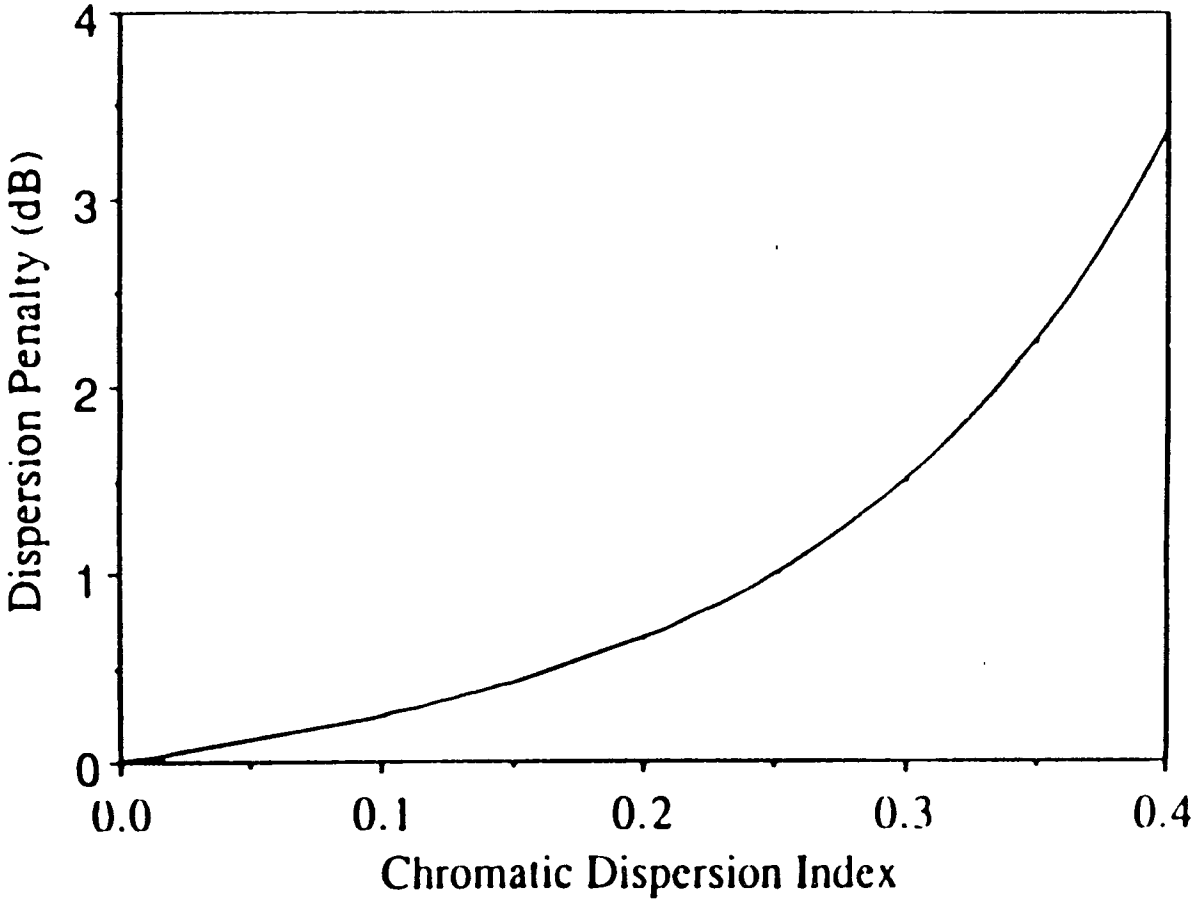

Fig. 6.8: Dispersion Penalty Versus Chromatic Dispersion Index γ for IM-DD systems.

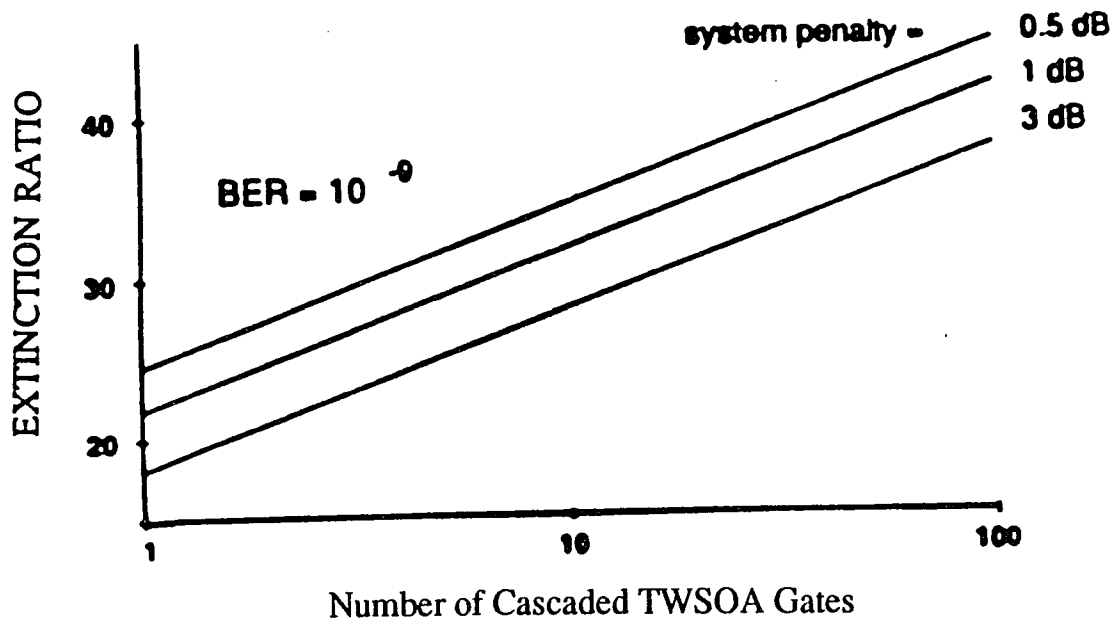

Fig. 6.9: Required extinction ratio versus the number of cascaded TWSOAs gates.

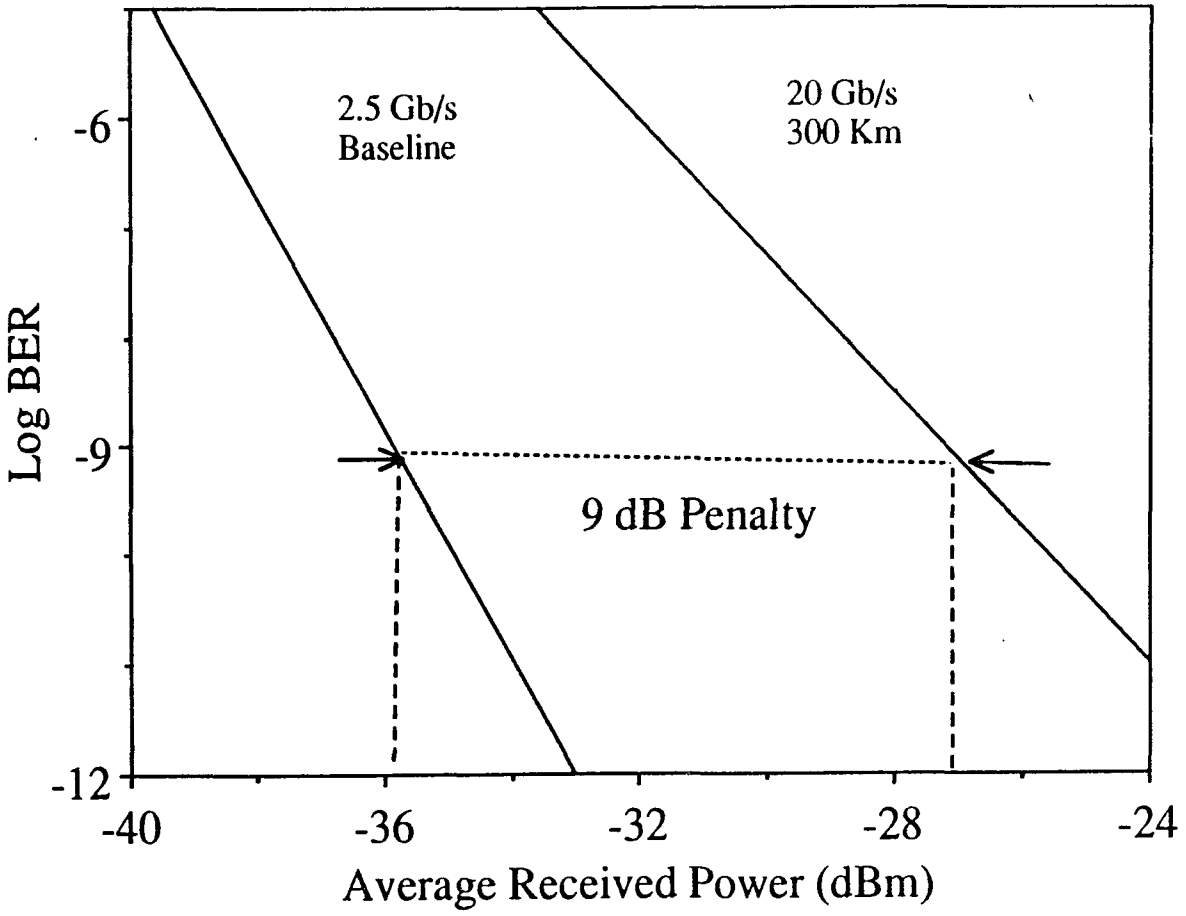

Fig. 6.10: BER versus Received Power.

CHAPTER 7
Multiple Access OTDM Networks

7.1. INTRODUCTION

The large potential bandwidth of optical fiber-theoretically on the order of 20 x 10^{12} Hz Cannot be realized by simply replacing the existing communications medium with optical fiber. To fully utilize the potential bandwidth of optical fiber in multiple-access applications such as local area communication networks and high speed computer interconnects, the large aggregate bandwidth of the network must be processed optically. This avoids the electronic bottleneck imposed if the network is implemented electronically. The bottleneck results because the network must process data at the rate N x B_E, where B_E is the bandwidth limit for electronic processors.

One approach which has the potential to achieve this objective is based on time-division multiple-access. Critical devices to implement such an optical time-division multiple-access (OTDMA) network include a high contrast ratio photoconductive AND device, a rapidly tunable optical delay device, a rapidly tunable optical delay device, and TWSOAs as switching elements for both modulation and demultiplexing.

In this chapter, we present a model of the OTDMA network architecture that relates parameters at the device-level to system-level performance measures such as BER and noise margin. Specifically, a fixed assignment TDMA synchronous accessing schemes using optical signal processing is investigated. It is shown that such a network can

accommodates more than 100 stations transmitting at 100 Mb/s each, using receiver-fixed assignment TDMA.

7.2 Fixed Assignment TDMA

Local area networks (LAN's) were originally proposed to interconnect computer facilities where the channel utilization was relatively low. Multiple access protocols were therefore designed to accommodate the low traffic demand in such networks in the most efficient way. Consequently, asynchronous contention protocols, such as token passing and carrier sense multiple access, are well suited to LAN's with low traffic demand. However, these asynchronous protocols suffer from cumulative delay as the traffic intensity increases.

Synchronous multiple access schemes, such as time division multiple access (TDMA), can accommodate higher traffic demands and do not suffer from cumulative delay [1-2]. In fixed assignment TDMA, each user is assigned a fixed time slot during which that user can receive a data packet or a bit information. In order to accommodate as many users as possible, the NRZ data are first converted into a low duty cycle signal by sampling them at the data rate. The low duty cycle signal is then transmitted in the selected destination time slot. This time division multiplexing process must be performed at a high speed. The cost of high speed electronics restricts the use of TDMA to networks where the traffic demand is heavy most of the time, in which case the high expenditure is justified. In any event, the speed limitation of electronics will ultimately restrict the minimum duty cycle of the sampled signal

(width of sample or TDMA slot) and hence the number of users that can be accommodated.

The user of fiber optics for the transmission channel alone does not reduce the bandwidth requirements of the electronic interfaces, nor does it mark a synchronous system more economical for network applications. It is proposed that the bandwidth requirements in the electronic interfaces for TDMA systems be reduced by performing the high bandwidth processing of the medium access protocols optically, and confining the slow electronic processing to relatively low-rate data handling.

7.3 SYSTEM ARCHITECTURE

A block diagram of the proposed TDMA system with optical signal processing is shown in Fig. 7.1. The system consists of an optical clock source, M stations with optical transmitters and optical receivers, and a passive optical star coupler. All interconnections utilize single-mode optical fibers. Although other configurations are possible, a star topology is chosen here to permit the maximum number of users given a fixed budget.

Using a fixed assignment TDMA, the optical signal at each station must be located in the correct time slot that corresponds to its destination. To synchronize all the transmitters, a centralized clock signal must be available to all stations. The clock signal can be distributed optically from a central mode-locked laser, as described in Fig. 7.2. The mode-locked laser generates a train of very narrow optical pulses at the data rate 1/T. The time between pulses T and the width of the pulses τ will determine

the maximum number of time slots T/τ that can be assigned. Using a mode-locked laser, a low duty cycle, high peak power pulses can be routinely generated. Consequently, many time slots can be assigned. The distance of any station from the mode-locked laser must be an integral multiple of Tc/n where c/n is the velocity of light in the fiber core.

At the transmitter, the data of each transmitting station must be optically sampled and multiplexed into the selected destination time slot. An optical sampler can be implemented by using the optical clock pulses in combination with an electrooptic modulator. The optical pulses are gated by the electrical data signal at the electrooptic modulator. The original electrical NRZ data signal is thus converted into a low duty cycle optical signal with the same data rate. By this procedure, conversion from a low bandwidth electrical signal into a high bandwidth optical signal is accomplished without resorting to high bandwidth electronics. The slow rise/fall time of the electrical data compared to the narrow optical pulses could result in a reduction in optical pulse amplitude if the optical pulses are gated during these transition times. To avoid this, some type of synchronization between the electrical signal and the optical pulses must be provided.

The optical data signal can be multiplexed into the correct destination time slot simply by using optical fiber delay lines. One possible schemes for a time division multiplexer (TDM) is shown in Fig. 7.3. M delay lines of length $i\tau c/n$, with i=1, 2, ...,M, are connected in parallel between two active electrooptic switches. To select the ith time slot, the first 1 x M

switch selects the fiber delay line of length $i\tau c/n$. The selected delay line is then switched into the output port using the M x 1 electrooptic switch.

At the receiver end of the network, the receiving station must be able to identify its own time slot within the TDMA frame. To accomplish this, the station uses the slot demultiplexer (Fig. 7.4). In order to recognize its own time slot, the ith receiver delays the clock signal by $i\tau$ and adds it to the incoming signal. The addition of the TDMA signal and the delayed clock results in the correct signal riding atop the clock signal. The signal can then be threshold detected. It is necessary that the TDMA frames arrive at the receiver in synchronism with the optical clock, so that the clock signal can be synchronized to the position of the receiver slot in the TDMA frame. Therefore, the length of fiber from each station to the star coupler must be an integral multiple of $L=Tc/n$.

The transmitted data are ultimately recovered by the threshold detector and pulse generator. The output of the slot demultiplexer has three well-defined signal levels: a low level corresponding to no data or a data 0 transmitted in another user's slot, a middle level corresponding to a data 1 transmitted in another user's slots or a data 0 transmitted in the receiver's own slot, and a high level corresponding to a data 1 transmitted in the receiver's own slot. The threshold detector level is set between the middle and high level. Whenever the optical signal crosses the threshold, a pulse of length T is emitted by the optical pulse generator. This optical pulse is subsequently converted by the photodetector into an electrical NRZ data signal of rate 1/T.

7.4 POWER REQUIREMENTS

The synchronous networks presented in section II require a mode-locked laser with sufficient peak optical power. The mode-locked laser must be able to drive the whole network, leaving a power margin for future expansion and network reliability. The power available for a station in an M-station network is divided between a transmitter clock and a receiver clock signal (see Fig. 7.2). The signal intensity P_{TC} of transmitter clock is given by

$$P_{TC} = P_L - 10 \log M - L_S - 10 \log \alpha - L'_S \qquad (1)$$

where:

P_L : laser peak power output into a fiber pigtail

L_S : the (1 x M) splitter excess loss

L'_S: the (1 x 2) splitter excess loss

α : the splitting ratio of input to transmitter-clock output of the (1 x 2) splitter.

It is assumed for simplicity that the loss in the fiber is negligible and the power is equally divided among M output fibers.

The power at the input to the receiver is given by

$$P_R = P_{TC} - L_M - L_{SS} - L_{SC} - 10 \log M \qquad (2)$$

Where

L_M : the modulator excess loss

L_{SS}: the multiplexer total loss

L_{SC}: the star coupler excess loss.

At the optical threshold detector, the signal power P_S for corresponds to the difference between the middle and high levels in Fig. 7.4. To maximize the signal power and reduce the effects of adjacent pulse interference, the clock pedestal should be at least as large as the surrounding interference, i.e., the middle level. To minimize the source power required, the amplitude of the clock pedestal is set equal to the maximum interference level. This is achieved by adjusting α to equalize the losses in the clock channel equal to the losses in the signal channel and solving for α yields

$$\alpha = 1 + 1/\{M \log^{-1} ((L_M + L_{SS} + L_{SC})/10)\} \quad (3)$$

With this choice of α , the signal power P_S at the optical threshold detector is

$$P_S = P_R - L'_S - 3 \quad (4)$$

where the splitting loss in the (2 x 1) combiner is assumed to be 3 dB. Substituting (1) and (2) in (4), the power required at the mode-locked laser to yield a given signal level at the input to the optical threshold detector is given by

$$P_L = P_S + 20 \log M + L_S + 2L'_S + L_M + L_{SS} + L_{SC} + 10 \log \alpha + 3. \quad (5)$$

For a TDMA system with a parallel line multiplexer [Fig. (7.3)], the multiplexer loss is:

$$L_{SS} = 2L_{SW} \quad (6)$$

where L_{SW} is the switch loss.

7.5 Results and Analysis

In this section, the appropriateness of the assumptions are discussed. Different configurations for the detection process are presented. Fiber length tolerances are specified. Finally. ways to avoid error arising from the imprecise gating of the electrooptic modulator by a low bandwidth signal are given.

In the preceding section, equal output power distribution from the optical splitter and star couplers was assumed. Equal power distribution is important because the slot synch. process. If the power distribution is unequal, false detection could result when interfering transmission are strong enough to cross the threshold level. Although most commercially available optical splitters are passive star couplers have unequal output power distribution, recently reported was a 100-node star coupler with low excess loss and approximately equal output power distribution.

For the network configurations 1 x M optical splitters and M x M star couplers are required. Such device are available for M up to 100. To implement a network with a larger number of users (M > 100), these devices could be implemented by cascading existing units of smaller size. One way of cascading these units with low loss is to interconnect $M^{1/2}$ x $M^{1/2}$ sized units in two columns of $M^{1/2}$ units each.

Nonlinear optical effects become nonnegligible in a single mode fiber when high power optical clock sources are used. To avoid these effects, the clock distribution can be done by coupling the output of the optical clock source into a bundle of M single mode fiber. Thus,

the power per fiber is reduced by a factor of M. Coupling efficiency can be maximized by reducing the fiber cladding thickness to just a few micrometers.

In order to maintain network synch., the distance of the stations from the mode-locked laser must be an integral multiple of TDMA frame lengths. The permissible fiber length tolerance is + $0.2\delta\ \tau$ m, where δ is the allowed percent of slot overlap and t is the pulse width in nanosecond. A propagation velocity of 0.2 m/ns is assumed.

At the slot demultiplexer, the delayed clock reference and the received signal must also be synchronized. The permissible tolerance in fiber delay lengths in this case is $0.2JT + 0.2\delta\ \tau$, where J is any integer. For picosecond pulses, fiber length tolerances would have to be kept within hundreds of microns.

7.6 REFERENCES

[1] Paul R. Prucnal, and Sanjay Sehgal, "Ultrafast all-optical synchronous multiple access fiber networks," IEEE J. Select. Areas Commun., vol. SAC-4, No 9, pp. 1484-11493 (1986).

[2] R. V. Schmidt, "Fiber netII: A fiber optic Ethernet," IEEE J. Select. Areas Commun., vol. SAC-1, pp. 701-711 (1983).

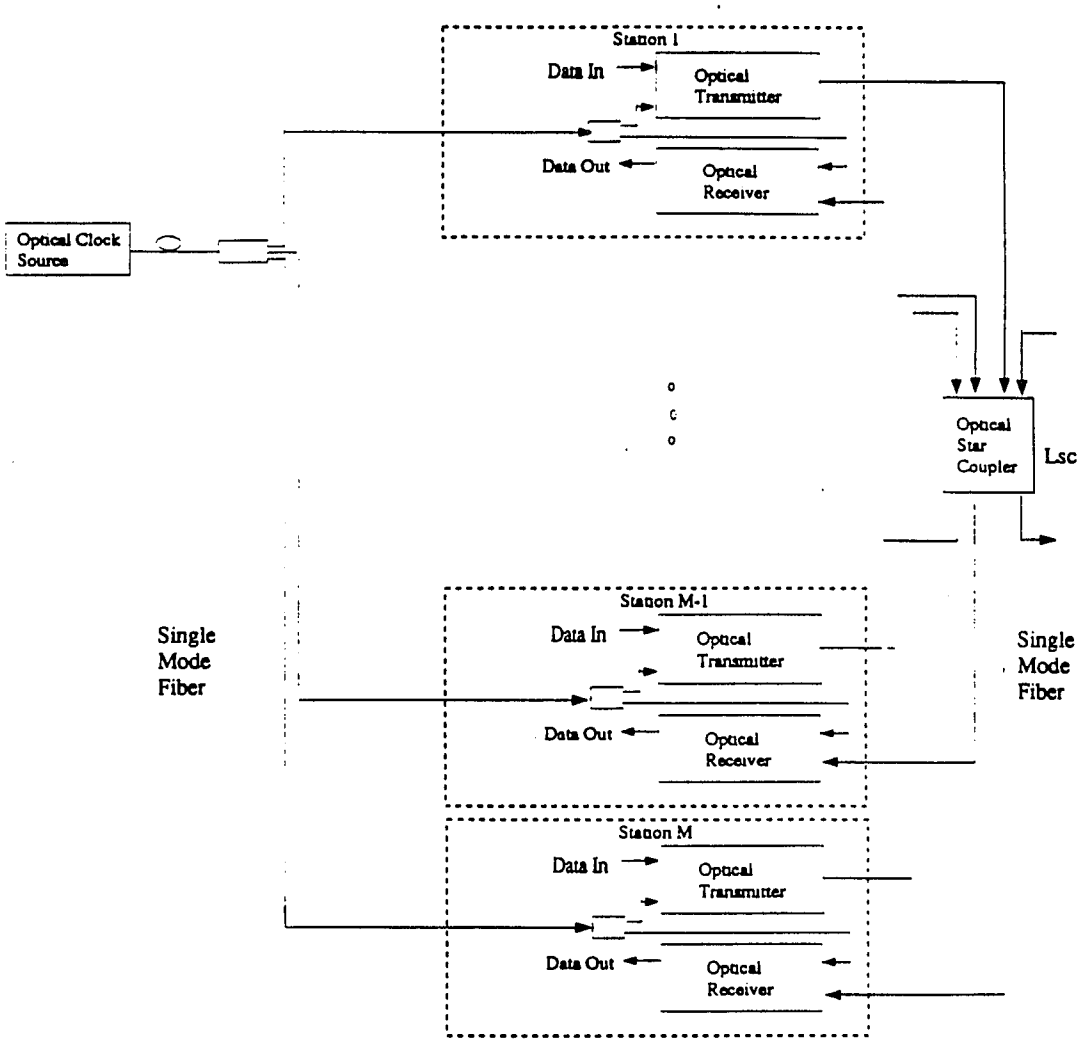

Fig. 7.1. Block diagram of a Synchronous fiber optic network with M stations in a star topology and a central optical clock. Lsc is the star coupler excess loss. Single mode fiber is used to interconnect the stations.

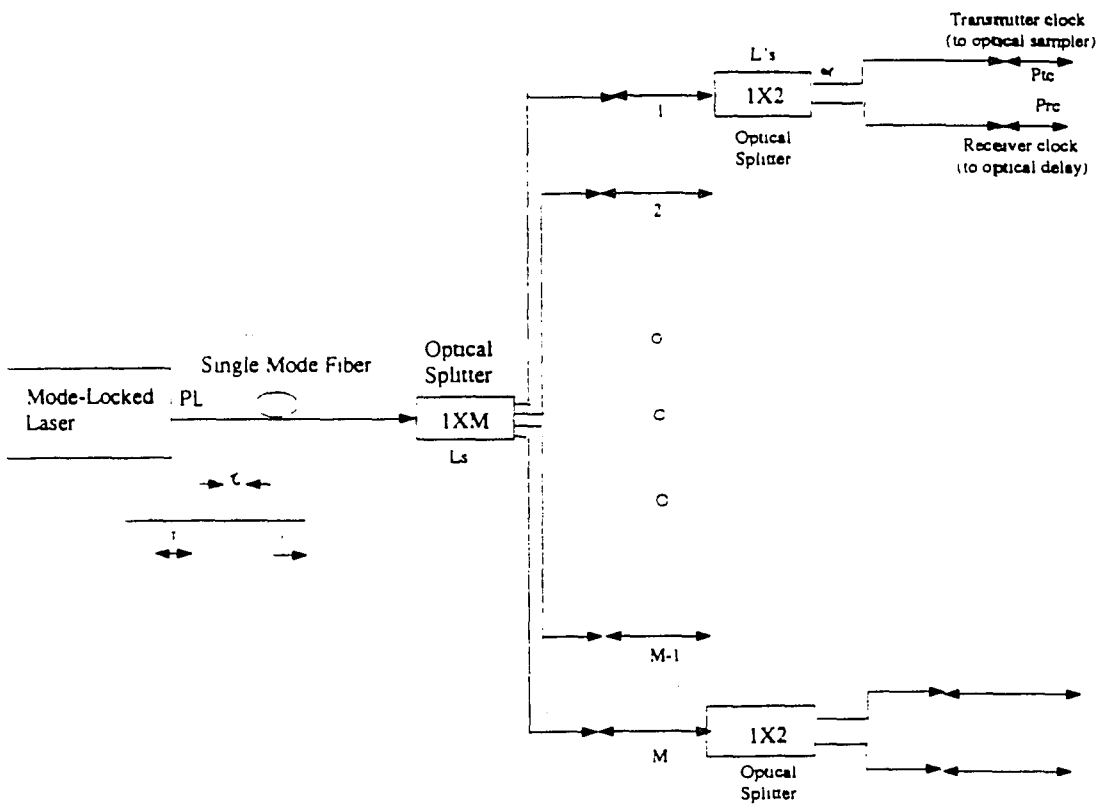

Fig 7.2. Optical clock signal distribution. $1/T$ is the optical pulse repetition rate. τ is the optical pulse width. PL is the laser peak power output. α is the splitting ratio of input to transmitter-clock-output of the 1 X 2 splitter. Ls is the 1 X M optical splitter excess loss, and L's is the 1 X 2 splitter excess loss. The distance of any station to the mode-locked laser is ki Tc/n where ki is an integer and c/n is the velocity of light in the fiber.

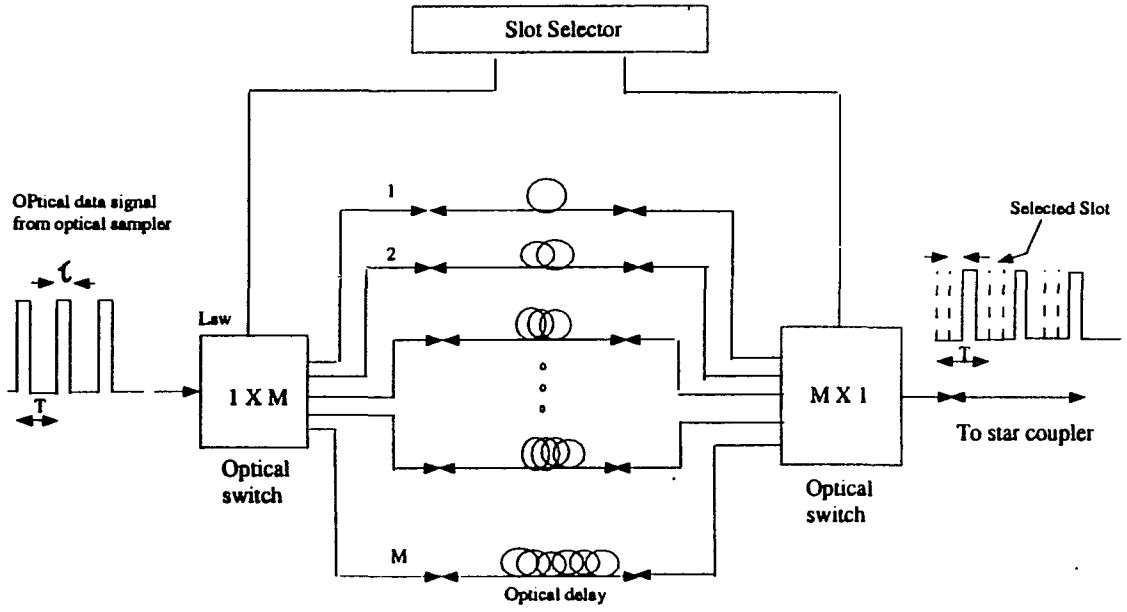

Fig 7.3. Optical Parallel multiplexer. Different fiber optic delay lines with length a multiple of $\tau c/n$ are attached to 1 X M and M X 1 electrooptic switches. The slot selector selects the desired fiber optic delay path by appropriately activating the 1 X M and M X 1 switches.

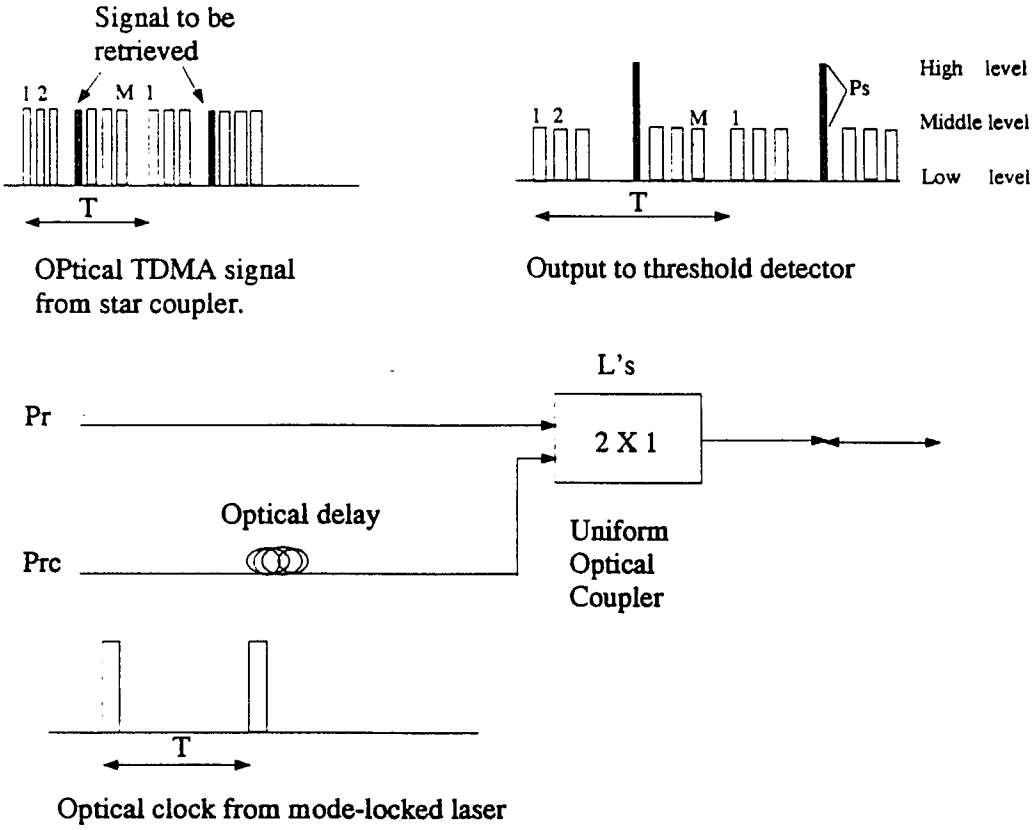

Fig. 7.4. Slot demultiplexer. The optical TDMA signal is combined with a delayed optical clock. In this way, information arriving in the correct slot is raised on the clock pedestal and is made easily distinguishible. Pr is the received peak power, L's is the coupler loss. Three signal levels are defined: a low level corresponding to no data or a data bit zero in other user's slots or a data 0 transmitted in the receivers own slot, a middle level corresponding to a data bit one in other user's slot, and a high level corresponding to a data bit one in the receiver's own slot. Ps is the signal power.

CHAPTER 8
SUMMARY

This thesis focused on developing a novel optical time-division multiplexing technique for use in ultra high-speed transmission systems. Our emphasis was on both very high bit-rate point-to-point transmission systems and multiple-access local loop networks. We have investigated and analyzed, through computer simulation and modeling, the performance of all the critical elements necessary for the implementation of high–capacity, high–performance, cost–effective, reliable point-to-point and multiaccess transmission systems based on time division optical fiber communications technology. OTDM networking architectures and technology as well as the potential and limitations of long-haul very high bit-rate point-to-point OTDM transmission systems have also been investigated. The network technology element of this work aimed to define the physical components and network elements that are necessary to assemble a reconfigurable, diverse OTDM network. The network architecture element specifically addressed several new topologies, such as rings and stars.

We have also presented a model of a novel optical time-division multiple-access (OTDMA) network architecture that related parameters at the device-level to system-level performance measures such as bit error rate (BER) and noise margin. This was accomplished by developing mathematical models of the optical and electronic devices in the system which are suitable for discrete-time simulation at the system-level. These simulation models were interconnected into a system level simulation

model of the OTDMA architecture. We demonstrated some of the capabilities of the simulation model through a number of examples at both device and system level.

The simulation modeling is characterized by its consideration of the full potential for exploiting travelling-wave semiconductor optical amplifiers (TWSOAs) as multifunction components in both long haul optical transmission systems and multiple-access broad-band fiber optic networks. Specifically, the nonlinear model is used to examine the switching characteristics of TWSOAs when used for external modulation and demultiplexing at both the transmitter and receiver ends of a multi-Gb/s OTDM system. Employing TWSOAs as high-speed optical gates at both the transmitter and receiver ends of OTDM systems will, (i) provide simultaneous gain and gating, and hence increase both information capacity and transmission distance, and (ii) replace the present inherently bulky and lossy Ti: $LiNbO_3$ waveguide external modulators and demultiplexers, required at each end of each channel, with compact ones suitable for opto-electronic integrated circuit (OEIC) implementation. This approach may allow for lossless devices and future monolithic integration of external modulators with lasers and of demultiplexers with detectors or with opto-electronic integrated front-ends. Optical gating with TWSOAs is also of particular interest for bus or broadcast network architectures where one channel on a bus is sampled and access to all channels is required.

The specific tasks of our simulation tools are two fold:

Simulation Tool: We have implemented a flexible, powerful computer modeling tool for evaluating the end to end performance of OTDM networks. The tool has included wavelength driven and time driven capabilities. The wavelength driven capability was required to model the effects of cascading many optical amplifiers and optical filters on the output signal to noise ratio and crosstalk level of any signal on the network. The time driven capability was required to model the effects of fiber chromatic and polarization dispersion, crosstalk from adjacent channels, timing jitter due to noise and crosstalk, thermal and shot noise in the receiver, and non-perfect extinction ratio in external modulators, on the signal quality in the network.

Device and subsystems Models: We have developed models for different subsystem components, like laser sources, TWSOAS, OTDM multiplexers and demultiplexers, optical filters, and external modulators. It was possible to combine these components in any combination, using the above tool, to allow the important network elements to be modeled. These networks elements were then combined in an arbitrary order to allow a variety of network architectures to be modeled.

The following summarizes the main results of this thesis:

By using TWSOAs as external modulators and demultiplexers at both the transmitter and receiver ends of the proposed multi-Gb/s OTDM system, the following has been achieved:

1) Satisfactory modulation performance at a bit rate ranging from 1 Gb/s up to 8 Gb/s, over a practically useful range of input signal levels, has been achieved provided that $E_{in}/E_{sat} \leq -10$ dB.

2) At high modulation speeds (> 2.5 Gb/s), such that the separation between pulses is comparable and/or shorter than the gain recovery time, satisfactory modulation performance was achieved by: a) Increasing the drive current pulses amplitude, however, subject to the constraint that the carrier level must be maintained below the lasing threshold to prevent significant emission from the amplifier itself; and, b) Using Zn-doped active layers with different doping concentrations.

3) The maximum achievable satisfactory demultiplexing speeds using conventional undoped active region TWSOA is 6 Gb/s.

4)The maximum demultiplexing speeds can be increased from the 6 Gb/s maximum speed achievable using undoped single TWSOA gate, to 10-12 Gb/s by using an optical gate consisting of two cascaded TWSOAs. Those satisfactory high speeds demultiplexing performances are also shown to be achievable over a wide range of input signal levels ($E_{in}/E_{sat} \leq 0$ dB), using an optical gate consisting of two cascaded TWSOAs, each with a 2 : 1 and/or 4 : 1 selection ratios.

5) Satisfactory demultiplexing performance at 10 Gb/s can also be achieved using a single Zn-doped active layer TWSOA gate.

6) Using TWSOAs as external modulators and demultiplexers at both the transmitter and receiver ends of the proposed multi-Gb/s OTDM system

provides adequate overall system performance for eight 2.5 Gb/s channels transmitted over a transmission distance of about 300 Km.

7) An OTDMA network architecture model has been presented. Specifically, a fixed assignment TDMA synchronous accessing schemes using TWSOAs was shown to be capable of accommodating more than 100 stations transmitting at 100 Mb/s each, using receiver-fixed assignment TDMA.

Eventually, we were able to model the end-to-end performance of any signal that passes through the network. This permitted us to compare and devise candidate survivable OTDM architectures and determine the appropriate field of use for each. In addition, this has enabled us to determine how to use the capabilities of each architecture to best advantage and provide insight into which OTDM architecture should be stressed by yielding estimates of comparative networking costs.

Bibliography

Adams, M. J., J. V. Collins, and I. D. Henning, "Analysis of semiconductor laser optical amplifiers," Proc. IEE, Optoelectron., Vol. 132, pp. 58-63 (1985).

Agrawal, G. P., and N. A. Olsson, "Self-phase modulation and spectral broadening of optical pulses in semiconductor laser amplifiers," IEEE J. QE., vol. 25, pp. 2279-2306, (1989).

Alferness, R. C., "optical amplifiers for photonic circuits," Technical Digest on Optical Amplifiers and their Applications Topical Meeting, SANTA FE, New Mexico, Vol. 17, Paper FA1-1 (1992).

Ali, M., A. Elrefaie, and S. Ahmed, "Simulation of 12.5 Gb/s optical time-division multiplexer using semiconductor optical amplifiers as external modulators," IEEE PTL., Vol. 11, PP. 1018-1020, Mar. (1992).

Ali, M., and S. Ahmed, "Simulation of semiconductor optical amplifiers for external modulation and demultiplexing in multi-Gb/s optical time-division multiplexed systems," International Conf. on lasers, 91, Proceedings, Session WD.7.

Ali, M., H. Issa, A. Elrefaie, and S. Ahmed, " High speed optical time-division demultiplexer using semiconductor optical amplifiers," IEEE J. Lightwave Technol., Vol. , NOv. (1992).

Andrekson, P. A., N. A. Olsson, J. R. Simpson, T. Tanbun-EK, R. A. Logan, and M. Haner, "16 Gb/s all-optical demultiplexing using four-wave mixing," Electron. Lett., vol 27, pp 922-924, 1991.

Beattie, A.,R. and P. T. Landsberg, "Auger effects in semiconductors," Proc. Roy. Soc. London, Vol. 249, PP. 16-29, 1956.

Brackett, C. A., "dense wavelength division multiplexing networks: principles and application," IEEE J. on Selected Areas in communication, Vol. 8, No, 6, pp. 948-964, August (1990).

Denton, R. T., and T. S. Kinsel, "Terminals for a high-speed optical pulse code modulation communication system: I. 224-Mbit/s single channel," Proceedings of the IEEE, Vol. 56, No. 2, Feb.(1968). PP. 140.

Dutta, N. K., and R. J. Nelson, "The case of Auger combination InGaAsP," J. Appl. Phys., Vol 53, PP. 74-92, Jan. 1982.

Ehrhardt, A., et.al., "Semiconductor laser amplifier as optical switching gate," IEEE JLT., Vol. 11, No, 8, pp. 1287-1295 (1993).

Eisenstien, G., R. S. Tucker, G. Raybon, and S. K. Korotky, "8-Gb/s transmission over 40 km in a two-channel single-laser optical time-division multiplexed system experiment," OFC' 89

Eisenstien, G., R. S. Tucker, and G. Raybon, "Optical time-division multiplexed transmission at 8 Gb/s using single laser and semiconductor optical power amplifier," Electron. Lett., Vol. 25, No 16, pp., 1034-1036, Aug. (1989).

Elrefaie, A., H. Izadpanah, and A. Alhamdan, "8 Gb/s current modulation of semiconductor optical amplifiers," ECOC' (1990).

Elrefaie, A., R. Wagner, and D. Daut, "Chromatic dispersion limitations in coherent lightwave transmission systems," IEEE JLT., Vol. 6, No, 5, pp. 704-709 (1988).

Hansen, P.B., and R. Tucker, " Repetition-rate dependence of gain compression in InGaAsP optical amplifiers using picosecond optical pulses," IEEE J. Qu. Elec., Vol. 25, PP. 2611-2619 (1984).

Haug, A., "Auger recombination in InGaAsP," Appl. phys. lett., Vol. 42, PP. 512-514, Mar. 1983.

Henry, C. H., " theory of spontaneous emission noise in open resonators and its application to lasers and optical amplifiers," IEEE J. Lightwave Technol., Vol. LT-4, pp. 288-297 (1986).

Henry, P., "Lightwave primer," IEEE J. Qu. Elec., Vol. 21, No. 12, PP. 1862-1879 (1985).

Kamite, K., H. Sudo, and H. Ishikawa, "14 GHZ single-mode picosecond optical pulse train generation in Zn-doped distributed-feedback lasers," App. Phys. Lett., 45 (3), PP. 208-209, (1989).

Kinsel, T. S., and Richard T. Denton, "Terminals for high-speed optical pulse code modulation communication system : Optical

multiplexing and demultiplexing," Proceedings of the IEEE, Vol. 56, No. 2, Feb. (1968).

Kinsel, T. S., "Wide-band optical communication systems : Part I -- Time division multiplexing," Proceeding of the IEEE, Vol. 58, No. 10, Oct. (1970) .

Korotky, S. K., and J. J. Veselka, "Efficient switching in a 72-Gb/s Ti:$LiNbO_3$ binary multiplexer/ demultiplexer," Conf. Opt. Fiber Commun., Paper TuH2, San Francisco, CA, 1990.

Lee, C. H., and P. J. Delfyett, "limits on amplification of picosecond pulses by using semiconductor laser traveling-wave amplifiers," IEEE J. QE., vol. 25, pp. 2279-2306, (1991).

Lomax, A., and I. White, "Modulation of picosecond pulses using semiconductor laser amplifiers," IEE Proc., Part J, Vol.138, no. 3, PP. 178-184, (1991).

Mukai, T., Y. Yamamoto, and T. Kimura, "S/N and error ra performance in AlGaAs semisonductor laser preamplifier and linear repeater systems," IEEE Trans. Microwave Theory Tech., Vol. MIT-30, No. 10, PP. 1548-1554 (1982).

Olshansky, R., C. Su, and W. Powazink, " Measurement of radiative and nonradiative recombination rates in InGaAsP and AlGa As light sources," IEEE J. Qu. Elec., Vol. 20, PP. 838-854 (1984).

Olsson, N.A."Lightwave system with optical amplifiers," IEEE J. Lightwave Technol., Vol. 7, No. 7, pp. 1071-1082 (1989).

O'Mahony, M. J., "Semiconductor laser amplifier for use in future systems," IEEE J. Lightwave Technol., Vol. 5, No. 4, pp. 531-543, Apr. (1988).

Prucnal, R. Paul, "Ultrafast all-optical synchronous multiple access fiber networks," IEEE J. Select. Areas Commun., vol. SAC-4, No 8, pp. 1484-11493 (1986).

Saito, S., and T. Ito, "System performance of coherent transmission over cascaded in-line amplifiers," (Invited paper), IEEE J. Lightwave Technol., Vol. 11, No, 2, pp. 331-342, (1993).

Saitoh, T., and T. Mukai,"Gain saturation characteristics of traveling-wave semiconductor laser amplifiers in short optical pulse amplification," IEEE J. QE., vol. 26, pp. 2086-2094, (1990).

Saitoh, T., and T. Mukai, "1.5-μm GaInAs TWSOA," IEEE J. Qu. Elec., Vol. 23, No. 6, PP. 1010-1020 (1987).

Saleh, A., "Modeling of nonlinearity in semiconductor optical amplifiers," IEEE Globecom, (1989).

Saleh, A., "Nonlinear models of traveling-wave optical amplifiers," Electron. Lett., Vol. 24, No 14, pp., 835-837, July (1988).

Siegman, A. E., Lasers. Mill Valley, CA: University Science Books, 1986, Ch. 10.

Schmidt R. V., "Fiber netII: A fiber optic Ethernet," IEEE J. Select. Areas Commun., vol. SAC-1, pp. 701-711 (1983).

Simon, J. C., "GaInAsP semiconductor laser amplifiers for single mode fiber comunications," J. Lightwave Technol., vol. 5, No 9, pp. 1286-1295 (1987).

Smith, R. G., and S. D. Personic, "Receiver design for optical fiber communication systems," Topics in App. Phys., H. Kressel, Ed. New York: Spring-Verlag, 1987, Vol. 39, ch. 4.

Su, C. B., and V. Lanzisera, App. Phys. Lett. 45, PP. 1302 (1984).

Su, C. B., J. Schlafer, J. Manning, and R. Olshansky, "Measurement of radiative and Auger recombination rates in p-type InGaAsP diode lasers," Elect. Lett., Vol. 18, PP. 595-596, July 1982.

Sugimura, A., "Band-to-band Auger recombination in InGaAsP lasers," Appl. phys. lett., Vol. 39, PP. 21-23, July 1981.

Takada, A., K. Aida, and M. Jinno, "Demultiplexing of a 40- Gb/s optical signal to 2.5 Gb/s using a nonlinear fiber loop mirror driven by amplified, gain-switched laser diode pulses," Conf. Opt. Fiber Commun., Paper TuN3, San Diego, CA, 1991.

Thompson, G. H. B., "Analysis of radiative and nonradiative recombination law in lightly doped InGaAsP lasers," Elect. Lett., Vol. 19, PP. 154-155, Mar. 1983.

Tucker, R. S., G. Eisenstien, and S. K. Korotky, "Optical time-division multiplexing for very high bit-rate transmission," IEEE J. Lightwave Technol., Vol. 6, No, 11, pp. 1737-1749, Nov. (1988).

Tucker, R. S., G. Eisenstien, S. K. Korotky, L. L. Buhl, "16 Gbit/s Fiber transmission experiment using Optical Time-Division Multiplexing," Electronics Lett., Vol. 23, Nov. (1987).

Uji, T., K. Iwamato, and R. Lang, "Dominance of Auger recombination in InGaAsP light emitting diode current-power characteristics," IEEE Trans. Electron Dev., Vol. ED-30, PP. 316-320, Apr. 1983.

Uji, T., K. Iwamoto, and R. Lang, "Non-radiative recombination in InGaAsP/InP light sources causing light emitting diode output saturation and strong laser-threshold-current temperature sensitivity," Appl. phys. lett. Vol. 38, PP. 193-195, Feb. 1981.